Development of Oxidation Technology in Water Treatment: Pulsed Corona Discharge Plasma Combined with Peroxocompounds

Dmitri Nikitin

Development of Oxidation Technology in Water Treatment: Pulsed Corona Discharge Plasma Combined with Peroxocompounds

DMITRI NIKITIN

TALLINN UNIVERSITY OF TECHNOLOGY
School of Engineering
Department of Materials and Environmental Technology
This dissertation was accepted for the defence of the degree 01/07/2024

Supervisor: Dr. Niina Dulova, Senior Researcher
                          School of Engineering
                          Tallinn University of Technology
                          Tallinn, Estonia

Co-supervisor: Professor Sergei Preis
                          School of Engineering
                          Tallinn University of Technology
                          Tallinn, Estonia

Opponents: Asst. Prof. Anton Yu. Nikiforov
                          Department of Applied Physics
                          Ghent University
                          Ghent, Belgium

                          Dr. Monica Magureanu, Senior Researcher
                          Dept. of Plasma Physics and Nuclear Fusion
                          National Institute for Laser, Plasma and Radiation Physics
                          Bucharest, Romania

Defence of the thesis: 23/08/2024, Tallinn

Declaration:
Hereby I declare that this doctoral thesis, my original investigation and achievement, submitted for the doctoral degree at Tallinn University of Technology has not been submitted for doctoral or equivalent academic degree.

Dmitri Nikitin

European Union
European Regional
Development Fund

Investing
in your future

_____
                                  signature

Oksüdatsioonitehnoloogia arendamine veepuhastuses: peroksoühenditega kombineeritud impulss koroona elektrilahendus

DMITRI NIKITIN

Contents

List of publications

The list of author's publications, on the basis of which the thesis has been prepared:

I **Nikitin, D.**, Kaur, B., Preis, S., Dulova, N., 2022. Persulfate contribution to photolytic and pulsed corona discharge oxidation of metformin and tramadol in water. Process Saf. Environ. Prot. 165, pp 22–30. https://doi.org/10.1016/j.psep.2022.07.002

II **Nikitin, D.**, Kaur, B., Preis, S., Dulova, N., 2023. Degradation of antibiotic vancomycin by UV photolysis and pulsed corona discharge combined with extrinsic oxidants. Catalysts 13, 466. https://doi.org/10.3390/catal13030466

III **Nikitin, D.**, Preis, S., Dulova, N., 2024. Degradation of imidazolium-based ionic liquids by UV photolysis and pulsed corona discharge: The effect of persulfates addition. Sep. Purif. Technol. 344, 127235. https://doi.org/10.1016/j.seppur.2024.127235

Author's contribution to the publications

Contributions of the author to the published papers in this thesis are:

I   The author carried out experiments and respective analyses, supervised the experimental work of an MSc student, interpreted the obtained data and wrote the paper in cooperation with co-authors.

II   The author fulfilled the majority of experiments, interpreted the obtained data, and wrote the paper in cooperation with co-authors.

III   The author carried out the experiments, supervised the experimental work of two MSc students, interpreted the obtained data and wrote the paper in cooperation with co-authors.

Introduction

The technological development in the 20th century and the growing quality of life led to the appearance and massive consumption of synthetic substances, including components of plastics, resins, fibres, pharmaceuticals, personal care products, steroid hormones, etc., released into the environment. Synthetic organic compounds possessing better stability and resistance to environmental factors accumulate in the environment. The occurrence of man-made pollutants resistant to biodegradation in surface water, groundwater and soil in concentrations ranging from ng L^{-1} to µg L^{-1} has raised environmental concerns. Conventional wastewater treatment plants were not designed for the treatment of such recalcitrant compounds, resulting in accumulated micropollutants that pose a threat to aquatic life and ecosystems.

Advanced oxidation processes (AOPs) are actively studied as effective treatment methods against recalcitrant compounds. These processes are based on the *in-situ* generation and use of strong oxidants, such as hydroxyl radicals, as well as sulfate and chlorine radicals.

Among the emerging AOPs, persulfate and non-thermal plasma processes show the greatest potential in producing reactive oxygen species (ROS). The pulsed corona discharge (PCD) applied to the water dispersed in the discharge zone outperforms other types of plasma in energy efficiency of oxidation. On the other hand, there is a growing interest in the activation of peroxocompounds by the non-thermal plasma. It is believed that in plasma treatment of aqueous media, a part of the energy is radiated without being fully utilized, opening the certain possibility for better energy utilisation in, e.g., activation of extrinsic peroxocompounds.

This thesis provides data about the impact of peroxocompounds on the oxidation efficiency of PCD for selected water pollutants to improve energy efficiency. The degradation of pharmaceuticals, including the anti-diabetic metformin, the analgesic tramadol, and the antibiotic vancomycin, was described for the process chemistry. The imidazolium-based ionic liquid, 1-ethyl-3-methylimidazolium chloride, 1-octyl-3-methylimidazolium chloride, and 1-ethyl-3-methylimidazolium bromide were also studied for oxidation in PCD accompanied with the extrinsic oxidant additions. The choice of the pollutants as the study subjects was dictated by their omnipresent character, as metformin and tramadol. Vancomycin represents one of the most potent antibiotics in the world, the release of which into the environment may contribute to the development of antibiotic-resistant bacteria. Imidazolium-based liquids, the novel compounds known for their exceptional properties and promising applications, exhibit potential persistence in the environment and toxicity to aquatic organisms. The current thesis addresses a gap in knowledge in the degradation of target pollutants using non-thermal plasma technology.

The thesis provides an overview of ROS present in plasma and possible activation pathways of peroxocompounds in PCD. Impacts of basic operating parameters including pH and pulse repetition frequency on the degradation of target pollutants in unassisted PCD treatment were evaluated. The effects of peroxydisulfate, peroxymonosulfate, and hydrogen peroxide in combination with PCD on degradation were disclosed. The results were compared with conventional UV-based treatment combined with peroxocompounds under the same conditions performed in parallel with the PCD experiments for chemistry and energy efficiency.

The knowledge gained in this doctoral research contributes to the further development of non-thermal plasma technology, particularly pulsed corona discharge oxidation, and the promotion of its application as an energy-efficient method for the degradation of persistent micropollutants in water treatment. By exploring the impact of various peroxocompounds on PCD's oxidation efficiency, this study provides valuable insights for enhancing the degradation of micropollutants.

Abbreviations

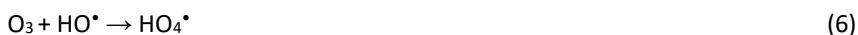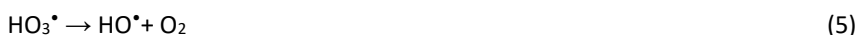|	
ACN	Acetonitrile
AOPs	Advanced oxidation processes
BDD	Boron doped diamond
DBD	Dielectric barrier discharge
EtOH	Ethanol
HP	Hydrogen peroxide
HPLC	High-performance liquid chromatography
ILs	Ionic liquids
MS	Mass spectrometer
MTF	Metformin
NTP	Non-thermal plasma
PCD	Pulsed corona discharge
PDA	Photo diode array
PDS	Peroxydisulfate
pps	Pulse per second
PMS	Peroxymonosulfate
ROS	Reactive oxygen species
TOC	Total organic carbon
TMD	Tramadol
t-BuOH	$tert$-Butanol
UV	Ultraviolet
VMN	Vancomycin
VUV	Vacuum ultraviolet
WWTPs	Wastewater treatment plants
ZVI	Zero-valent iron
[Emim][Br]	1-ethyl-3-methylimidazoilum bromide
[Emim][Cl]	1-ethyl-3-methylimidazoilum chloride
[Omim][Cl]	1-methyl-3-octylimidazolium chloride

1 Literature review

1.1 Advanced oxidation processes

Advanced oxidation processes (AOPs) are being actively investigated as a means of water treatment efficiency improvement towards recalcitrant compounds. AOPs are processes based on the *in situ* generation and use of strong oxidants like hydroxyl radicals (HO$^\bullet$), sulfate radicals (SO$_4^{\bullet-}$), or chlorine radicals (Cl$^\bullet$). Among these, the hydroxyl radical is the preferred one due to its non-selectivity, reactivity, and safety. Established AOPs include ozone-based processes (O$_3$/H$_2$O$_2$, O$_3$/UV), UV-based combinations such as UV/H$_2$O$_2$, UV/Cl$_2$, Fenton (Fe^{2+}/H$_2$O$_2$) and photo-Fenton processes (Miklos et al., 2018). Emerging AOPs are persulfate-based processes, electrochemical oxidation, non-thermal plasma (NTP), ultrasound, and microwave-based oxidation processes (Priyadarshini et al., 2022). Among them, persulfate and plasma-based processes show the greatest potential (Wang & Wang, 2018; Priyadarshini et al., 2022).

1.1.1 Ozonation and ozone-based AOPs

Ozone has been widely used in water treatment for disinfection since the late 19th century. Due to the highest standard redox potential (E^o=2.07 V) among conventional oxidants (chlorine, chlorine dioxide, permanganate and hydrogen peroxide (HP)), ozone can easily deactivate microorganisms and oxidize a wide range of organic compounds in direct reaction (Lukes et al., 2012; Lim et al., 2022). The direct reaction, however, occurs mostly under acidic conditions, where ozone attacks specific functional groups in organic molecules. These include unsaturated bonds and aromatic rings with substituents such as hydroxyl, methyl or amino groups. Ozone reacts mainly through 1,3-dipolar cycloaddition and electrophilic substitution (Lukes et al., 2012), being thus considered as a selective oxidant. However, ozone in its reactions with aqueous organic compounds, decomposes producing hydroxyl radicals, which are unselective and highly reactive with standard redox potential up to E^o = 2.70 V (Wardman, 1989; Miklos et al., 2018). Ozonation is thus considered an AOP under alkaline conditions (pH > 8.5), where ozone tends to degrade generating hydroxyl radicals (Sonntag & Gunten, 2012). Ozone is decomposed in chain reactions involving two main steps: chain initiation and chain propagation. At the slow initiation step, hydroperoxide ion (HO$_2^-$) and superoxide anion-radical O$_2^{\bullet-}$ are formed by the reaction between ozone and hydroxide ion (HO$^-$) (Eq. 1). Ozone reacts with hydroperoxide ion to form ozonide anion-radical O$_3^{\bullet-}$ and HO$_2^{\bullet-}$(Eq. 2). Then, in the fast propagation step, ozone reacts with O$_2^{\bullet-}$ and produce ozonide anion-radical O$_3^{\bullet-}$ (Eq. 3). Formed hydrogen trioxy-radical (HO$_3^\bullet$) (Eq. 4) is converted to HO$^\bullet$ (Eq. 5). The hydroxyl radical can react with O$_3$ to form HO$_4^\bullet$ (Eq. 6) followed by its decomposition of HO$_4^\bullet$ to HO$_2^\bullet$ (Eq. 7). The final step is a termination that involves recombination of HO$^\bullet$ with other reactive species (Umar et al., 2013).

$$O_3 + HO^- \rightarrow HO_2^- + O_2^{\bullet-} \tag{1}$$

$$O_3 + HO_2^- \rightarrow HO_2^{\bullet-} + O_3^{\bullet-} \tag{2}$$

$$O_3 + O_2^{\bullet-} \rightarrow O_3^{\bullet-} + O_2 \tag{3}$$

$$O_3^{\bullet-} + H^+ \rightarrow HO_3^\bullet \tag{4}$$

$$HO_3^\bullet \rightarrow HO^\bullet + O_2 \tag{5}$$

$$O_3 + HO^\bullet \rightarrow HO_4^\bullet \tag{6}$$

$$HO_4^\bullet \rightarrow HO_2^\bullet + O_2 \tag{7}$$

Ozone-based AOPs include ozonation at alkaline pH, in O_3/H_2O_2, O_3/UV, and O_3/catalyst combinations, where oxidation of organic compounds with hydroxyl radicals dominates. Increasing the pH influences also on dissociation of organic compounds, which can significantly change their reaction rate with ozone molecules or hydroxyl radicals (Miklos et al., 2018).

The most convenient AOP is the combination of hydrogen peroxide with ozone also called peroxone process. It improves the oxidation of organic substances by forming hydroxyl radicals from hydrogen peroxide. However, the direct reaction of ozone with HP is very slow ($k < 0.01$ M^{-1} s^{-1}), while the reaction rate of ozone with hydroperoxide ion is much faster ($k = 9.6 \times 10^6$ M^{-1} s^{-1}). The first introduced mechanism of $HO^\bullet$ formation (Staehelin & Holgné, 1982) in practice showed only 50% efficiency of its stoichiometry (Sonntag & Gunten, 2012). Another formation mechanism was proposed as starting with the formation of an adduct (Eq. 8) (Sonntag & Gunten, 2012):

$$HO_2^- + O_3 \rightarrow HO_5^- \tag{8}$$

Decomposition of the adduct takes place in two reactions (Eqs. 9–10), which have, possibly, similar constant rates:

$$HO_5^- \rightarrow HO_2^\bullet + O_3^{\bullet-} \tag{9}$$
$$HO_5^- \rightarrow 2O_2 + HO^- \tag{10}$$

The ozonide radical $O_3^{\bullet-}$ rapidly reaches the equilibrium with O_2 and $O^{\bullet-}$ and the latter is in equilibrium with $HO^\bullet$ in water (Eqs. 11–12). However, hydroxyl radical does not react with O_2, shifting the balance to the formation of $HO^\bullet$ and O_2.

$$O_3^{\bullet-} \rightleftarrows O_2 + O^{\bullet-} \tag{11}$$
$$O^{\bullet-} + H_2O \rightleftarrows HO^- + HO^\bullet \tag{12}$$

Hydrogen peroxide also plays an important role in O_3/UV process. During photolysis of ozone, it is decomposed to oxygen atoms in their excited state $O(^1D)$ and O_2 molecule (Eq. 13). Singlet oxygen atoms react with water forming "hot" H_2O_2 (Eq. 14), which may be cooled down in water or fragmented due to excess energy. The majority of the $O(^1D)$ atoms are transformed to HP due to the solvent-cage effect described earlier (Sonntag & Gunten, 2012; Miklos et al., 2018), thus providing the peroxone process also in the O_3/UV combination.

$$O_3 + h\nu \rightarrow O_2 + O(^1D) \tag{13}$$
$$O(^1D) + H_2O \rightarrow H_2O_2(hot) \tag{14}$$

O_3/catalyst combinations use homogeneous or heterogeneous catalysts in an attempt to reduce ozone consumption and costs. Heterogeneous catalysts such as transition metal oxides (TiO_2, NiO, MnO_2) accelerate aqueous ozone decomposition with the production of $HO^\bullet$ in complex multiphase mechanisms. In addition to water pH, the efficiency of catalysis depends on various factors – physical properties include the catalyst surface area, porosity, pore size and volume, and chemical properties include the catalyst's chemical stability and the surface density of active surface sites for catalytic reactions. Homogeneous catalysts include metal ions such as Fe^{2+}, Zn^{2+}, Mn^{2+}, and Co^{2+}, which have a certain positive effect on ozonation, accelerating ozone decomposition and the production of $HO^\bullet$ (Kasprzyk-Hordern et al., 2003; Sonntag & Gunten, 2012; Miklos et al., 2018). The reaction rate varies with the character of the catalyst, for example, Fe^{2+} and Mn^{2+} exhibit the second-order reaction rate constants k as big as 8.5×10^5 and

1.3×10^3 M^{-1} s^{-1}, respectively. The production of HO$^\bullet$ can also be inhibited in various ways (Sonntag & Gunten, 2012; Miklos et al., 2018). It is considered, according to the practical application (Legager et al., 1992), that ozone reacts with Fe^{2+} by an O-transfer (Eq. 15). Formed FeO^{2+} is highly reactive and participates in HO$^\bullet$ production from water (Eq. 16), although the reaction with Fe^{2+} is more favourable (Eq. 17) (Jacobsen et al., 1997).

$$Fe^{2+} + O_3 \rightarrow FeO^{2+} + O_2 \qquad k = 8.5 \times 10^5 \text{ M}^{-1}\text{s}^{-1} \qquad (15)$$
$$FeO^{2+} + H_2O \rightarrow Fe^{3+} + HO^\bullet + HO^- \qquad k = 1.3 \times 10^{-2} \text{ M}^{-1}\text{s}^{-1} \qquad (16)$$
$$FeO^{2+} + Fe^{2+} + 2H^+ \rightarrow 2Fe^{3+} + H_2O \qquad k = 7.2 \times 10^4 \text{ M}^{-1}\text{s}^{-1} \qquad (17)$$

In recent years, the combination of ozone with peroxymonosulfate (PMS) has gained attention (Deniere et al., 2018; Shao et al., 2019). In the reaction of PMS ions with ozone, sulfate and hydroxyl radicals can be formed accelerating the oxidation of pollutants. The reaction proceeds likely through the formation of an adduct $^-O_3SO_5^-$ (Eq. 18), which decomposes to $SO_5^{\bullet-}$and $O_3^{\bullet-}$ (Eq. 19). The former produces $SO_4^{\bullet-}$ (Eqs. 20–21), HO$^\bullet$ (Eqs. 11–12), and non-reactive species (Eq. 23) (Yang et al., 2015).

$$^-O_3SOO^- + O_3 \rightarrow {}^-O_3SO_5^- \qquad k = 2.1 \times 10^4 \text{ M}^{-1}\text{s}^{-1} \qquad (18)$$
$$^-O_3SO_5^- \rightarrow SO_5^{\bullet-} + O_3^{\bullet-} \qquad\qquad (19)$$
$$SO_5^{\bullet-} + O_3 \rightarrow SO_4^{\bullet-} + 2O_2 \qquad k = 1.6 \times 10^5 \text{ M}^{-1}\text{s}^{-1} \qquad (20)$$
$$2SO_5^{\bullet-} \rightarrow 2SO_4^{\bullet-} + O_2 \qquad k = 2.1 \times 10^8 \text{ M}^{-1}\text{s}^{-1} \qquad (21)$$
$$2SO_5^{\bullet-} \rightarrow S_2O_8^{2-} + O_2 \qquad k = 2.2 \times 10^8 \text{ M}^{-1}\text{s}^{-1} \qquad (22)$$
$$^-O_3SO_5^- \rightarrow SO_4^{2-} + 2O_2 \qquad\qquad (23)$$

1.1.2 Ozone generation and non-thermal plasma technology

Ozone in its conventional application is typically generated remotely on site with the ozone-containing gas transported to water. Nowadays, ozone generators work using non-thermal dielectric barrier discharge at an energy requirement of about 15 kWh per kg of O_3 (Sonntag & Gunten, 2012). High-energy electrons driven by an electric field transfer their energy to surrounding atoms depending on the gas composition, which leads to excited atomic and molecular states of oxygen or nitrogen. Thus, excited states of oxygen dissociate to atomic oxygen (Eq. 24), which participates in a three-body reaction with oxygen and M (O_2, O_3, O$^\bullet$, or in the case of air, N_2) (Eq. 25) (Locke et al., 2012; Sonntag & Gunten, 2012).

$$O_2 + e^- \rightarrow 2O^\bullet + e^- \qquad\qquad (24)$$
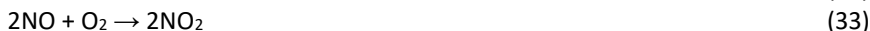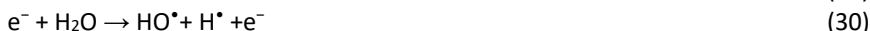$$O^\bullet + O_2 + M \rightarrow O_3 + M \qquad\qquad (25)$$
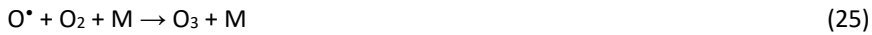
However, pure and dry oxygen is needed to achieve a high concentration of ozone (8–16%) (Sonntag & Gunten, 2012). The presence of water vapours negatively affects the yield of ozone due to the formation of hydroxyl radicals (Eq. 26) reacting with ozone in the gas phase (Eq. 27) (Sehested et al., 1984).

$$e^- + H_2O \rightarrow HO^\bullet + H^\bullet + e^- \qquad\qquad (26)$$
$$O_3 + HO^\bullet \rightarrow HO_2^\bullet + O_2 \qquad k = 4.1 \times 10^7 \text{ M}^{-1}\text{s}^{-1} \qquad (27)$$

Although hydroxyl radicals are unwanted in ozone production, they may be used effectively when applied directly to the aqueous pollutant. For this purpose, various electric discharge or non-thermal plasma technologies are being developed to be operated at atmospheric pressure and room temperature (Nijdam et al., 2012; Kyere-Yeboah et al., 2023; Yusuf et al., 2023). In addition to ozone and hydroxyl radicals (Eqs. 24–26)

electrical discharges produce a variety of oxidant species (Eqs. 28–31). The presence of nitrogen also induces the formation of nitrogen oxides (Eqs. 32–35) (Malik et al., 2001; Lukes et al., 2012; Chu, 2013; Kyere-Yeboah et al., 2023).

$$O_2 + e^- \rightarrow O^+ + O^\bullet + 2e^- \tag{28}$$
$$e^- + 2H_2O \rightarrow H_2O_2 + H_2 + e^- \tag{29}$$
$$e^- + H_2O \rightarrow HO^\bullet + H^\bullet + e^- \tag{30}$$
$$e^- + N_2 \rightarrow 2N^\bullet + e^- \tag{31}$$
$$N^\bullet + O_2 \rightarrow NO + O^\bullet \tag{32}$$
$$2NO + O_2 \rightarrow 2NO_2 \tag{33}$$
$$NO + O_3 \rightarrow NO_2 + O_2 \tag{34}$$
$$2NO_2(aq) + H_2O \rightarrow NO_2^- + NO_3^- + 2H^+ \tag{35}$$

Non-thermal plasma technologies vary according to the type of electrical discharge and its implementation. The most common discharges are corona and barrier discharge similar to ozone generators. Discharges are separated into two different categories: continuous and pulsed. Unlike continuous discharges, pulsed discharges avoid the formation of spark discharge, having sharp high-voltage pulses producing more reactive oxygen species (ROS) per unit of delivered energy (Malik et al., 2001; Yusuf et al., 2023). Pulses are typically of a nanosecond or microsecond range duration time, allowing the pause between pulses ensuring more efficient utilisation of long-living oxidants, which otherwise are uselessly destroyed by the following pulse.

Dielectric barrier discharge (DBD) reactors for water treatment consist of parallel plates or cylindrical coaxial electrodes divided by a dielectric layer. Typically, an alternating or pulsed high voltage of about 15 kV is applied to the electrodes. The high-voltage electrode creates a high electric field on the dielectric, which leads to ionization of the air gap and formation of the plasma discharge. Barrier discharges work best with an electrode separation of a few millimetres. The aqueous solution can also act as the second electrode in the DBD system (Malik et al., 2001; Li et al., 2020; Ansari et al., 2021). It showed high removal efficiency towards recalcitrant compounds, but some studies reported the pulsed corona discharge being more energy efficient (Malik, 2010; Ajo et al., 2017).

1.2 Pulsed corona discharge

Corona discharge occurs when the discharge propagates from a needle or wire electrode into outer space due to a high electric field around an electrode, but when the streamers reach the low electric field, the discharge is no longer sustained (D'Agostino, 2008). If the electric field exceeds the dielectric strength of the air, air molecules are ionized by electron collisions, resulting in an electron avalanche process that forms streamers (Riba et al., 2018). In the case of pulsed corona discharge (PCD), ultrashort (ns to µs) sharp voltage pulses are applied, making streamers more efficient in the gas ionization, while being limited in travelled distance due to the finite duration of the voltage pulse (Chu, 2013). The practical advantage of the short pulse is in ensuring no transition of corona to the spark. Usually, corona discharge is of two polarities, positive and negative corona according to the polarity of the active, i.e., sharp/corona electrode. Negative corona discharge is larger in volume and produces a greater number of electrons, and, therefore, more ozone (Chen & Davidson, 2003; Briels et al., 2008). However, the positive corona discharge was reported as more energy efficient in producing ozone (Riba et al., 2018). Corona discharge includes various geometries, such as point-to-plane, wire-to-cylinder,

or wire-to-plane ones. Point-to-plane geometry is typical for laboratory scale studies, while wire-to-cylinder and wire-to-plane electrode systems are more practical providing a high volume of stable and homogenous plasma.

When applying NTP technologies for water treatment, achieving a short distance between reactive species formed in the discharge and the target pollutant molecules is crucial. Corona discharge is applied in water with gas bubbling, on the water surface, in air over a thin film of water, and in air in contact with water spray or water showering (Malik, 2010; Kyere-Yeboah et al., 2023). Those exploiting the still water surface or its film face the problem of low energy efficiency or high energy consumption, the configuration of pulsed corona discharge in the air with water spray or water showering is considered the most efficient (Malik et al., 2001; Gerrity et al., 2009; Magureanu et al., 2015). While the formation of aerosol requires additional expenses, the gas-phase PCD with water showering provides higher flow-through capacities. This configuration, however, requires a specific pulse shape eliminating the potential formation of high-temperature spark discharges due to interference of water droplets with high conductivity (Kornev et al., 2017). Water spraying in the form of droplets, jets and films up to a few millimetres in size, provides a sufficient plasma-liquid interface at minor energy required by sprinkling. It was confirmed that compounds reacting rapidly with ozone, such as phenol, are degraded at rather low plasma-liquid contact surfaces (Tikker et al., 2020), while the ozone-resistant compounds benefit from the increased contact surface for ROS formed at the plasma-liquid interface. In PCD reactors with water sprinkling, the plasma-liquid contact surface depends on the flow rate of water: the higher is flow rate the higher is surface area (Tikker et al., 2020).

The PCD application acts on pollutants by hydroxyl radicals, ozone, hydrogen peroxide and other reactive species like e^{-*}, $O^{\bullet}$, $H^{\bullet}$, $N^{\bullet}$, and $NO^{\bullet}$. Above mentioned combinations like O_3/H_2O_2 and O_3/Fe^{2+} are also present to some extent in the process which might also generate hydroxyl radicals depending on the condition of treated water. Besides, the plasma glow emits in the near-UV wavelength range, potentially activating hydrogen peroxide and producing additional hydroxyl radicals (Eq. 36). By all means, the energy dose determines the amount of generated ROS and is regulated by variation of pulse repetition frequency (Preis et al., 2013).

$$H_2O_2 + h\nu \rightarrow 2HO^{\bullet} \tag{36}$$
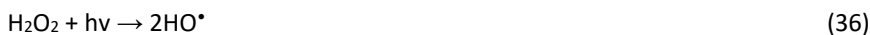
As described in earlier publications, besides the electric discharge parameters, there are several ways to enhance the pollutants removal efficiency in NTP reactors, e.g., treatment in specific conditions – the discharge atmosphere, water conductivity and pH, the use of catalysts, such as activated carbon, TiO_2, MnO_2, Fe^{2+}, and combinations with other AOPs and extrinsic oxidants (Jiang et al., 2014; Ansari et al., 2021; Kyere-Yeboah et al., 2023; Yusuf et al., 2023). Amongst them, the use of persulfates gained attention, being actively studied for applications in various oxidation processes including NTP (Wang & Wang, 2018; Lee et al., 2020; Guo et al., 2023).
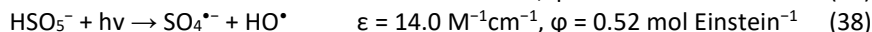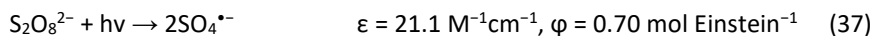
1.3 Persulfate-based AOPs

Persulfate-based AOPs employ highly reactive sulfate radicals to abate organic pollutants. Different from hydroxyl radical, which is unselective, sulfate radical reacts selectively, mostly through electron transfer, since it has a redox potential of 2.6–3.1 V comparable with the one of hydroxyl radical, but a longer half-life time (30–40 µs) than hydroxyl radical (0.02 µs) (Guerra-Rodríguez et al., 2018; Lee et al., 2020). Sulfate radicals

are obtained from peroxydisulfate (PDS, $S_2O_8^{2-}$) and peroxymonosulfate (PMS, HSO_5^-) ions. While non-radicalized persulfates have high redox potentials of about 2 V, they react poorly with the majority of organic compounds and need activation by transferring to the radical forms (Matzek & Carter, 2016). Formation of sulfate radicals from persulfates occurs by various activation methods including heat, UV, alkaline medium, transition metal ions, electric discharges, etc. (Wang & Wang, 2018; Lee et al., 2020).

1.3.1 UV activation

Activation by UV-light is a type of activation, which inputs radiant energy provoking the fission of O-O bond (Eqs. 37–38). The energy required for the fission of PDS and PMS differs substantially. The asymmetrical HSO_5^- anion has the O-O bond dissociation energy of 377 kJ mol^{-1}, compared to 92 kJ mol^{-1}, for the symmetrical peroxydisulfate anion. This makes breaking the O-O bond in PDS more probable (Shang et al., 2022). Irradiated at neutral pH, PDS decomposes faster: in Eqs. 37–38, illustrating activation of persulfates, ε is the molar extinction coefficient at a wavelength of 254 nm, and φ is the quantum yield of the UV photolysis (Luo et al., 2015). At alkaline pH, however, the HSO_5^- anion dissociates to SO_5^{2-}, having a molar extinction coefficient ε as big as 149.5 M^{-1}cm^{-1}, thus significantly enhancing its decomposition (Guan et al., 2011).

$$S_2O_8^{2-} + h\nu \rightarrow 2SO_4^{\bullet -} \qquad \varepsilon = 21.1 \text{ M}^{-1}\text{cm}^{-1}, \varphi = 0.70 \text{ mol Einstein}^{-1} \quad (37)$$
$$HSO_5^- + h\nu \rightarrow SO_4^{\bullet -} + HO^{\bullet} \qquad \varepsilon = 14.0 \text{ M}^{-1}\text{cm}^{-1}, \varphi = 0.52 \text{ mol Einstein}^{-1} \quad (38)$$

Application of submerged UV sources to the treated water is complicated by the sediments formed at the surface of lamps thus requiring continuous sophisticated cleaning of their surfaces. Replacement of burnt-out lamps also presents a substantial article of expense thus making UV activation rather expensive.
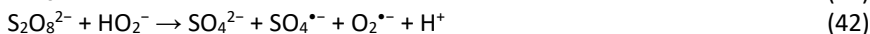
1.3.2 Thermal activation

Heat activation is technically simple requiring no addition of chemicals. However, high energy consumption makes it inapplicable for large-scale water supply or wastewater treatment. This approach may still find its application in, e.g., *in situ* thermal remediation of soil (Ji et al., 2015). Similar to UV, thermal activation produces sulfate radicals (Eq. 39), which react fast with water at high temperatures forming hydroxyl radicals (Eq. 40) (Wang & Wang, 2018).

$$S_2O_8^{2-} + heat \rightarrow 2SO_4^{\bullet -} \qquad\qquad\qquad\qquad\qquad\qquad\qquad (39)$$
$$SO_4^{\bullet -} + H_2O \rightarrow HO^{\bullet} + SO_4^{2-} + H^+ \qquad\qquad\qquad\qquad\qquad (40)$$

1.3.3 Alkaline activation

Activation of PDS and PMS in alkaline media has been considered to be effective in the degradation of organic contaminants. Several issues need to be addressed in this approach: alkaline activation requires pH adjustment as high as 11–12 by using relatively expensive sodium or potassium hydroxide additions (Matzek & Carter, 2016).

For alkaline activation of PDS, a nucleophilic attack of hydroperoxide anion on the O-O bond is likely to be the main activation mechanism (Eqs. 41–43) (Wang & Wang, 2018). Alkaline activation is also possible for PMS (Eqs. 44–47) (Qi et al., 2016). Recombination of active species takes place with the formation of singlet oxygen and hydrogen peroxide (Eqs. 48–49). It was found that singlet oxygen and superoxide radicals were the main reactive species during the degradation of Acid Orange 7 (Qi et al., 2016).

$$S_2O_8^{2-} + H_2O \rightarrow 2SO_4^{2-} + HO_2^- + H^+ \tag{41}$$
$$S_2O_8^{2-} + HO_2^- \rightarrow SO_4^{2-} + SO_4^{\bullet-} + O_2^{\bullet-} + H^+ \tag{42}$$
$$SO_4^{\bullet-} + HO^- \rightarrow SO_4^{2-} + HO^\bullet \tag{43}$$
$$HSO_5^- \rightarrow SO_5^{2-} + H^+ \tag{44}$$
$$SO_5^{2-} + H_2O \rightarrow H_2O_2 + SO_4^{2-} \tag{45}$$
$$H_2O_2 \rightarrow H^+ + HO_2^- \tag{46}$$
$$HSO_5^- + HO_2^- \rightarrow H_2O + SO_4^{\bullet-} + {}^1O_2 \tag{47}$$
$$HO^\bullet + O_2^{\bullet-} \rightarrow {}^1O_2 + HO^- \tag{48}$$
$$2O_2^{\bullet-} + 2H^+ \rightarrow {}^1O_2 + H_2O_2 \tag{49}$$

1.3.4 Activation by transition metal ions

Transition metal ions and oxides have a potential for activation of persulfates, being classified as homogeneous and heterogeneous catalysts, respectively (Matzek & Carter, 2016). Among homogeneous catalysts, silver and cobalt ions (Eqs. 50-52), interacting with PDS and PMS respectively, provided the highest efficiency in removing pollutants (Anipsitakis & Dionysiou, 2004; Hu & Long, 2016; Wang & Wang, 2018). Other metals are actively studied to replace expensive silver: relatively non-toxic iron is a cost-effective reagent (Eq. 53) (Matzek & Carter, 2016).

$$S_2O_8^{2-} + M^{n+} \rightarrow SO_4^{2-} + SO_4^{\bullet-} + M^{[n+1]+} \tag{50}$$
$$Co^{2+} + HSO_5^- \rightarrow Co^{3+} + SO_5^{\bullet-} + H^+ \tag{51}$$
$$2SO_5^{\bullet-} \rightarrow 2SO_4^{\bullet-} + O_2 \tag{52}$$
$$S_2O_8^{2-} + Fe^{2+} \rightarrow SO_4^{2-} + SO_4^{\bullet-} + Fe^{3+} \tag{53}$$

In homogeneous systems metal ions react freely, and mass transfer is not a limiting factor. However, the metal ions create a problem of secondary pollution, requiring their recovery from treated water. This makes heterogeneous catalysts better controllable over the processes overcoming the limitations of homogeneous catalysts, although with somewhat reduced efficiency (Wang & Wang, 2018). Heterogeneous catalysts, in turn, are not completely free from the secondary pollution problem. Similarly, zero-valent iron (ZVI) showing catalytic properties slowly releases iron ions in acidic solutions (Eq. 54):

$$Fe^0 \rightarrow Fe^{2+} + 2e^- \tag{54}$$

1.3.5 Non-thermal plasma

In recent years, there has been a growing interest towards the NTP activation of persulfates. This is approached from the consideration, that during the plasma treatment, some of its effects remain unused, e.g., radiation or short-living reactive species, which results in certain energy waste. It is presumed, that various active species formed in plasma may be used for the activation of persulfates resulting in secondary longer-living reactive species with strong oxidation potential (Guo et al., 2023). Possibly, the activation of persulfates takes place by solvated electrons and active species diffused into water. Thus, in water radiolysis experiments, solvated electrons (e_{aq}^-) react rapidly with PDS and PMS (Eqs. 55–56) (Neta et al., 1977; Shang et al., 2022).

$$S_2O_8^{2-} + e_{aq}^- \rightarrow SO_4^{2-} + SO_4^{\bullet-} \qquad k = 1.1 \times 10^{10}\ M^{-1}\ s^{-1} \tag{55}$$
$$HSO_5^- + e_{aq}^- \rightarrow HO^- + SO_4^{\bullet-}/SO_4^{2-} + HO^\bullet \quad k = 8.4 \times 10^9\ M^{-1}\ s^{-1} \tag{56}$$

The activation by other reactive species is also possible, although at a considerably lower reaction rate (Eqs. 57–59) (Shang et al., 2019).

$$S_2O_8^{2-} + HO^{\bullet} \rightarrow SO_4^{\bullet-} + HSO_4^- + \tfrac{1}{2}O_2 \qquad k = 8.0 \times 10^4 \; M^{-1} \; s^{-1} \qquad (57)$$
$$S_2O_8^{2-} + H^{\bullet} \rightarrow SO_4^{\bullet-} + SO_4^{2-} + H^+ \qquad k = 2.5 \times 10^7 \; M^{-1} \; s^{-1} \qquad (58)$$
$$S_2O_8^{2-} + O_2^{\bullet-} \rightarrow SO_4^{\bullet-} + SO_4^- + O_2 \qquad k = 2.4 \times 10^3 \; M^{-1} \; s^{-1} \qquad (59)$$

Certain role in NTP activation may also be played by the plasma glow of UV light, ozone, hydrogen peroxide, alkali, and metal ions (Shang et al., 2022; Guo et al., 2023).

1.4 Emerging contaminants and water treatment

The emerging problem of micropollutants is a major concern for the sustainability of water resources, including the challenges of modern water treatment and its increasing costs (Luo et al., 2014; Margot et al., 2015; Patel et al., 2019). Due to inefficient removal of micropollutants at conventional wastewater treatment plants, they are discharged into the environment where accumulate and pose a threat to aquatic life and ecosystems (Wang et al., 2018; Kanaujiya et al., 2019). In addition, micropollutants present a challenge in any attempt to recycle or reuse treated wastewater (Xu et al., 2020). Micropollutants include pharmaceuticals, illicit drugs, perfluorinated compounds, nanomaterials, bactericides, hormones, flame-retardants, disinfection by-products, algal toxins, prions, ionic liquids, etc. (Richardson & Kimura, 2017). Only a small fraction of them have been studied in terms of their impact on human health and the environment.

1.4.1 Pharmaceuticals

The development of the pharmaceutical industry has saved millions of lives, increased life expectancy and contributed to population growth. However, a growing population requires more pharmaceuticals to be produced, not only for human healthcare but also for animal husbandry to provide food for mankind. Amongst pharmaceuticals, analgesics, anti-diabetics and antibiotics are of great importance, i.e., massive production and usage.

Pharmaceuticals include a wide range of chemicals that have different chemical, physical and structural properties. Pharmaceuticals can be classified according to their structure, mechanism or mode of action, and therapeutic perspective. The most known classes are antibiotics, anti-inflammatory drugs, analgesics, opioids, antidepressants, and steroids. Out of 713 compounds tested in 71 countries, 631 pharmaceuticals were found to be present in the environment above analytical detection limits (aus der Beek et al., 2016). Concentrations of pharmaceuticals appeared to follow the descending order industrial effluents > hospital effluents > wastewater treatment plant effluents > surface water > groundwater > drinking water (Patel et al., 2019).

According to data presented at the Estonian Water Works Association seminar, the pharmaceuticals most often found in Estonia's environment are metformin (MTF) and tramadol (TMD) which were observed in 89% and 98% of surface water samples, respectively. One should note, however, that metformin consumption comprises about 25,000 kg per year, whereas tramadol is consumed in the amount of only 600 kg per year (Eesti Vee-ettevõtete Liit, 2019), nominating TMD as persistent, and MTF – pseudo-persistent compound.

The resistance of bacteria towards antibiotics shows a sustainable growth reflected in research reports. In Estonia, vancomycin resistance in outpatient clinics increased from

5.8% in 2017 to 7.2% in 2021 (ECDC, 2023). Meanwhile, across the EU/EEA countries, *Enterococcus faecium* resistance to vancomycin rose from 10.4% in 2014 to 17.6% in 2022 (ECDC, 2023).

1.4.1.1 Metformin

Metformin (3-(diaminomethylidene)-1,1-dimethylguanidine) is a drug that is used for 2-class diabetes treatment, improving the sensitivity of cells to insulin and increasing the ability of cells to uptake glucose. It decreases glucose production in the liver and reduces the intestinal absorption of glucose. Metformin hydrochloride has become one of the most prescribed drugs in the World (Briones et al., 2016). A total of 463 million people are estimated to have diabetes, of which approximately 90% with the 2-class disease (Saeedi et al., 2019). The number of people suffering from diabetes will rise to 700 million by 2045, by severe increase in developing countries in Asia. Together with the growth of the number of people with diabetes, also the amount of consumed metformin will increase leading to environmental pollution, especially in developing countries. Recent studies showed that MTF can inhibit the growth, survival, and metastasis of certain types of tumour cells including those of breast, liver, bone, pancreas, endometrial, colorectal, kidney, and lung cancers (Morales & Morris, 2015; Podhorecka et al., 2017; Lv & Guo, 2020). Furthermore, there is evidence of metformin having beneficial effects on obesity, and liver, cardiovascular, age-related and renal diseases, thus finally decreasing the death risk (Lv & Guo, 2020). Based on new possibilities, one can assume that MTF consumption may skyrocket in the near future resulting in growing pressure on the environment since wastewater treatment plants (WWTPs) insufficiently remove MTF (Golovko et al., 2021).

Metformin is not metabolized in the human body, being excreted and, therefore, released into the environment in its original form (Briones et al., 2016). It is a water-soluble and polar compound, with the partition coefficient log K_{OW} of −4.90 suggesting high solubility in the aqueous phase. Metformin is the most frequent pharmaceutical found in surface water worldwide (Briones et al., 2016). The concentration of MTF in surface waters depends on the respective wastewater burden of an aquatic system and is typically in the range of about 1 µg L^{-1} (Scheurer et al., 2012; Blair et al., 2013; Briones et al., 2016). In the influent of WWTPs, the MTF concentration is found up to 100 µg L^{-1} (Scheurer et al., 2012). For example, the median value of three WWTPs in Germany was found as big as 112 µg L^{-1} (Briones et al., 2016). The median and average MTF removal efficiencies at 84 conventional WWTPs comprised 94% and 79%, respectively (Straub et al., 2019).

According to cytotoxicity testing, MTF has no toxic effect at its highest concentration of 414.05 mg L^{-1} (Caminada et al., 2006). The half-maximum effective concentration (EC$_{50}$) for *Daphnia magna* was found at 60 mg L^{-1} in 48 h (Hanisch & Abbas, 2004). Metformin showed acute toxicity to *Aliivibrio fischeri* at EC$_{10}$ of 871 mg L^{-1} in 30 min suggesting that it is not a toxic compound (Jacob et al., 2020). Despite the low acute toxicity of MTF, aquatic life as fishes or mussels exposed to MTF suffers negative consequences. For example, a study by Niemuth & Klaper (2018) showed that MTF has endocrine-disrupting effects on fish *Pimephales promelas* at 40 µg L^{-1} in one year of exposure. Previously, they found that MTF causes changes in vitellogenin (a yolk protein used as a specific biomarker of estrogenic activity) synthesis at environmentally relevant concentrations. According to the review made by Elizalde-Velázquez & Gómez-Oliván (2020), metformin and guanylurea have a variety of effects on aquatic organisms concluding that those compounds are toxic to non-target organisms.

High efficiency of MTF removal was shown by UV/H_2O_2 (Maćerak et al., 2018), UV/Fe^{2+} (Aseman-Bashiz & Sayyaf, 2020), UV/PMS (Karimian et al., 2020), UV/TiO_2 (Chinnaiyan et al., 2019), UV/TiO_2-ZrO_2 (Carbuloni et al., 2020), electro-Fenton system (Orata et al., 2019), and electrochemically activated PDS (Aseman-Bashiz & Sayyaf, 2020). Other methods of MTF oxidation, operation conditions and application results are shortly described in Table 1.

Table 1. Metformin degradation by AOPs

Type	Water matrix	Initial conc.	Combination	Time	Degradation	Total organic carbon (TOC) removal	Source
UV-based	Ultrapure water	2 µM	$UVC/H_2O_2/Fe^{2+}$	60 min	<24.0%	-	Neamţu et al., 2014
UV-based	Ultrapure water	10 mg L^{-1}	UVC/TiO_2	30 min	31.0%	-	Quintão et al., 2016
UV-based	Deionized water	10 mg L^{-1}	UV/H_2O_2	180 min	100.0%	99.0%	Maćerak et al., 2018
UV-based	Distilled water	50 mg L^{-1}	Vacuum-UV(VUV), 5.7 W	60 min	87.5%	57.1%	Karimian et al., 2020
			VUV/Fe^{2+}	30 min	86.1%	55.0%	
			VUV/PMS	30 min	89.7%	58.6%	
			$VUV/Fe^{2+}/PMS$	60 min	99.0%	70.3%	
			UV/PMS	30 min	34.9%	4.0%	
Electro-Fenton	Distilled water	0.2 mM	H_2O_2/Fe^{2+}, 300 mA	30 min	99.6%	-	Orata et al., 2019
Electro-activation	Distilled water	15 mg L^{-1}	Pyrite/PDS, 50 mA	60 min	89.0%	68.4%	Aseman-Bashiz & Sayyaf, 2020
			Nano-Fe$_3$O$_4$/PDS, 40 mA	60 min	76.9%	55–57%	
UV-based	Synthetic water	10 mg L^{-1}	UVA/TiO_2	150 min	92.6%	-	Chinnaiyan et al., 2019
		50 mg L^{-1}	UVA/TiO_2	150 min	69.1%	-	
UV-based	Deionized water	1 mg L^{-1}	UVB/Polymer	60 min	99.0%	-	Kumar et al., 2021
UV-based	-	10 mg L^{-1}	$UVA/TiO_2–ZrO_2$	30 min	50–60%	-	Carbuloni et al., 2020
Ozonation	Tap water	1 µg L^{-1}	O_3	60 min	45–50%	-	Scheurer et al., 2012

1.4.1.2 Tramadol

Tramadol (2-(dimethylamino)-methyl)-1-(3'-methoxyphenyl) cyclohexanolhydro chloride) is an opioid analgesic used to treat moderate to severe acute or chronic pain. Even though TMD is a weak opioid, it is used as a drug of abuse at supra-therapeutic doses. It has the advantage of less respiratory depression or risk of addiction compared to strong opioids (Miotto et al., 2017). Worldwide consumption of medical tramadol increased from 290 tons in 2006 to 424 tons in 2012 (Radbruch et al., 2013), inducing, however, cytotoxic and genotoxic effects (Antonopoulou & Konstantinou, 2016). Despite its low consumption, TMD is one of the most frequently detected compounds in concentrations ranging from ng L^{-1} to µg L^{-1} (Kostanjevecki et al., 2019; Golovko et al., 2021). Tramadol poorly degrades at WWTPs reaching only 40% removal (Lindim et al., 2016), having adverse effects on aquatic life (Sehonova et al., 2016; Ložek et al., 2019; Bachour et al., 2020; Plhalova et al., 2020). Effective degradation of TMD was achieved by photocatalysis (Antonopoulou et al., 2016; Majhi et al., 2019), Fenton process (Mackuľak et al., 2015), electro-Fenton system (Monteil et al., 2020), and electro-chemical oxidation (Ghalwa et al., 2014; Lütke Eversloh et al., 2015) (Table 2).

1.4.1.3 Vancomycin

Vancomycin (VMN) is an amphoteric glycopeptide antibiotic used to treat infections caused by Gram-positive organisms (Gotvajn et al., 2021). This antibiotic and its modifications are considered drugs of last resort, i.e., the World's last line of defence against resistant pathogens, making these of extreme importance from the environmental point of view due to the emergence and spread of antimicrobial resistance in bacteria (Okano et al., 2017; Azuma et al., 2024). Vancomycin was detected in French rivers in concentrations reaching up to 90 ng L^{-1} (Tuc Dinh et al., 2011), and in the effluents of the wastewater treatment plants of Milan and Varese, Italy, as high as 17.4 ± 1.7 ng L^{-1} and 24.4 ± 31 ng L^{-1}, respectively (Zuccato et al., 2010). Limited data is available for VMN removal from water: in recent years, a few studies demonstrated the application of AOPs to VMN removal such as ZVI-Fenton (Furia et al., 2021), and photocatalytic oxidation TiO_2/UV (Dehghani et al., 2022).

Table 2. Tramadol degradation by AOPs

Type	Water matrix	Initial conc.	Combination	Time	Degradation	TOC removal	Source
UV-based	Ultrapure water	10 mg L^{-1}	UVA, 500 W m^{-2}	240 min	70%	40%	Antonopoulou et al., 2020
UV-based	Deionized water	10 mg L^{-1}	UV/NiS/Bi_2O_3	180 min	94%	91%	Majhi et al., 2019
UV-based	-	10 mg L^{-1}	UVA/TiO_2, 500 W m^{-2}	20 min	95%	80% @4 h	Antonopoulou & Konstantinou, 2016
Anodic oxidation	Distilled water	100 mg L^{-1}	Pb/PbO_2, 1 A cm^{-2}	25 min	90%	-	Ghalwa et al., 2014
Electro-Fenton	Ultrapure water	26.3 mg L^{-1}	Boron doped diamond (BDD)/Fe^{2+}	8 min	100%	100% @6 h	Monteil et al., 2020
Electro-oxidation	Osmosis brine	100 µM	BDD/Pt, 12 A m^{-2}	60 min	99%	-	Lütke Eversloh et al., 2015
Fenton process	Wastewater	600-800 ng L^{-1}	Fe^0/H_2O_2/H_2SO_4	60 min	99%+	-	Mackuľak et al., 2016

1.4.2 Ionic liquids

Ionic liquids (ILs) are an emerging class of compounds, which are also called 'green' chemicals. Classically, they are defined as organic salts with melting points below 100°C, composed of inorganic/organic anions and organic cations. Ionic liquids may potentially become widespread chemicals in the near future due to their exceptional properties, such as low vapour pressure, high thermal and chemical stability, and tunability (Kaur et al., 2022). The latter means that one can change the chemical and physical properties of ILs by altering anions or cations. The search in Scopus for publications issued within the last four years showed about 7,000 articles published on ILs yearly. Although ILs do not evaporate and cannot cause atmospheric pollution, they, being hygroscopic and water-soluble, will inevitably enter the environment via aquatic ways, and may cause adverse environmental effects (Frade & Afonso, 2010). The toxic character of ILs was revealed in recent years: several studies reported bacterial toxicity and slow biodegradability (Garcia et al., 2005; Romero et al., 2008; Jordan & Gathergood, 2015; Cho et al., 2021). The data about the presence of ILs in wastewaters and natural water systems are limited. Available studies suggest that ILs found in effluent water originate from their synthesis and use in industry, providing generally low concentrations of ILs (Mena et al., 2021).

Among ILs, imidazolium-based compounds have gained attention becoming the most studied ones (Plechkova & Seddon, 2008). The toxicity of imidazolium-based ILs is of great concern being mainly attributed to the alkyl chain, the length of which positively correlates with toxicity (Romero et al., 2008; Gomez-Herrero et al., 2020). For example, [Omim][Cl] and [Omim][Br] show acute toxicity to *Vibrio fischeri* (logEC$_{50}$, µM) of 0.94 ± 0.14 and 0.63 ± 0.06, whereas [Emim][Cl] is less toxic with logEC$_{50}$ of 4.02 ± 0.14 (Romero et al., 2008).

According to the review made by Mena et al. (2021), Fenton-based, electrochemical, or photocatalytic AOPs have been actively studied for the degradation of ILs. However, ozone-based and plasma-based AOPs have not yet been studied for the degradation of ionic liquids.

1.5 Objectives of the study

Summing up the literature review, the presence of micropollutants and their potential threat is of great concern. Micropollutants such as pseudo-persistent metformin, persistent and toxic tramadol, potent antibiotic vancomycin, or recalcitrant imidazolium-based ionic liquids require proper treatment technology. Different types of AOPs and their combinations may be applied to degrade micropollutants, while only a few of them might be considered economically feasible. Amongst them, the emerging NTP approach is the most promising technology combining different oxidation species, while conventional UV/PDS and UV/PMS combinations showed a high potential for sulfate radicals. Moreover, the combination of NTP and persulfates is a new path in AOPs development.

Objectives of this study include:
- establishing oxidation efficiency of pharmaceuticals and imidazolium-based ILs oxidation in unassisted PCD treatment at varied operating parameters, pH and pulse repetition frequency;
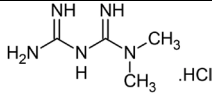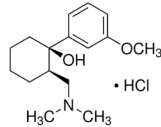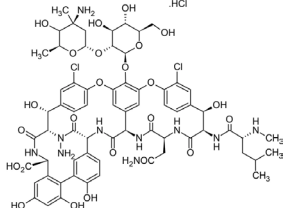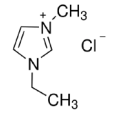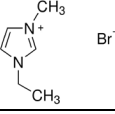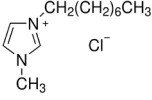
- establishing the dependence of oxidation efficiency of PCD in combinations with extrinsic oxidants on their doses and operation parameters in the degradation of pharmaceuticals and imidazolium-based ILs;
- comparative analysis of assisted PCD treatment and conventional UV-based treatment in oxidation and energy efficiency within the span of operation parameters;
- evaluation of the PCD/oxidant and UV/oxidant methods applicability at their energy efficiencies and oxidant dosing at their current costs.

2 Materials and methods

2.1 Chemicals and materials

Descriptions of target compounds are given in Table 3. 1-Ethyl-3-methylimidazolium chloride and 1-ethyl-3-methylimidazolium bromide were obtained from Arcos Organics. 1-Octyl-3-methylimidazolium and metformin hydrochloride chloride was purchased from Alfa Aesar. Tramadol hydrochloride, vancomycin hydrochloride, sodium persulfate ($Na_2S_2O_8$), potassium peroxymonosulfate (Oxone®, $KHSO_5 \cdot 0.5KHSO_4 \cdot 0.5K_2SO_4$), hydrogen peroxide ($H_2O_2$, PERDROGEN™), ethanol ($C_2H_5OH$, EtOH), and *tert*-butyl alcohol (($CH_3)_3COH$, *t*-BuOH) were obtained from Sigma-Aldrich. Acetonitrile (CH_3CN, ACN, LiChrosolv®) and formic acid (CH_2O_2) were obtained from Merck KGaA. Chemicals were of analytical grade used without further purification.

Table 3. Target compounds

Abbreviation	Compound	Elementary formula	Structure	Molecular mass, g mol^{-1}	pKa
MTF	Metformin hydrochloride	$C_4H_{11}N_5 \cdot HCl$		129.2 165.6 (HCl)	12.4 (Jones et al., 2002)
TMD	Tramadol hydrochloride	$C_{16}H_{25}NO_2 \cdot HCl$		263.4 299.8 (HCl)	9.41 (O'Neil & Britain, 2013)
VMN	Vancomycin hydrochloride	$C_{66}H_{75}Cl_2N_9O_{24} \cdot xHCl$		1485.7	2.9, 7.2, 8.6, 9.6, 10.5, 11.7 (Dodd et al., 2006)
[Emim][Cl]	1-Ethyl-3-methylimidazolium chloride	$C_6H_{11}ClN_2$		111.1 146.6 (Cl$^-$)	-
[Emim][Br]	1-Ethyl-3-methylimidazolium bromide	$C_6H_{11}BrN_2$		111.1 191.1 (Br$^-$)	-
[Omim][Cl]	1-Octyl-3-methylimidazolium chloride	$C_{12}H_{23}ClN_2$		195.3 230.8 (Cl$^-$)	-

2.2 Experimental procedures

2.2.1 Pulsed corona discharge reactors

The PCD experiments were conducted in devices made by Flowrox Oy (Finland) described in (Ajo et al., 2017; Kornev et al., 2017) with characteristics given in Table 4. The device features a PCD stainless steel reactor with a storage tank, pulse generator, and circulation pump (Figure 1). The latter controls the water flow rate by a frequency regulator. Within the plasma reactor, high voltage wire electrodes are positioned horizontally between two grounded vertical parallel plates. The generator administers high-voltage pulses to the electrode system at regulated pulse repetition frequencies. The output-input ratio of the pulse generator stands at 65%. The solution undergoes treatment by being dispersed through a perforated plate positioned above the wire electrodes, at a specific spray density calculated as the flow rate divided by the planar cross-sectional area of the plasma zone. Subsequently, the treated solution is directed back to a storage tank after passing through the plasma zone, from where it is recirculated to the top of the reactor.

Table 4. Characteristics of PCD reactors

Reactor parameters	Value	
	Reactor 1 (Paper I, III)	Reactor 2 (Paper II)
Reactor full volume, L	110	80
Perforated plate size for water distribution, mm	500×30	565×97
Number of perforations	51	24
Diameter of perforations, mm	1	3
Water flow rate, L min^{-1}	2.0–28.5	2.0–18.0
Spray density, m s^{-1}	0.002–0.0243	0.002–0.0177
Plasma zone volume, m^3	0.013	0.011
Contact surface area at flow rate of 1 m^3 h^{-1}, m^{-1}	91.9	130.0
Electrode configuration		
High voltage wire length, m	20	12
Wire diameter, mm	0.5	0.6
Distance between high-voltage electrodes and grounded plates, mm	18	17
Distance between high-voltage electrodes, mm	30	30
Voltage pulse generator's characteristics		
Pulse repetition frequency, pps	50–880	25–800
Output power, W	9.0–123.2	8.0–112.0
Peak voltage, kV	18	22
Peak current, A	380	290
Current pulse duration, ns	100	70
Pulse energy, J	0.14–0.18	0.14–0.16
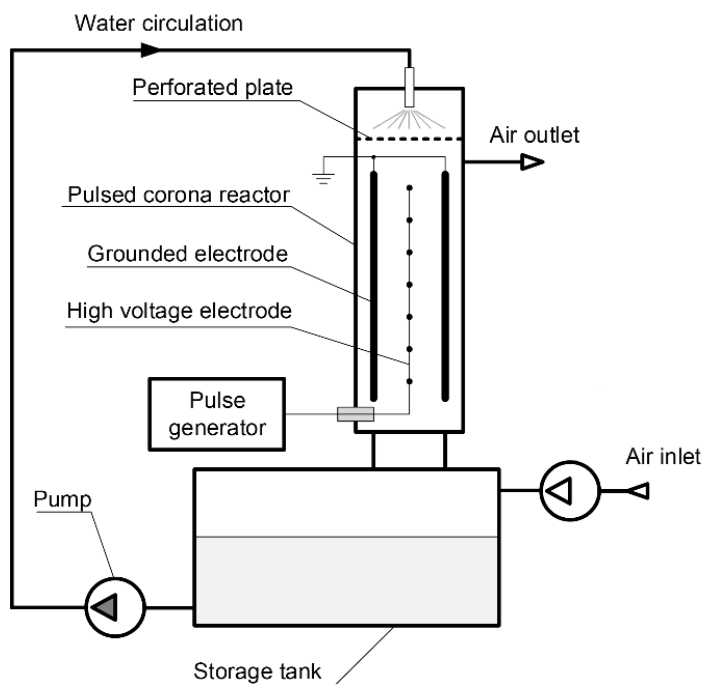
Figure 1. Schematic diagram of PCD reactor

2.2.2 UV reactor

The photochemical experiments in Papers I–III were conducted using a 1-L cylindrical glass reactor in batch mode. Within the reactor, a low-pressure mercury germicidal lamp (11 W, Philips TUV PL-S) was positioned in a quartz sleeve to serve as the UVC source. The input-output power of the lamp is approximately 32%. The incident photon flux at 254 nm was measured by ferrioxalate actinometry and comprised 2.55×10^{-7} Einstein s^{-1}. The lamp was turned on at least 10 min before the trial to provide a constant radiation output. A water-cooling jacket was used to keep the constant temperature in the reactor.

2.2.3 Experimental

Both PCD and UV experiments were performed at an ambient room temperature of $21 \pm 2°C$. Concentrations of target pollutants and oxidants are present in Table 5, including unadjusted pH average values. For acidic (pH 3) or alkaline (pH 11) conditions, pH was regulated by adding 0.1–5.0 M solutions of H_2SO_4 or NaOH. In experiments with oxidants, the oxidation reaction was quenched with ethanol or methanol added at the sample to alcohol volume ratio of 10 for HPLC analysis. For the TOC analysis, sodium sulfite was used at the Na_2SO_3 to oxidant molar ratio of 10 (Paper I, II).

In UV/oxidant trials, a solution with an IL (0.8 L) was prepared in bidistilled water and treated for 2 h with permanent stirring using a magnetic stirrer. After the addition and dissolution of oxidants, the UVC-lamp inserted into the reactor initialized oxidation.

PCD experiments were performed at the water flow rate of 1 m^3 h^{-1}. In Paper III, the pulse repetition frequency was 50, 200, and 880 pulses per second (pps) with the power input of 9.0, 32.0 and 123.2 W, respectively. For Papers I and II, the pulse repetition frequency was 50 pps, and the power input of 9 and 8 W, respectively.

The stock solutions for PCD experiments were prepared in a 100-mL volumetric flask using bidistilled water, followed by dilution to a total volume of 10 L (Paper I and III) or 5 L (Paper II) by distilled water in the reactor tank constantly stirred with the circulation pump. Pre-selected amounts of oxidants were dissolved in a 100-mL volumetric flask and added to the tank immediately before the start of the treatment. For proper sampling, the treated solutions were circulated in the reactor for four minutes after the pulse generator was turned off to equalize the concentrations in the reactor.

Table 5. Concentrations of target pollutants and oxidants

Compound	C_M, µM	C, mg L^{-1}	Unadjusted pH$_{average}$	C_{ox}, µM, (oxidant to pollutant molar ratio)		
				PDS	PMS	HP
MTF	60.4	7.8	6.4 ± 0.8	60.4–604.0 (1, 2.5, 5, 10)	-	-
TMD	33.4	8.8	6.1 ± 0.5	38–380 (1.1, 2.8, 5.5, 11.4)	-	-
VMN	13.5	20.0	6.3 ± 0.4	13.5–135.0 (1, 5, 10)		
[Emim][Cl]	100.0	11.1	6.9 ± 0.7	50–500 (0.5, 1, 2.5, 5)		-
[Emim][Br]	100.0	11.1	6.2 ± 0.8			-
[Omim][Cl]	100.0	19.5	6.0 ± 0.7			-

2.3 Analytical methods

Concentrations of target pollutants were determined using high-performance liquid chromatography combined with a mass spectrometer or a photo array detector (HPLC-MS/HPLC-PDA, Shimadzu LC-MS, 2020) equipped with a Phenomenex Gemini (150 × 2 mm, 1.7 mm) NX-C18 (110 Å, 5 µm) column. Table 6 demonstrates chromatography parameters for each target compound. The analysis was performed using a mobile phase composed of 10% vol. of acetonitrile and 90% vol. of 0.3-% formic acid aqueous solution. Mass spectra were acquired in full-scan (scanning in the range of 50–500 m/z) and SIM (130 (MTF) and 111 ([Emim]$^+$) m/z) modes. The instrument was operated in positive ESI mode, and the results obtained with the MS detector were handled using Shimadzu Lab Solutions software.

Table 6. Parameters of HPLC analysis

Compound	Analysis type	Flow rate, mL min^{-1}	Eluent mixture, ACN:H$_2$O vol. %	Injection volume, µL	SIM, m/z	λ, nm
MTF	HPLC-MS	0.20	10:90	20	130	-
[Emim]$^+$					111	-
TMD	HPLC-PDA	0.20	15:85	40	-	275
VMN		0.25	9:91	75	-	220
[Omim]$^+$		0.20	25:75	60	-	205

Total organic carbon was measured using a TOC analyzer multi N/ C® 3100 (Analytik Jena, Germany) in 20-mL samples with an injection volume of 500 μL for each replicate (Paper I, III). Solution pH was measured using a digital pH/Ion meter (Mettler Toledo S220). Utilisation of persulfate was controlled by the quantification of residual PS concertation in the treated samples spectrophotometrically (Genesys 10 S, Thermo Scientific, USA) at $\lambda = 352$ nm by an excess KI reaction with residual persulfate towards the formation of I_2 (Liang et al., 2008). The residual hydrogen peroxide concentration in the treated samples was measured spectrophotometrically at $\lambda = 410$ nm with titanyl sulfate by a H_2O_2-Ti^{4+} complex formation (Eisenberg, 1943).

2.3.1 Reaction rate constant and energy efficiency

Due to the different treated water volumes and applied powers, the UV- and PCD-based oxidation may not be compared by the decrease in pollutants' concentrations in time. Delivered energy dose relative to the treated solution volume and treatment time was implemented to compare the pollutant removal results in reactors of different principles of action. To evaluate the effect of oxidant addition on the removal efficiency, an energy-related pseudo-first-order reaction rate coefficient k_1 was implemented (Eq. 60) being calculated using slopes k_1 of the straight lines by plotting $\ln (C_t/C_0)$ as a function of delivered energy dose D (Eq. 61) through the linear regression:

$$\frac{d[C]}{dD} = -k_1 \cdot [C] \qquad (60)$$

$$D = \frac{P \cdot t}{V} \qquad (61)$$

where k_1 is the pseudo-first-order reaction rate coefficient, m^3 kWh^{-1}; C is the concentration of target compound; D is the delivered energy dose, kWh m^{-3}, P is the power applied in pulsed corona discharge or UV photolysis, kW; V is the volume of treated solution, m^3.

To evaluate the energy efficiencies of the reactors under the scope, energy yields E_{90} at 90% conversion (E_{90}, mmol kWh^{-1}) of target pollutant were calculated taking into account the energy consumed during the treatment together with the cost of extrinsic oxidant. The latter was considered as 1.0 EUR kg^{-1}, 1.5 EUR kg^{-1} and 2.5 EUR kg^{-1} for HP, PDS and PMS, respectively, as average wholesale prices on the market in 2023. Thus, the cost of the oxidant used was converted to equivalent energy expense considering the average European non-household electric energy price in 2023 of EUR 0.21 kWh^{-1} and added to the energy expense (Eurostat, 2023).

The energy efficiency E, mmol kWh^{-1}, was calculated using the equation Eq. 62:

$$E = \frac{\Delta C \cdot V}{W} \qquad (62)$$

where ΔC – a decrease of target compound concentration, mmol m^{-3}, W – energy consumption derived from the generator power output and the time of treatment, kWh.

3 Results and discussion

3.1 Evaluation of degradation in unassisted PCD

3.1.1 Pharmaceuticals

Degradation of studied pharmaceuticals in blank hydrolysis experiments at unadjusted pH in PCD reactors showed no significant changes ($\leq 5\%$) in concentration for all target pollutants in 2 h of treatment. Figure 2 demonstrates the kinetics of pollutant degradation in the energy-related pseudo-first-order reaction for PCD treatment ($r^2 > 0.98$). Thus, the application of PCD at pulse repetition frequency of 50 pps achieved 90% removal of MTF, TMD, and VMN at energy doses of 0.58, 0.42, and 0.10 kWh m^{-3}, respectively, which corresponds to the energy-related reaction rate constants of 3.1 ± 0.1, 5.8 ± 0.2, and 30.3 ± 1.8 m^3 kWh^{-1}. The VMN molecule degraded faster due to its large structure containing numerous moieties potentially available for the electrophilic attack, including deprotonated moieties and unsaturated benzene rings (Table 3). At alkaline pH, most of its moieties are deprotonated leading to better oxidation of VMN achieving k_1 of 73.3 ± 3.5 m^3 kWh^{-1} (Table 7). A similar was seen for TMD degradation: having pKa of 9.41, TMD molecule at pH 11 is fully deprotonated reacting fast with electrophilic ROS and resulting in k_1 as high as 29.1 ± 1.1 m^3 kWh^{-1}. However, MTF has a dissociation constant at higher pH (pKa = 11.6–12.4), resulting in a low effect of alkaline pH on its degradation (Jones et al., 2002; Scheurer et al., 2012).
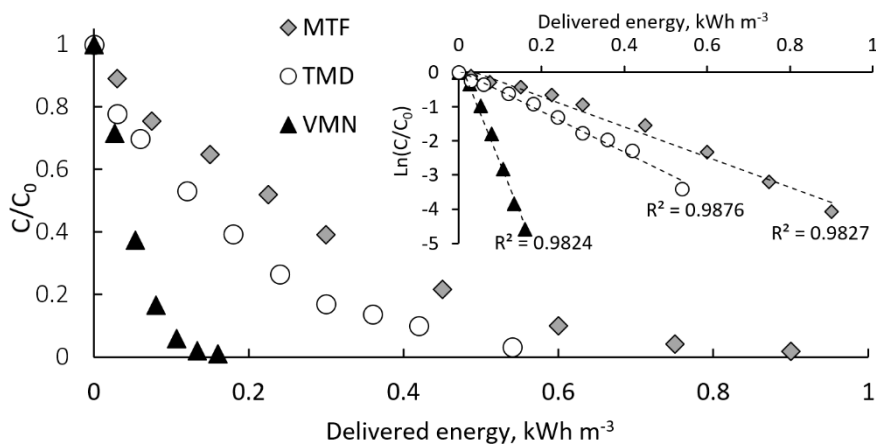
Figure 2. Degradation of MTF, TMD and VMN as a function of delivered energy ([MTF]$_0$ = 60.4 µM, [TMD]$_0$ = 33.4 µM, [VMN]$_0$ = 13.5 µM, pulse repetition frequency 50 pps, unadjusted pH)

   TOC removal achieved 24.8% and 61.4% for MTF and TMD, respectively, showing better oxidation of TMD degradation products. In the case of VMN at unadjusted pH, TOC removal reached 76.9%. Acidic pH contributed to better mineralization showing 85.7% TOC removal, while alkaline pH obstructed the mineralization achieving only 47.9%. The latter is due to potential scavenging by accumulated carbonates and/or bicarbonates in alkaline pH (Paper II).

Table 7. Energy-related reaction rate constants in degradation of MTF, TMD and VMN in unassisted PCD treatment ($V_{MTF} = V_{TMD} = 10$ L, $[MTF]_0 = 60.4$ µM, $[TMD]_0 = 33.4$ µM, $V_{VMN} = 5$ L, $[VMN]_0 = 13.5$ µM, pulse repetition frequency 50 pps, treatment time for TOC removal 2 h)

Compound	pH	k_1, m³ kWh⁻¹	TOC removal, %
Metformin	3	2.5 ± 0.2	-
	Unadjusted	3.1 ± 0.1	24.8
	11	3.1 ± 0.1	-
Tramadol	3	6.6 ± 0.5	-
	Unadjusted	5.8 ± 0.2	61.4
	11	29.1 ± 1.1	-
Vancomycin	3	20.0 ± 0.6	85.7
	Unadjusted	30.3 ± 1.8	76.9
	11	73.3 ± 3.5	47.9

3.1.2 Ionic liquids

Similar to studied pharmaceuticals, ILs were stable in blank hydrolysis experiments. The degradation kinetics at unadjusted pH and 200 pps for ILs degradation is shown in Figure 3. The 90% degradation of [Emim][Cl], [Omim][Cl], and [Emim][Br] in PCD experiments was achieved at energy doses of 1.27, 1.96, and 3.36 kWh m⁻³, respectively, with corresponding reaction rate constants 1.72, 1.03, and 0.68 m³ kWh⁻¹.

The difference in reaction rates between [Emim][Cl] and [Omim][Cl] may be explained by the length of the side chains. The size of the octyl alkyl chain hinders the oxidation of the imidazolium ring by screening off part of the hydroxyl radicals, which are inefficiently utilized due to their low reactivity towards saturated side chains: these chains confer certain surfactant properties to ILs by being oriented towards the gas phase at the gas-liquid interface (Derevshchikov et al., 2021). Thus, the longer side chain of [Omim]⁺ is the reason for its slower degradation compared to [Emim]⁺ paired with chloride. Degradation of [Emim]⁺ paired with chloride anion was about 2.4 faster than [Emim]⁺ paired with bromide anion. This observation may be explained by a) generation of less reactive radicals or b) scavenging reactions with bromide anion. Chloride and bromide anions might participate in reactions forming chlorine and bromine radicals. Chlorine radical (Cl•) ($E^o = 2.55$ V) is highly reactive towards organic compounds, while bromine radical (Br•) ($E^o = 1.93$ V) has lower redox potentials leading to lower oxidation efficiency (Wardman, 1989). However, different to chloride, bromide anion is known to be oxidized by ROS in acidic and neutral media to bromate via hypobromite (von Gunten, 2003; Tyrovola & Diamadopoulos, 2005). Oxidation of bromide competes effectively with the target reaction, consuming a substantial portion of oxidants. This competitive oxidation potentially contributes to the decreased [Emim]⁺ oxidation. Supporting this, data suggest that bromide oxidizes to hypobromite (Eq. 63), which then undergoes reduction, likely catalyzed by hydrogen peroxide formed from hydroxyl radicals' recombination (Eq. 64). Bromide thus degrades hydrogen peroxide, which contributes to overall oxidant waste. Previous findings by the authors indicated hydrogen peroxide accumulation during PCD treatment. In this study, hydrogen peroxide concentration reached 0.07 mM after a half-hour treatment of [Emim][Cl], while no

accumulation was observed after one hour of [Emim][Br] oxidation. This indirectly suggests bromide's competitive role in ILs' PCD oxidation.
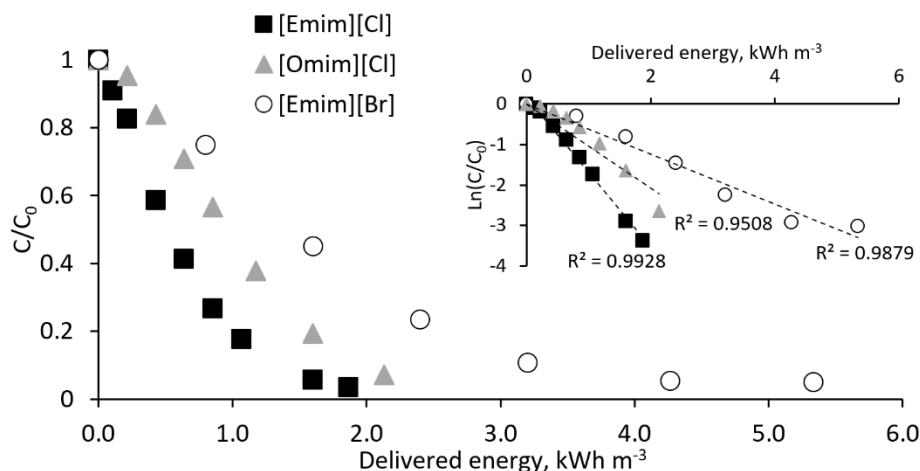
$$H_2O_2 + Br^- + H^+ \rightarrow H_2O + HBrO \qquad k = 1.5 \times 10^4 \ M^{-1} \ s^{-1} \qquad (63)$$
$$H_2O_2 + HBrO \rightarrow H_2O + O_2 + H^+ + Br^- \qquad k = 2.3 \times 10^4 \ M^{-1} \ s^{-1} \qquad (64)$$

Figure 3. Degradation of ILs as a function of delivered energy ($[IL]_0 = 100 \ \mu M$, pulse repetition frequency 200 pps, unadjusted pH)

Figure 4a shows the effect of pulse repetition frequency and pH on the ILs in the energy-related reaction rate constant. The difference between degradation at 50, 200, and 880 pps was similar to the previous observations which reflect the roles of ROS in oxidation. In turn, oxidation at 50 pps achieved the highest yield, and at 880 pps – the lowest: high repetition frequency destroyed a part of unused ROS.

The degradation of ILs showed similar trends with respect to the character of the hydrocarbon chains and the nature of anions: at 880 pps the degradation of [Emim][Cl] was 1.41 and 2.86 times faster than that of the [Omim][Cl] and [Emim][Br], respectively, with the k_1 values 1.09, 0.77, and 0.41 m^3 kWh^{-1}.

The effect of pH on the degradation of ILs was studied in acidic (pH 3), circum-neutral (pH unadjusted), and alkaline (pH 11) media (Figure 4b). During the plasma treatment at unadjusted pH, the oxidation of atmospheric nitrogen to nitrate in plasma leads to a noticeable decrease in pH (Paper II). The effect of pH was similar to VMN degradation: high reaction rates at high pH were observed for all ILs under consideration with k_1 of 2.71, 2.61, and 1.08 m^3 kWh^{-1} for [Emim][Cl], [Omim][Cl], [Emim][Br], respectively. The substantial positive effect of alkaline conditions can be explained by the fact that the organic cation is a desirable target for nucleophiles such as hydroxide, transforming the imidazolium cation to a neutral molecule with the hydroxyl group. Further deprotonation of the molecule in the alkaline medium enhances its reactivity with electrophilic hydroxyl radicals improving degradation efficiency (Figure 5).
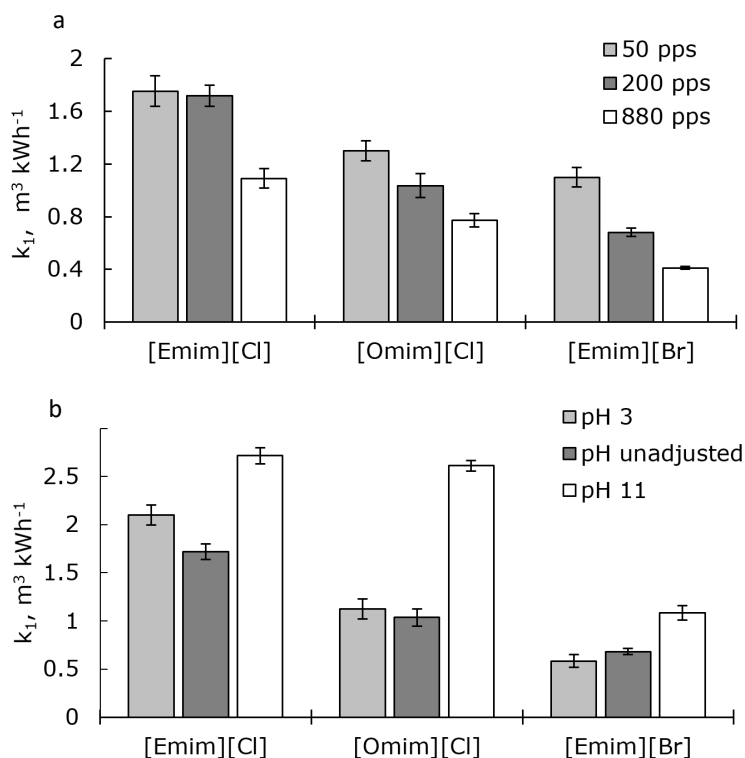
Figure 4. Effect of the pulse repetition frequency and pH on the ILs energy-related degradation rate constant k_1 in PCD oxidation ([IL]$_0$ = 100 µM)
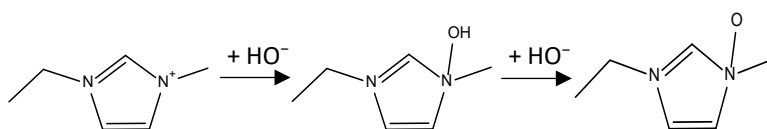
Figure 5. Transformation of 1-ethyl-3-methylimidazolium cation in alkaline solution

3.1.3 Comparison of degradation rates in unassisted PCD

Comparison between the studied pollutants in terms of their yields in PCD oxidation is made for their initial molar concentrations, counting the energy dose required to degrade a mole of pollutant at a given level of degradation. Figure 6 demonstrates the degradation of pharmaceuticals considering their molar concentrations. Degradation rates followed the descending order VMN > MTF > TMD> [Emim][Cl] > [Omim][Cl] > [Emim][Br]. One can see that for MTF, TMD, VMN, and [Emim][Cl] a similar pattern is observed suggesting certain limitation in the number of generated and rapidly reacting ROS. Therefore, for the PCD treatment, low initial pollutant concentrations within the interval 10−100 µM have a minor effect on the degradation rate, limited by the amount of ROS applied to a certain number of molecules. However, the VMN degradation was slightly faster compared to others, which might be determined by reactions in their large structure. In relation to the others, the degradation of [Omim][Cl] and [Emim][Br] was obstructed by the long alkyl chain and bromide anion, respectively.
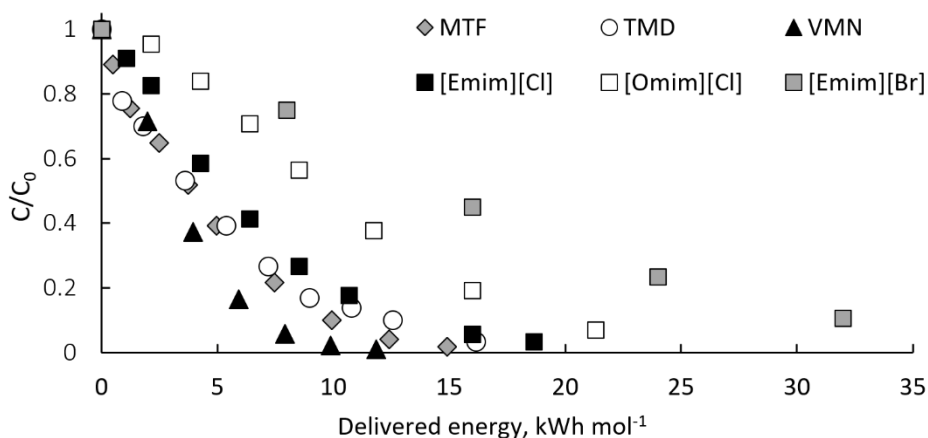
Figure 6. Degradation of pollutants as a function of delivered energy per mol of pollutant ([MTF]$_0$ = 60.4 μM, [TMD]$_0$ = 33.4 μM, [VMN]$_0$ = 13.5 μM, [IL]$_0$ = 100 μM, pharmaceuticals pulse repetition frequency 50 pps, ILs pulse repetition frequency 200 pps, unadjusted pH)

3.2 Evaluation of degradation in PCD assisted with peroxocompounds

3.2.1 Pharmaceuticals

Effects of PDS, PMS and HP additions on energy-related reaction rate constants are shown in Table 8. The addition of PDS at a pollutant/oxidant molar ratio of 1/10 enhanced the reaction rate constant of MTF oxidation from 3.1 to 7.9 m^3 kWh^{-1}. However, no positive effect in TMD degradation was observed in PCD/PDS combinations, even showing decreased oxidation rates with PDS additions. One can see from the experiments with MTF, that PDS is activated by PCD. It is logical to consider PDS activated also in the presence of TMD, although no oxidation enhancement was observed. Presumably, the sulfate radicals formed in PDS activation were not usefully utilized in TMD degradation and may have been lost in recombination reactions with hydroxyl radicals and other ROS. This assumption is supported by observations in MTF and TMD mineralization: the TMD mineralization comprised approximately 60% with or without PDS addition, whereas MTF mineralization increased from 24.8 to 31.6% as a result of PDS presence. The low reactivity between sulfate radicals and TMD might be the reason for the negative PDS effect.

In VMN oxidation, the addition of PDS, PMS, and HP at a pollutant/oxidant molar ratio of 1/10 improved the constants of oxidation rates as high as 59.3, 56.4, and 46.1 m^3 kWh^{-1}, respectively, from the unassisted PCD reaction rate constant of 30.3 m^3 kWh^{-1}. This confirms, like in MTF degradation, a more effective production of radicals in the PCD/PDS combination. Further oxidation of the VMN degradation products with sulfate radicals also showed a positive effect compared to unassisted PCD. For instance, at the lowest VMN/PDS molar ratio of 1/1, TOC removal reached 92.5%, whereas unassisted PCD achieved 76.9% removal in circum-neutral solutions. However, increasing the PDS dose exhibited a negative trend in VMN mineralization, reducing TOC removal to 82.1% at the maximum VMN/PDS ratio of 1/10.

In contrast, the PCD/PMS combination demonstrated further improvement with increased PMS dose in the mineralization of VMN oxidation products, achieving 96.4% removal. The differing activation pathways of PDS and PMS, as well as the types of active

species involved, contribute to the superior performance of PMS in combination with PCD.

The use of the PCD/HP combination resulted in the lowest effect on the k_1 value. The accumulation of HP was observed even in unassisted PCD treatment due to hydroxyl radicals' recombination, indicating that PCD is a weak activator for hydrogen peroxide. This is consistent with the rather low VMN mineralization degree fluctuating from 71.8% to 73.5%.

Table 8. Energy-related reaction rate constants of MTF, TMD and VMN degradation in assisted PCD treatment ($V_{MTF} = V_{TMD} = 10$ L, $[MTF]_0 = 60.4$ μM, $[TMD]_0 = 33.4$ μM, $V_{VMN} = 5$ L, $[VMN]_0 = 13.5$ μM, pulse repetition frequency 50 pps, treatment time for TOC removal 2 h)

Compound	Oxidant	Pollutant/oxidant molar ratio	k_1, m^3 kWh^{-1}	TOC removal, %
MTF	Unassisted	-	3.1 ± 0.1	24.8
	PDS	1/1	3.3 ± 0.1	-
		1/10	7.9 ± 0.3	31.6
TMD	Unassisted	-	5.8 ± 0.1	61.4
	PDS	1/1.1	4.7 ± 0.1	-
		1/11.4	5.3 ± 0.2	60.2
VMN	Unassisted	-	30.3 ± 1.8	76.9
	PDS	1/1	40.3 ± 2.1	92.5
		1/10	59.3 ± 3.4	82.1
	PMS	1/1	42.3 ± 2.7	94.0
		1/10	56.4 ± 1.4	96.4
	HP	1/1	40.5 ± 2.2	71.8
		1/10	46.1 ± 1.9	73.5

3.2.2 Ionic liquids

The results of ILs oxidation in PCD/oxidant treatment at unadjusted circum-neutral pH dependent on the IL/oxidant molar ratio are shown in Figure 7. The use of PDS or PMS mostly negatively affected the oxidation efficiency of ILs in PCD. While there were instances where the addition of persulfates at small IL/oxidant molar ratios exhibited a minor positive effect, this effect diminished with increased oxidant dosage. Persulfate ions and sulfate radicals may compete for the plasma-generated ROS responsible for oxidizing ILs, thereby diminishing the overall effectiveness of the treatment. In general, the performance of the PCD/PDS combination for [Omim][Cl] and [Emim][Br] remained comparable to that of unassisted PCD. This observation may suggest that there is nearly equal substitution of the discharge-generated ROS with sulfate radicals, which could explain the similarity in performance between the PCD/PDS combination and unassisted PCD.

The PCD/PMS combination resulted in k_1 values for [Emim][Cl] ranging from 1.4 to 1.58 m^3 kWh^{-1}, noticeably lower than unassisted PCD. The PMS activation likely produces hydroxyl radicals, unlike PDS (Eqs. 55−56). This may explain the PCD/PMS combination's better performance compared to PDS at high PMS dosages, possibly due to hydroxyl radicals' dominance in reactions with [Emim][Cl], reducing extrinsic scavenging effects. Increasing the PMS dose slightly enhanced the oxidation efficiency of [Omim][Cl], with k_1

reaching 1.1 m^3 kWh^{-1} at an IL/oxidant molar ratio of 1/5, surpassing unassisted PCD oxidation. However, for [Emim][Br], PMS addition showed no effect on oxidation, with only a slight reduction observed at the highest IL/oxidant molar ratio of 1/5. This lack of significant degradation changes suggests a compensatory oxidation mechanism, where PMS-derived secondary oxidation species evenly replace ROS reacted with PMS.
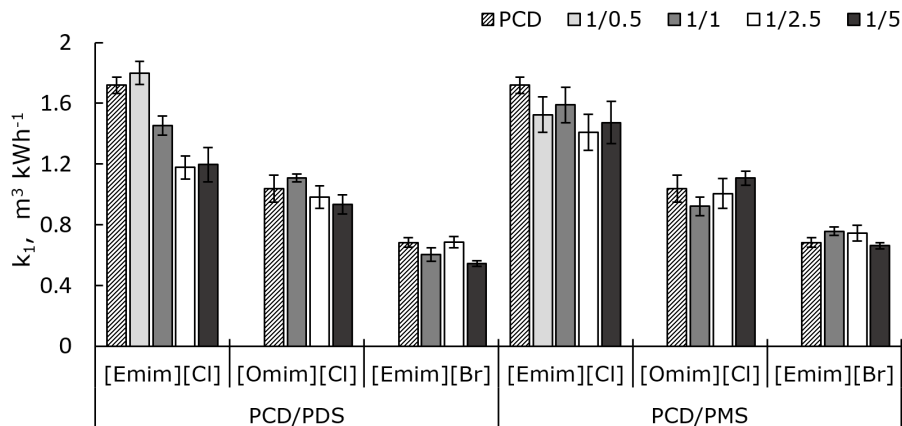

Figure 7. Energy-related ILs degradation rate constants in assisted PCD treatment dependent on the IL/oxidant molar ratios (V = 10 L, [ILs]$_0$ = 100 µM, pulse repetition frequency 200 pps)

3.2.3 Contribution of hydroxyl and sulfate radicals

To assess the role of radicals in assisted PCD oxidation, ethanol (EtOH) and *tert*-butanol (*t*-BuOH) were used as radical scavengers. EtOH reacts with hydroxyl radicals at second-order reaction rate constants ranging from $1.2·10^9$ to $2.8·10^9$ M^{-1} s^{-1}, and with sulfate radicals at $1.6·10^7$ to $7.7·10^7$ M^{-1} s^{-1}, while *t*-BuOH is more effective against hydroxyl radicals with reaction rate constants from $3.8·10^8$ to $7.6·10^8$ M^{-1} s^{-1}, compared to sulfate radicals, where the rate constants are much smaller, ranging from $4.0·10^5$ to $9.1·10^5$ M^{-1} s^{-1} (Anipsitakis & Dionysiou, 2004). Using both scavengers allows distinguishing the inhibition extent in the degradation of target compounds: an excess of *t*-BuOH highlights the effect of hydroxyl radicals while alternating excess amounts of EtOH and *t*-BuOH reveals the impact of sulfate radicals.

Scavenging studies were performed in assisted PCD oxidation with MTF, TMD and ILs, and inhibition results are presented in Table 9. The addition of *t*-BuOH reduced the MTF and TMD degradation efficiencies by 41% and 26%, respectively, indicating the presence of hydroxyl radicals in both systems. The addition of excess EtOH substantially inhibited oxidation of MTF and TMD resulting similarly to *t*-BuOH in 45% and 30%, respectively, showing a small impact of sulfate radicals. Therefore, hydroxyl radicals turn out to be the predominant oxidative species in the degradation of MTF and TMD in the PCD/PDS combination.

With ILs, various inhibitions in PCD/PDS oxidation were observed: the addition of *t*-BuOH reduced the degradation of [Emim][Cl], [Omim][Cl], and [Emim][Br] by 39%, 54%, and 17%, respectively. The strongest inhibition in [Omim][Cl] oxidation showed the great effect of hydroxyl radicals, indicating possible obstruction of oxidation of the long alkyl chain oriented towards the gas phase at the gas-liquid interface. The weak scavenging effect in [Emim][Br] oxidation might be explained by the significant part of hydroxyl

radicals consumed in reactions with easily oxidizable bromide ions. This observation aligns with the low oxidation efficiency observed for the brominated IL previously. The formation of smaller amounts of hydroxyl radicals in the oxidation of [Emim][Br] is less likely due to their predominant formation at the gas-plasma interface, as confirmed earlier, suggesting their consumption within the liquid bulk. Experiments with EtOH further inhibited the degradation of all ILs, pointing to the key role of sulfate radicals. Similar or even better contribution of sulfate radicals demonstrated PMS, possibly due to the reaction with ozone. The significant presence of sulfate radicals in PCD/persulfate-treated solutions, coupled with the limited effect of persulfates on the degradation rate of ILs, supports the hypothesis that ROS generated by PCD are consumed by persulfates, resulting in the production of sulfate radicals as substitutes. This process occurs with minimal change in the degradation rate of ILs.

Table 9. Results of hydroxyl and sulfate radical scavenging study in PCD/oxidant combinations ([MTF]$_0$ = 60.4 µM, [TMD]$_0$ = 33.4 µM, [ILs]$_0$ = 100 µM, pH unadjusted, MTF and TMD pulse repetition frequency 50 pps, ILs pulse repetition frequency 200 pps)

Target compound	Extrinsic oxidant	Pollutant/ oxidant molar ratio	[EtOH]$_0$/ [t-BuOH]$_0$, mM	Time, min	Degradation, %		
					Scavenger -free	EtOH	t-BuOH
MTF	PDS	1/5	15.1	40	96	51	55
TMD	PDS	1/5.7	8.4	40	91	61	65
[Emim][Cl]	PDS	1/1	25.0	6	83	24	44
	PMS	1/1		20	85	16	48
[Omim][Cl]	PDS	1/1		10	86	26	32
	PMS	1/1		20	87	11	38
[Emim][Br]	PDS	1/1		40	87	23	70
	PMS	1/1		60	89	25	65

3.3 Comparison with UV-based oxidation

3.3.1 Evaluation of degradation in UV/oxidant combinations

All studied compounds were treated in UV/oxidant combinations at the same initial concentrations as in PCD. Amongst target oxidants, TMD and VMN may be completely degraded in unassisted UV photolysis due to the presence of aromatic moieties in their structures providing better absorption of photons with further excitation of the substrate molecules. Other compounds were stable under UV radiation even after two hours of exposure.

Expectedly, the oxidants added to the UV-irradiated solutions actively oxidized all target compounds. Increasing the dose of oxidants showed mostly linear progression in the degradation rate of compounds. With TMD and MTF, about a ten-fold increase in the PDS concentration led to an increase in energy-related reaction rate constants by 2.5 and 8.0 times achieving k_1 of 5.74 and 7.83 m^3 kWh^{-1}, respectively, indicating the impact of generated radicals. Thus, the difference between TMD and MTF can expose their reactivity with sulfate radicals. While MTF molecules reacted fast with sulfate radicals, TMD molecules were prone to react with hydroxyl radicals. The fact that TMD showed a

negligible difference in reaction rates of UV oxidation and in the UV/PDS combinations at low PDS concentrations was explained by the substitution of UV-photons decomposing TMD molecules with sulfate radicals producing further hydroxyl radicals. The removal of TOC achieved about 60–65% for MTF and TMD at the highest PDS dose in two hours of treatment.

For VMN oxidation, unassisted UV photolysis was fast achieving complete degradation in ten minutes of treatment. The best performance in terms of reaction rate constant was demonstrated in the UV/HP combination achieving k_1 of 10.1 m^3 kWh^{-1}. Rapid activation of hydrogen peroxide with a generation of hydroxyl radicals contributed to oxidation enhancement. Among persulfates, faster oxidation was shown by PDS addition resulting in k_1 of 9.0 m^3 kWh^{-1} compared to 6.53 m^3 kWh^{-1} of PMS with relative increase of 89.2% and 37.8%, respectively, at the VMN/oxidant molar ratio of 1/10. These results are consistent with the difference in molar extinction coefficients presumably resulting in different amounts of produced radicals: slower activation of PMS at the fast unassisted UV photolysis of VMN resulted in a smaller effect of PMS addition. The removal of TOC was consistent with the reaction rates: mineralization of 18.1%, 24.2%, and 7.9% was observed in UV/PDS, UV/HP, and UV/PMS combinations, respectively, at the VMN/oxidant molar ratio of 1/10. These observations suggest hydroxyl radicals produced from HP being utilized in the oxidation of by-products more effectively for their unselective reactions.

The ILs/PDS molar ratio increased from 1/1 to 1/5 at circum-neutral unadjusted pH, resulting in an increase in k_1 value from 0.76, 0.71, and 0.14 to 4.49, 5.39, and 1.46 m^3 kWh^{-1} for [Emim][Cl], [Omim][Cl], and [Emim][Br], respectively. Different to PCD oxidation, a long alkyl chain does not have a substantial impact on the degradation rate, [Omim][Cl] oxidation was faster than [Emim][Cl]. However, the impact of anion remained similar to the PCD treatment: bromide anions inhibit the reaction. The UV/PMS combination at a molar ratio of 1/5 showed about 2.5-fold lower reaction rate constants than PDS addition, reaching 1.96, 2.1, and 0.44 m^3 kWh^{-1} for [Emim][Cl], [Omim][Cl], and [Emim][Br], respectively. The possible reasons for decreased efficiency include the difference in generated radicals and slower activation rate of PMS due to higher dissociation energy of the O-O bond in PDS and PMS molecules, 92 and 372 kJ mol^{-1}, respectively.

3.3.2 Energy efficiency

The reaction rate constant k_1 considers the energy needed for oxidation, but does not consider the contribution of extrinsic oxidants, creating a gap in the economic evaluation of treatment methods. To address this, energy efficiency or energy yield (E_{90}, mmol kWh^{-1}), offers a more comprehensive assessment. It accounts for the energy consumption in both UV irradiation and PCD treatment required for achieving 90% conversion of target compounds along with associated costs of extrinsic oxidants. The latter was considered as 1.0, 1.5, and 2.5 EUR kg^{-1} for HP, PDS and PMS, respectively, as average wholesale prices on the market in 2023. The cost of oxidant dose was then converted to the equivalent energy expense considering the average European non-household electric energy price of EUR 0.21 kWh^{-1} and added to the energy expense (Eurostat, 2023). The results of unassisted PCD, PCD/oxidant, and UV/oxidant combinations are shown in Table 10.

Treatment of target compounds with unassisted PCD at the pulse repetition frequency of 50 pps demonstrated better oxidation of pharmaceutical molecules, e.g., with VMN achieving energy efficiency of 126.1 mmol kWh^{-1}. The oxidation of ILs was slower than the one of pharmaceuticals, although the energy efficiency of [Emim][Cl] was comparable

to MTF. At higher pulse repetition rates of 200 and 880 pps, the energy efficiency decreased since the shortened time between pulses prevented the long-lived oxidants from useful utilisation in reactions. Interestingly, increasing the pulse repetition frequency from 50 to 880 pps, the energy efficiency of [Emim][Cl] and [Omim][Cl] oxidation was reduced by about 26%, while the energy efficiency of [Emim][Br] disproportionally dropped by 63%. This shows a serious impact of long-living species on the oxidation of [Emim]$^+$ in the presence of bromide anion.

Table 10. Energy efficiencies of target compounds oxidation in unassisted PCD, PCD/oxidant, and UV/oxidant combinations ([MTF]$_0$ = 60.4 μM, [TMD]$_0$ = 33.4 μM, [ILs]$_0$ = 100 μM, unadjusted circumneutral pH, MTF, TMD, and VMN pulse repetition frequency 50 pps, ILs pulse repetition frequency 200 pps)

Treatment process	Condition	Energy efficiency, mmol kWh^{-1}					
		MTF	TMD	VMN	[Emim][Cl]	[Omim][Cl]	[Emim][Br]
PCD	50	75.2	81.4	126.1	68.4	49.7	47.6
	200	-	-	-	67.2	45.9	26.8
	880	-	-	-	50.6	35.9	17.7
PCD/PDS	1/1	72.4	63.6	83.2	53.0	46.0	25.1
	1/2.5	70.7	67.8	-	42.6	37.1	25.4
	1/5	61.3	72.0	57.2	37.9	30.7	18.5
PCD/PMS	1/1			75.1	47.8	37.0	26.0
	1/2.5		-	-	35.8	31.0	21.7
	1/5			36.2	28.8	24.3	18.4
PCD/HP	1/1			107.2			
	1/5		-	111.9		-	
	1/10			91.3			
UV/PDS	1/1	*	30.6	27.3	28.0	26.0	*
	1/2.5	41.0	31.0	-	59.7	57.8	14.1
	1/5	50.8	31.2	28.3	71.8	70.5	42.0
UV/PMS	1/1			24.5	*	12.8	*
	1/2.5		-	-	25.0	29.5	*
	1/5			17.7	30.6	31.0	11.7
UV/HP	1/1			32.1			
	1/5		-	39.7		-	
	1/10			51.5			

*Degradation did not achieve 90% removal

As was found earlier, the PCD/oxidant combinations improved the oxidation of MTF and VMN. Accordingly, the addition of PDS at pollutant/oxidant molar ratios of 1/1 and 1/2.5 slightly decreased the energy efficiency of MTF oxidation from 75.2 to 72.4 and 70.7 mmol kWh^{-1}, respectively. However, the effect on mineralization makes this combination more economically viable. With VMN, the energy efficiency decreased from 126.1 to 83.2, 75.1 and 107.2 mmol kWh^{-1} at VMN/oxidant molar ratio of 1/1 for PDS, PMS, and HP, respectively. Considering some improvement in the mineralization of VMN, the addition of PDS and PMS at low dosages looks reasonable.

In the UV/oxidant treatment, the increased oxidant dose resulted in pronounced improvement in the energy efficiency of target compounds oxidation, however, with exceptions. These include oxidation of TMD in UV/PDS combination, and VMN oxidation in UV/PDS and UV/PMS ones. The impact of increased doses of extrinsic oxidants was negligible, attaining energy efficiencies at the same or even reduced levels, although with substantially increased TOC removal. Compared to pharmaceuticals, the use of UV/PDS combination demonstrated more promising results in ILs degradation, achieving higher energy efficiencies. Thus, oxidation of [Emim][Cl] and [Omim][Cl] achieved at IL/oxidant molar ratio of 1/5 energy efficiencies of 71.8 and 70.5 mmol kWh^{-1} with PDS, and 30.6 and 31.0 mmol kWh^{-1} with PMS addition, respectively. More expensive PMS reacted slower, being unable to achieve high energy efficiencies.

Finally, the PCD process proved capable of activating extrinsic oxidants providing faster degradation and mineralization of MTF and VMN. However, if the cost of extrinsic oxidants is converted into an energy equivalent, the PCD/oxidant combinations have not proven to be economically justified. Moreover, the addition of oxidants makes the combined treatment less convenient in terms of chemical delivery, storage, and handling. Therefore, unassisted PCD treatment provided acceptably high energy efficiency, comparable to or superior to UV/oxidant combinations, in the oxidation of recalcitrant compounds using only electric energy without added extrinsic oxidants.

Conclusions

Oxidation of aqueous pollutants was successfully performed in PCD, PCD/oxidant and UV/oxidant combinations. Degradation of pharmaceuticals and imidazolium-based ILs was evaluated in unassisted PCD treatment at variable operating parameters, including pH and pulse repetition frequency. Efficiencies of PCD combinations with extrinsic oxidants at variable dosages of peroxydisulfate, peroxymonosulfate, and hydrogen peroxide in the oxidation of pharmaceuticals and imidazolium-based ILs were assessed. Results were compared with UV/oxidant combinations and the applicability of approaches was evaluated.

Unassisted PCD treatment showed degradation rates in the descending order: VMN > MTF > TMD > [Emim][Cl] > [Omim][Cl] > [Emim][Br]. Being at different initial concentrations, similar degradation patterns of VMN, MTF, TMD, and [Emim][Cl] suggest quantitative limitations in reactive species. The longer alkyl chain in [Omim][Cl] reduced the oxidation rate by 40%, explained by its screening effect in surface reaction characteristic for PCD. Bromide anions diminished the oxidation efficiency of [Emim]$^+$ by 2.8 times due to their significant reactivity toward oxidation. For all the compounds studied, except MTF, the degradation rates increased by about 2−4 times in alkaline media due to the deprotonation of the molecules favourable for electrophilic attacks of hydroxyl radicals. The involvement of ozone and possibly other long-living oxidants in the oxidation of ILs is evident through the difference in oxidation efficiencies at variations on pulse repetition frequency: lower frequency provides higher efficiency on account of long-living oxidants realizing their oxidation potential within longer pauses between pulses.

Amongst studied compounds, a certain effect of extrinsic oxidants addition to PCD-treated solutions was observed in the degradation of MTF and VMN: the addition of PDS was more effective in the degradation of MTF, while PDS, PMS, and HP contributed to better oxidation of VMN. Degradation of other compounds showed a low to moderate negative impact on the oxidation efficiency. In turn, studies in radical scavenging demonstrated an important role of sulfate radicals in PCD/persulfate treatment. The sulfate radicals, however, demonstrated negligible or negative impact on the pollutants' oxidation efficiency, supporting the hypothesis of primary reactive oxygen species substituted with sulfate radicals.

The UV/oxidant combinations showed high efficiency in the degradation of target compounds, although it is worth noting that for some of them, complete degradation was achieved only at increased dosages of the oxidant. Expectedly, UV/persulfate combinations provided high energy efficiencies, confirming their applicability at optimal oxidant doses. In turn, unassisted PCD treatment provided acceptably high energy efficiency, comparable to or superior to UV/oxidant combinations using only electric energy. The addition of peroxocompounds verified the potential to improve the rates of oxidation and mineralization of target compounds, but not the energy efficiency. Moreover, the use of chemicals makes the combined treatment less convenient in terms of chemical delivery, storage, and handling.

References

Ajo, P., Kornev, I., & Preis, S. 2017. Pulsed corona discharge induced hydroxyl radical transfer through the gas-liquid interface. *Scientific Reports*, *7*(1), 1–6. https://doi.org/10.1038/s41598-017-16333-1

Anipsitakis, G. P., & Dionysiou, D. D. 2004. Radical generation by the interaction of transition metals with common oxidants. *Environ. Sci. Technol. y*, *38*(13), 3705–3712. https://doi.org/10.1021/es035121o

Ansari, M., Sharifian, M., Ehrampoush, M. H., Mahvi, A. H., Salmani, M. H., & Fallahzadeh, H. 2021. Dielectric barrier discharge plasma with photocatalysts as a hybrid emerging technology for degradation of synthetic organic compounds in aqueous environments: A critical review. *Chemosphere* 263. https://doi.org/10.1016/j.chemosphere.2020.128065

Antonopoulou, M., Hela, D., & Konstantinou, I. 2016. Photocatalytic degradation kinetics, mechanism and ecotoxicity assessment of tramadol metabolites in aqueous TiO_2 suspensions. *Sci. Total Environ.*, *545–546*, 476–485. https://doi.org/10.1016/j.scitotenv.2015.12.088

Antonopoulou, M., & Konstantinou, I. 2016. Photocatalytic degradation and mineralization of tramadol pharmaceutical in aqueous TiO_2 suspensions: Evaluation of kinetics, mechanisms and ecotoxicity. *Appl. Catal. A Gen.*, *515*, 136–143. https://doi.org/10.1016/j.apcata.2016.02.005

Antonopoulou, M., Thoma, A., Konstantinou, F., Vlastos, D., & Hela, D. 2020. Assessing the human risk and the environmental fate of pharmaceutical Tramadol. *Sci. Total Environ.*, *710*. https://doi.org/10.1016/j.scitotenv.2019.135396

Aseman-Bashiz, E., & Sayyaf, H. 2020. Metformin degradation in aqueous solutions by electro-activation of persulfate and hydrogen peroxide using natural and synthetic ferrous ion sources. *J. Mol. Liq.*, *300*, 112285. https://doi.org/10.1016/j.molliq.2019.112285

aus der Beek, T., Weber, F. A., Bergmann, A., Hickmann, S., Ebert, I., Hein, A., & Küster, A. 2016. Pharmaceuticals in the environment-Global occurrences and perspectives. *Environ. Toxicol. Chem.*, *35*, 823–835. https://doi.org/10.1002/etc.3339

Azuma, T., Usui, M., & Hayashi, T. 2024. Inactivation of antibiotic-resistant bacteria in hospital wastewater by ozone-based advanced water treatment processes. *Sci. Total Environ.*, *906*. https://doi.org/10.1016/j.scitotenv.2023.167432

Bachour, R. L., Golovko, O., Kellner, M., & Pohl, J. 2020. Behavioral effects of citalopram, tramadol, and binary mixture in zebrafish (*Danio rerio*) larvae. *Chemosphere*, *238*, 124587. https://doi.org/10.1016/j.chemosphere.2019.124587

Blair, B. D., Crago, J. P., Hedman, C. J., & Klaper, R. D. 2013. Pharmaceuticals and personal care products found in the Great Lakes above concentrations of environmental concern. *Chemosphere*, *93*(9), 2116–2123. https://doi.org/10.1016/j.chemosphere.2013.07.057

Briels, T. M. P., Kos, J., Winands, G. J. J., Van Veldhuizen, E. M., & Ebert, U. 2008. Positive and negative streamers in ambient air: Measuring diameter, velocity and dissipated energy. *J. Phys. D: Appl. Phys.*, *41*(23), 234004–234015. https://doi.org/10.1088/0022-3727/41/23/234004

Briones, R. M., Sarmah, A. K., & Padhye, L. P. 2016. A global perspective on the use, occurrence, fate and effects of anti-diabetic drug metformin in natural and engineered ecosystems. *Environ. Pollut.*, *219*, 1007–1020. https://doi.org/10.1016/j.envpol.2016.07.040

Caminada, D., Escher, C., & Fent, K. 2006. Cytotoxicity of pharmaceuticals found in aquatic systems: Comparison of PLHC-1 and RTG-2 fish cell lines. *Aquat. Toxicol.*, *79*(2), 114–123. https://doi.org/10.1016/j.aquatox.2006.05.010

Carbuloni, C. F., Savoia, J. E., Santos, J. S. P., Pereira, C. A. A., Marques, R. G., Ribeiro, V. A. S., & Ferrari, A. M. 2020. Degradation of metformin in water by TiO_2–ZrO_2 photocatalysis. *J. Environ. Manag.*, *262*, 110347. https://doi.org/10.1016/j.jenvman.2020.110347

Chen, J., & Davidson, J. H. 2003. Ozone production in the negative DC corona: The dependence of discharge polarity. *Plasma Chem. Plasma Process., 23*(3), 501–518. https://doi.org/10.1023/A:1023235032455

Chinnaiyan, P., Thampi, S. G., Kumar, M., & Balachandran, M. 2019. Photocatalytic degradation of metformin and amoxicillin in synthetic hospital wastewater: effect of classical parameters. *Int. J. Environ. Sci. Techn.*, *16*(10), 5463–5474. https://doi.org/10.1007/s13762-018-1935-0

Cho, C.-W., Pham, T. P. T., Zhao, Y., Stolte, S., & Yun, Y.-S. 2021. Review of the toxic effects of ionic liquids. *Sci. Total Environ.*, *786*, 147309. https://doi.org/https://doi.org/10.1016/j.scitotenv.2021.147309

Chu, P. K. 2013. *Low temperature plasma technology: Methods and Applications.* CRC Press (an imprint of Taylor & Francis).

D'Agostino, Riccardo. 2008. *Advanced plasma technology*. Wiley-VCH.

Dehghani, F., Yousefinejad, S., Dehghani, M., Borghei, S. M., & Javid, A. H. 2022. Photocatalytic degradation of vancomycin using titanium dioxide and optimization by central composite design. *Int. J. Environ. Sci. Techn., 19*(9), 8957–8968. https://doi.org/10.1007/s13762-022-04117-8

Deniere, E., Van Hulle, S., Van Langenhove, H., & Demeestere, K. 2018. Advanced oxidation of pharmaceuticals by the ozone-activated peroxymonosulfate process: the role of different oxidative species. *J. Hazard. Mater.*, *360*, 204–213. https://doi.org/10.1016/j.jhazmat.2018.07.071

Derevshchikov, V., Dulova, N., & Preis, S. (2021). Oxidation of ubiquitous aqueous pharmaceuticals with pulsed corona discharge. *J. Electrostat.*, *110*(November 2020), 103567. https://doi.org/10.1016/j.elstat.2021.103567

Dodd, M. C., Buffle, M. O., & von Gunten, U. (2006). Oxidation of antibacterial molecules by aqueous ozone: Moiety-specific reaction kinetics and application to ozone-based wastewater treatment. *Environmental Science and Technology*, *40*(6), 1969–1977. https://doi.org/10.1021/es051369x

Eesti Vee-ettevõtete Liit. 2019. *Ravimijääke jõuab keskkonda liiga palju*. https://evel.ee/uudised/ravimijaake-jouab-keskkonda-liiga-palju-89-pinnaveeproovidest-sisaldas-nii-diabeediravimit-metformini-kui-ka-valuvaigistina-tuntud-diklofenaki/ (Accessed 15.04.2024)

Eisenberg, G. M. 1943. Colorimetric Determination of Hydrogen Peroxide. *Industrial and Engineering Chemistry - Analytical Edition*, *15*(5), 327–328. https://doi.org/10.1021/i560117a011

Elizalde-Velázquez, G. A., & Gómez-Oliván, L. M. 2020. Occurrence, toxic effects and removal of metformin in the aquatic environments in the world: Recent trends and perspectives. *Sci. Total Environ.*, *702*. https://doi.org/10.1016/j.scitotenv.2019.134924

European Centre for Disease Prevention and Control (ECDC). 2023. *Antimicrobial resistance in the EU/EEA (EARS-Net) - Annual epidemiological report for 2022*. https://atlas.ecdc.europa.eu/

European Centre for Disease Prevention and Control (ECDC). 2023. *Antimicrobial resistance surveillance in Europe*. https://doi.org/10.2900/63495

Eurostat. 2023. *Electricity prices for non-household consumers*. https://ec.europa.eu/eurostat/statistics-explained/index.php?title=Electricity_price_statistics (Accessed 15.02.2024)

Frade, R. F. M., & Afonso, C. A. M. 2010. Impact of ionic liquids in environment and humans: An overview. *Hum. Experim. Toxicol.*, *29*(12), 1038–1054. https://doi.org/10.1177/0960327110371259

Furia, F., Minella, M., Gosetti, F., Turci, F., Sabatino, R., Di Cesare, A., Corno, G., & Vione, D. 2021. Elimination from wastewater of antibiotics reserved for hospital settings, with a Fenton process based on zero-valent iron. *Chemosphere*, *283*. https://doi.org/10.1016/j.chemosphere.2021.131170

Garcia, M. T., Gathergood, N., & Scammells, P. J. 2005. Biodegradable ionic liquids Part II. Effect of the anion and toxicology. *Green Chem.,* *7*(1), 9–14. https://doi.org/10.1039/B411922C

Gerrity, D., Stanford, B. D., Trenholm, R. A., & Snyder, S. A. 2009. An evaluation of a pilot-scale nonthermal plasma advanced oxidation process for trace organic compound degradation. *Water Res.*, *44*, 493–504. https://doi.org/10.1016/j.watres.2009.09.029

Ghalwa, N. A., Abu-Shawish, H. M., Zaggout, F. R., Saadeh, S. M., Al-Dalou, A. R., & Abou Assi, A. A. 2014. Electrochemical degradation of tramadol hydrochloride: Novel use of potentiometric carbon paste electrodes as a tracer. *Arab. J. Chem.*, *7*(5), 708–714. https://doi.org/10.1016/j.arabjc.2010.12.007

Golovko, O., Örn, S., Sörengård, M., Frieberg, K., Nassazzi, W., Lai, F. Y., & Ahrens, L. 2021. Occurrence and removal of chemicals of emerging concern in wastewater treatment plants and their impact on receiving water systems. *Sci. Total Environ.*, *754*, 142122. https://doi.org/10.1016/j.scitotenv.2020.142122

Gomez-Herrero, E., Tobajas, M., Polo, A., Rodriguez, J. J., & Mohedano, A. F. 2020 Toxicity and inhibition assessment of ionic liquids by activated sludge. *Ecotoxicol. Environ. Saf.*, *187*. https://doi.org/10.1016/J.ECOENV.2019.109836

Gotvajn, A. Ž., Rozman, U., Antončič, T., Urbanc, T., Vrabel', M., & Derco, J. 2021. Fe^{2+} and UV catalytically enhanced ozonation of selected environmentally persistent antibiotics. *Processes*, *9*(3), 1–17. https://doi.org/10.3390/pr9030521

Guan, Y. H., Ma, J., Li, X. C., Fang, J. Y., & Chen, L. W. 2011. Influence of pH on the formation of sulfate and hydroxyl radicals in the UV/Peroxymonosulfate system. *Environ. Sci. Techn.*, *45*(21), 9308–9314. https://doi.org/10.1021/es2017363

Guerra-Rodríguez, S., Rodríguez, E., Singh, D. N., & Rodríguez-Chueca, J. 2018. Assessment of sulfate radical-based advanced oxidation processes for water and wastewater treatment: A review. *Water (Switzerland)*, *10*(12). https://doi.org/10.3390/w10121828

Guo, H., Pan, S., Hu, Z., Wang, Y., Jiang, W., Yang, Y., Wang, Y., Han, J., Wu, Y., & Wang, T. 2023. Persulfate activated by non-thermal plasma for organic pollutants degradation: A review. *Chem. Eng. J.*, *470*, 144094. https://doi.org/10.1016/j.cej.2023.144094

Hanisch, B., & Abbas, B. 2004. Human drugs in aquatic ecosystems: Approach for the environmental risk assessment of drug residues. Environ. Sci. 16, 223-238. https://doi.org/10.1065/uwsf2004.02.076

Hu, P., & Long, M. 2016. Cobalt-catalyzed sulfate radical-based advanced oxidation: A review on heterogeneous catalysts and applications. *App. Cat. B: Environ.,* 181, 103–117. https://doi.org/10.1016/j.apcatb.2015.07.024

Jacob, R. S., de Souza Santos, L. V., d'Auriol, M., Lebron, Y. A. R., Moreira, V. R., & Lange, L. C. 2020. Diazepam, metformin, omeprazole and simvastatin: a full discussion of individual and mixture acute toxicity. *Ecotoxicology*, *29*(7), 1062–1071. https://doi.org/10.1007/s10646-020-02239-8

Jacobsen, F., Holcman, J., & Sehested, K. 1997. Activation parameters of ferryl ion reactions in aqueous acid solutions. *Int. J. Chem. Kinet.*, *29*(1), 17–24. https://doi.org/10.1002/(SICI)1097-4601(1997)29:1<17::AID-KIN3>3.0.CO;2-O

Ji, Y., Fan, Y., Liu, K., Kong, D., & Lu, J. (2015). Thermo activated persulfate oxidation of antibiotic sulfamethoxazole and structurally related compounds. *Water Res.*, *87*, 1–9. https://doi.org/10.1016/j.watres.2015.09.005

Jiang, B., Zheng, J., Qiu, S., Wu, M., Zhang, Q., Yan, Z., & Xue, Q. 2014. Review on electrical discharge plasma technology for wastewater remediation. *Chem. Eng. J.,* 236, 348–368. https://doi.org/10.1016/j.cej.2013.09.090

Jones, O. A. H., Voulvoulis, N., & Lester, J. N. 2002. Aquatic environmental assessment of the top 25 English prescription pharmaceuticals. *Water Res.* 36. https://doi.org/10.1016/S0043-1354(02)00227-0

Jordan, A., & Gathergood, N. 2015. Biodegradation of ionic liquids-a critical review. *Chem. Soc. Rev.*, *44*(22), 8200–8237. https://doi.org/10.1039/C5CS00444F

Kanaujiya, D. K., Paul, T., Sinharoy, A., & Pakshirajan, K. 2019. Biological treatment processes for the removal of organic micropollutants from wastewater: a Review. *Curr. Pollution Rep.*, *5*(3), 112–128. https://doi.org/10.1007/s40726-019-00110-x

Karimian, S., Moussavi, G., Fanaei, F., Mohammadi, S., Shekoohiyan, S., & Giannakis, S. 2020. Shedding light on the catalytic synergies between Fe(II) and PMS in vacuum UV (VUV/Fe/PMS) photoreactors for accelerated elimination of pharmaceuticals: The case of metformin. *Chem. Eng. J.*, *400*, 125896. https://doi.org/10.1016/j.cej.2020.125896

Kasprzyk-Hordern, B., Ziółek, M., & Nawrocki, J. 2003. Catalytic ozonation and methods of enhancing molecular ozone reactions in water treatment. *Appl. Cat. B: Environ.*, *46*(4), 639–669. https://doi.org/10.1016/S0926-3373(03)00326-6

Kaur, G., Kumar, H., & Singla, M. 2022. Diverse applications of ionic liquids: A comprehensive review. *J. Mol. Liq.*, *351*. https://doi.org/10.1016/J.MOLLIQ.2022.118556

Kornev, I., Saprykin, F., & Preis, S. 2017. Stability and energy efficiency of pulsed corona discharge in treatment of dispersed high-conductivity aqueous solutions. *J. Electrostat.*, *89*, 42–50. https://doi.org/10.1016/j.elstat.2017.07.001

Kostanjevecki, P., Petric, I., Loncar, J., Smital, T., Ahel, M., & Terzic, S. 2019. Aerobic biodegradation of tramadol by pre-adapted activated sludge culture: Cometabolic transformations and bacterial community changes during enrichment. *Sci. Total Environ.*, *687*, 858–866. https://doi.org/10.1016/j.scitotenv.2019.06.118

Kumar, R., Akbarinejad, A., Jasemizad, T., Fucina, R., Travas-Sejdic, J., & Padhye, L. P. 2021. The removal of metformin and other selected PPCPs from water by poly(3,4-ethylenedioxythiophene) photocatalyst. *Sci. Total Environ.*, *751*, 142302. https://doi.org/10.1016/j.scitotenv.2020.142302

Kyere-Yeboah, K., Bique, I. K., & Qiao, X. chen. 2023. Advances of non-thermal plasma discharge technology in degrading recalcitrant wastewater pollutants. A comprehensive review. *Chemosphere, 320*. https://doi.org/10.1016/j.chemosphere.2023.138061

Lee, J., von Gunten, U., & Kim, J. H. 2020. Persulfate-based advanced oxidation: Critical assessment of opportunities and roadblocks. *Environ. Sci. Techn.*, *54*(6), 3064–3081. https://doi.org/10.1021/acs.est.9b07082

Legager, T., Holcman, J., Sehested, K., & Pedersen7, T. 1992. Oxidation of ferrous ions by ozone in acidic solutions. *Inorg. Chem., 31*. https://doi.org/10.1021/ic00043a009

Li, S., Dang, X., Yu, X., Abbas, G., Zhang, Q., & Cao, L. 2020. The application of dielectric barrier discharge non-thermal plasma in VOCs abatement: A review. *Chem. Eng. J., 388*, 124275. https://doi.org/10.1016/j.cej.2020.124275

Liang, C., Huang, C. F., Mohanty, N., & Kurakalva, R. M. 2008. A rapid spectrophotometric determination of persulfate anion in ISCO. *Chemosphere*, *73*(9), 1540–1543. https://doi.org/10.1016/j.chemosphere.2008.08.043

Lim, S., Shi, J. L., von Gunten, U., & McCurry, D. L. 2022. Ozonation of organic compounds in water and wastewater: A critical review. *Water Res.* 213. https://doi.org/10.1016/j.watres.2022.118053

Lindim, C., van Gils, J., Georgieva, D., Mekenyan, O., & Cousins, I. T. 2016. Evaluation of human pharmaceutical emissions and concentrations in Swedish river basins. *Sci. Total Environ.*, *572*, 508–519. https://doi.org/10.1016/j.scitotenv.2016.08.074

Locke, B. R., Lukes, P., & Brisset, J.-L. 2012. *Elementary chemical and physical phenomena in electrical discharge plasma in gas-liquid environments and in liquids*. (eds V.I. Parvulescu, M. Magureanu and P. Lukes). https://doi.org/10.1002/9783527649525.ch6

Ložek, F., Kuklina, I., Grabicová, K., Kubec, J., Buřič, M., Grabic, R., Randák, T., Císař, P., & Kozák, P. 2019. Behaviour and cardiac response to stress in signal crayfish exposed to environmental concentrations of tramadol. *Aquat. Toxicol.*, *213*, 105217. https://doi.org/10.1016/j.aquatox.2019.05.019

Lukes, P., Locke, B. R., & Brisset, J.-L. 2012. *Aqueous-phase chemistry of electrical discharge plasma in water and in gas-liquid environments*. (eds V.I. Parvulescu, M. Magureanu and P. Lukes). https://doi.org/10.1002/9783527649525.ch7

Luo, C., Ma, J., Jiang, J., Liu, Y., Song, Y., Yang, Y., Guan, Y., & Wu, D. 2015. Simulation and comparative study on the oxidation kinetics of atrazine by UV/H_2O_2, UV/HSO_5^- and $UV/S_2O_8^{2-}$. *Water Res.*, *80*, 99–108. https://doi.org/10.1016/j.watres.2015.05.019

Luo, Y., Guo, W., Ngo, H. H., Nghiem, L. D., Hai, F. I., Zhang, J., Liang, S., & Wang, X. C. 2014. A review on the occurrence of micropollutants in the aquatic environment and their fate and removal during wastewater treatment. *Sci. Total Environ.*, *473–474*, 619–641. https://doi.org/10.1016/j.scitotenv.2013.12.065

Lütke Eversloh, C., Schulz, M., Wagner, M., & Ternes, T. A. 2015. Electrochemical oxidation of tramadol in low-salinity reverse osmosis concentrates using boron-doped diamond anodes. *Water Res.*, *72*, 293–304. https://doi.org/10.1016/j.watres.2014.12.021

Lv, Z., & Guo, Y. 2020. Metformin and Its Benefits for Various Diseases. *Front. Endocrinol.*, *11*, 1–10. https://doi.org/10.3389/fendo.2020.00191

Maćerak, A. L., Kerkez, Đ., Bečelić-Tomin, M., Pilipović, D. T., Kulić, A., Jokić, J., & Dalmacija, B. 2018. Removal of diclofenac and metformin from water in laboratory photo reactor. *Proceedings*, *2*(20), 1288. https://doi.org/10.3390/proceedings2201288

Mackuľak, T., Birošová, L., Bodík, I., Grabic, R., Takáčová, A., Smolinská, M., Hanusová, A., Híveš, J., & Gál, M. 2016. Zerovalent iron and iron(VI): Effective means for the removal of psychoactive pharmaceuticals and illicit drugs from wastewaters. *Sci. Total Environ.*, *539*, 420–426. https://doi.org/10.1016/j.scitotenv.2015.08.138

Mackuľak, T., Mosný, M., Grabic, R., Golovko, O., Koba, O., & Birošová, L. 2015. Fenton-like reaction: A possible way to efficiently remove illicit drugs and pharmaceuticals from wastewater. *Environ. Toxicol. Pharmacol.*, *39*(2), 483–488. https://doi.org/10.1016/j.etap.2014.12.016

Magureanu, M., Mandache, N. B., & Parvulescu, V. I. 2015. Degradation of pharmaceutical compounds in water by non-thermal plasma treatment. *Water Res.*, *81*, 124–136. https://doi.org/10.1016/j.watres.2015.05.037

Majhi, D., Samal, P. K., Das, K., Gouda, S. K., Bhoi, Y. P., & Mishra, B. G. 2019. α-NiS/Bi_2O_3 nanocomposites for enhanced photocatalytic degradation of tramadol. *ACS Appl. Nano Mater.*, *2*(1), 395–407. https://doi.org/10.1021/acsanm.8b01974

Malik, M. A. 2010. Water purification by plasmas: Which reactors are most energy efficient? *Plasma Chem. Plasma Process.*, *30*(1), 21–31. https://doi.org/10.1007/s11090-009-9202-2

Malik, M. A., Ghaffar, A., & Malik, S. A. 2001. Water purification by electrical discharges. *Plasma Sources Sci. Technol.*, *10*(1), 82–91. https://doi.org/10.1088/0963-0252/10/1/311

Margot, J., Rossi, L., Barry, D. A., & Holliger, C. 2015. A review of the fate of micropollutants in wastewater treatment plants. *Wiley Interdisciplinary Reviews: Water*, *2*(5), 457–487. https://doi.org/10.1002/wat2.1090

Matzek, L. W., & Carter, K. E. 2016. Activated persulfate for organic chemical degradation: A review. *Chemosphere*, *151*, 178–188. https://doi.org/10.1016/j.chemosphere.2016.02.055

Mena, I. F., Diaz, E., Rodriguez, J. J., & Mohedano, A. F. 2021. An overview of ionic liquid degradation by advanced oxidation processes. *Crit. Rev. Environ. Sci. Techn.*, *0*(0), 1–44. https://doi.org/10.1080/10643389.2021.1896273

Miklos, D. B., Remy, C., Jekel, M., Linden, K. G., Drewes, J. E., & Hübner, U. 2018. Evaluation of advanced oxidation processes for water and wastewater treatment – A critical review. *Water Res. 139*, 118–131. https://doi.org/10.1016/j.watres.2018.03.042

Miotto, K., Cho, A. K., Khalil, M. A., Blanco, K., Sasaki, J. D., & Rawson, R. 2017. Trends in tramadol: Pharmacology, metabolism, and misuse. *Anesth. Analg.*, *124*(1), 44–51. https://doi.org/10.1213/ANE.0000000000001683

Monteil, H., Oturan, N., Péchaud, Y., & Oturan, M. A. 2020. Electro-Fenton treatment of the analgesic tramadol: Kinetics, mechanism and energetic evaluation. *Chemosphere*, *247*. https://doi.org/10.1016/j.chemosphere.2020.125939

Morales, D. R., & Morris, A. D. 2015. Metformin in cancer treatment and prevention. *Annu. Rev. Med.*, *66*, 17–29. https://doi.org/10.1146/annurev-med-062613-093128

Neamţu, M., Grandjean, D., Sienkiewicz, A., Le Faucheur, S., Slaveykova, V., Colmenares, J. J. V., Pulgarín, C., & De Alencastro, L. F. 2014. Degradation of eight relevant micropollutants in different water matrices by neutral photo-Fenton process under UV_{254} and simulated solar light irradiation - A comparative study. *Appl. Cat. B: Environ.*, *158–159*, 30–37. https://doi.org/10.1016/j.apcatb.2014.04.001

Neta, P., Madhavan, V., Zemel, H., & Fessenden, R. W. 1977. Rate constants and mechanism of reaction of sulfate radical with aromatic compounds. *J. Am. Chem. Soc.*, *99*(1), 163–164. https://doi.org/10.1021/ja00443a030

Niemuth, N. J., & Klaper, R. D. 2018. Low-dose metformin exposure causes changes in expression of endocrine disruption-associated genes. *Aquat. Toxicol.*, *195*, 33–40. https://doi.org/10.1016/j.aquatox.2017.12.003

Nijdam, S., Van Veldhuizen, E., Bruggeman, P., & Ebert, U. 2012. *An introduction to nonequilibrium plasmas at atmospheric pressure*.

Okano, A., Isley, N. A., & Boger, D. L. 2017. Peripheral modifications of [Ψ[CH$_2$NH]Tpg^4]vancomycin with added synergistic mechanisms of action provide durable and potent antibiotics. *Proc. Natl. Acad. Sci. USA*, *114*(26), E5052–E5061. https://doi.org/10.1073/pnas.1704125114

Royal Society of Chemistry (Great Britain). 2013. The Merck index: an encyclopedia of chemicals, drugs, and biologicals (Ed. O'Neil, M. J.; Fifteenth edition).

Orata, E. D., De Leon, P. D. P., & Doma, B. T. 2019. Degradation of metformin in water using electro-Fenton process. *IOP Conf. Ser.: Earth Environ. Sci.*, *344*(1). https://doi.org/10.1088/1755-1315/344/1/012007

Patel, M., Kumar, R., Kishor, K., Mlsna, T., Pittman, C. U., & Mohan, D. 2019. Pharmaceuticals of emerging concern in aquatic systems: Chemistry, occurrence, effects, and removal methods. *Chem. Rev.*, *119*(6), 3510–3673. https://doi.org/10.1021/acs.chemrev.8b00299

Plechkova, N. V., & Seddon, K. R. 2008. Applications of ionic liquids in the chemical industry. *Chem. Soc. Rev.*, *37*(1), 123–150. https://doi.org/10.1039/B006677J

Plhalova, L., Sehonova, P., Blahova, J., Doubkova, V., Tichy, F., Faggio, C., Berankova, P., & Svobodova, Z. 2020. Evaluation of tramadol hydrochloride toxicity to juvenile zebrafish - Morphological, antioxidant and histological responses. *Appl. Sci. (Switzerland)*, *10*(7). https://doi.org/10.3390/app10072349

Podhorecka, M., Ibanez, B., & Dmoszyńska, A. 2017. Metformin-its potential anti-cancer and anti-aging effects. *Advan. Hyg. Experim. Med.*, *71*, 170–175. https://doi.org/10.5604/01.3001.0010.3801

Preis, S., Panorel, I. C., Kornev, I., Hatakka, H., & Kallas, J. 2013. Pulsed corona discharge: The role of ozone and hydroxyl radical in aqueous pollutants oxidation. *Water Sci. Technol.*, *68*(7), 1536–1542. https://doi.org/10.2166/wst.2013.399

Priyadarshini, M., Das, I., Ghangrekar, M. M., & Blaney, L. 2022. Advanced oxidation processes: Performance, advantages, and scale-up of emerging technologies. In *J. Environ. Manag.* 316. https://doi.org/10.1016/j.jenvman.2022.115295

Qi, C., Liu, X., Ma, J., Lin, C., Li, X., & Zhang, H. 2016. Activation of peroxymonosulfate by base: Implications for the degradation of organic pollutants. *Chemosphere*, *151*, 280–288. https://doi.org/10.1016/j.chemosphere.2016.02.089

Quintão, F. J. O., Freitas, J. R. L., de Fátima Machado, C., Aquino, S. F., de Queiroz Silva, S., & de Cássia Franco Afonso, R. J. 2016. Characterization of metformin by-products under photolysis, photocatalysis, ozonation and chlorination by high-performance liquid chromatography coupled to high-resolution mass spectrometry. *Rapid Commun. Mass Sp.*, *30*(21), 2360–2368. https://doi.org/10.1002/rcm.7724

Radbruch, L., Glaeske, G., Grond, S., Münchberg, F., Scherbaum, N., Storz, E., Tholen, K., Zagermann-Muncke, P., Zieglgänsberger, W., Hoffmann-Menzel, H., Greve, H., & Cremer-Schaeffer, P. 2013. Topical review on the abuse and misuse potential of tramadol and tilidine in Germany. *Subst. Abus.* 34, 313–320. https://doi.org/10.1080/08897077.2012.735216

Riba, J. R., Morosini, A., & Capelli, F. 2018. Comparative study of ac and positive and negative dc visual corona for sphere-plane gaps in atmospheric air. *Energies*, *11*(10). https://doi.org/10.3390/en11102671

Richardson, S. D., & Kimura, S. Y. 2017. Emerging environmental contaminants: Challenges facing our next generation and potential engineering solutions. *Environ. Technol. Innov.*, *8*, 40–56. https://doi.org/10.1016/j.eti.2017.04.002

Romero, A., Santos, A., Tojo, J., & Rodríguez, A. 2008. Toxicity and biodegradability of imidazolium ionic liquids. *J. Hazard. Mater.*, *151*(1), 268–273. https://doi.org/10.1016/J.JHAZMAT.2007.10.079

Saeedi, P., Petersohn, I., Salpea, P., Malanda, B., Karuranga, S., Unwin, N., Colagiuri, S., Guariguata, L., Motala, A. A., Ogurtsova, K., Shaw, J. E., Bright, D., & Williams, R. 2019. Global and regional diabetes prevalence estimates for 2019 and projections for 2030 and 2045: Results from the International Diabetes Federation Diabetes Atlas, 9th edition. *Diabetes Res. Clin. Pract.*, *157*, 107843. https://doi.org/10.1016/j.diabres.2019.107843

Scheurer, M., Michel, A., Brauch, H. J., Ruck, W., & Sacher, F. 2012. Occurrence and fate of the antidiabetic drug metformin and its metabolite guanylurea in the environment and during drinking water treatment. *Water Res.*, *46*(15), 4790–4802. https://doi.org/10.1016/j.watres.2012.06.019

Sehested, K., Holcman, J., Bjergbakke, E., & Hart, E. J. 1984. A pulse radiolytic study of the reaction OH + O_3 in aqueous medium. *J. Physic. Chem.*, *88*(18), 4144–4147. https://doi.org/10.1021/j150662a058

Sehonova, P., Plhalova, L., Blahova, J., Berankova, P., Doubkova, V., Prokes, M., Tichy, F., Vecerek, V., & Svobodova, Z. 2016. The effect of tramadol hydrochloride on early life stages of fish. *Environ. Toxicol. Pharmacol.*, *44*, 151–157. https://doi.org/10.1016/j.etap.2016.05.006

Shang, K., Li, W., Wang, X., Lu, N., Jiang, N., Li, J., & Wu, Y. 2019. Degradation of p-nitrophenol by DBD plasma/Fe^{2+}/persulfate oxidation process. *Sep. Pur. Technol.*, *218*, 106–112. https://doi.org/10.1016/j.seppur.2019.02.046

Shang, K., Morent, R., Wang, N., Wang, Y., Peng, B., Jiang, N., Lu, N., & Li, J. 2022. Degradation of sulfamethoxazole (SMX) by water falling film DBD Plasma/Persulfate: Reactive species identification and their role in SMX degradation. *Chem. Eng. J.*, *431*. https://doi.org/10.1016/j.cej.2021.133916

Shao, Y., Pang, Z., Wang, L., & Liu, X. 2019. Efficient degradation of acesulfame by ozone/peroxymonosulfate advanced oxidation process. *Molecules*, *24*(16). https://doi.org/10.3390/molecules24162874

Sonntag, C. von Clemens, & von Gunten, U. 2012. *Chemistry of ozone in water and wastewater treatment: from basic principles to applications*. IWA Publishing.

Staehelin, J., & Holgné, J. 1982. Decomposition of ozone in water: Rate of initiation by hydroxide ions and hydrogen peroxide. *Environ. Sci. Technol.* 16, 676–681. https://doi.org/10.1021/es00104a009

Straub, J. O., Caldwell, D. J., Davidson, T., D'Aco, V., Kappler, K., Robinson, P. F., Simon-Hettich, B., & Tell, J. 2019. Environmental risk assessment of metformin and its transformation product guanylurea. I. Environmental fate. *Chemosphere*, *216*, 844–854. https://doi.org/10.1016/j.chemosphere.2018.10.036

Tikker, P., Kornev, I., & Preis, S. 2020. Oxidation energy efficiency in water treatment with gas-phase pulsed corona discharge as a function of spray density. *J. Electrostat.*, *106*, 103466. https://doi.org/10.1016/j.elstat.2020.103466

Tuc Dinh, Q., Alliot, F., Moreau-Guigon, E., Eurin, J., Chevreuil, M., & Labadie, P. 2011. Measurement of trace levels of antibiotics in river water using on-line enrichment and triple-quadrupole LC-MS/MS. *Talanta*, *85*(3), 1238–1245. https://doi.org/10.1016/j.talanta.2011.05.013

Tyrovola, K., & Diamadopoulos, E. 2005. Bromate formation during ozonation of groundwater in coastal areas in Greece. *Desalination*, *176*(1–3), 201–209. https://doi.org/10.1016/j.desal.2004.10.018

Umar, M., Roddick, F., Fan, L., & Aziz, H. A. 2013. Application of ozone for the removal of bisphenol A from water and wastewater - A review. *Chemosphere*, *90*(8), 2197–2207. https://doi.org/10.1016/j.chemosphere.2012.09.090

von Gunten, U. 2003. Ozonation of drinking water: Part II. Disinfection and by-product formation in presence of bromide, iodide or chlorine. *Water Res.*, *37*(7), 1469–1487. https://doi.org/10.1016/S0043-1354(02)00458-X

Wang, J., Tian, Z., Huo, Y., Yang, M., Zheng, X., & Zhang, Y. 2018. Monitoring of 943 organic micropollutants in wastewater from municipal wastewater treatment plants with secondary and advanced treatment processes. *J. Environ. Sci. (China)*, *67*, 309–317. https://doi.org/10.1016/j.jes.2017.09.014

Wang, J., & Wang, S. 2018. Activation of persulfate (PS) and peroxymonosulfate (PMS) and application for the degradation of emerging contaminants. *Chem. Eng. J. 334*, 1502–1517. https://doi.org/10.1016/j.cej.2017.11.059

Wardman, P. 1989. Reduction potentials of one electron couples involving free radicals in aqueous solution. *J. Phys. Chem. Ref. Data*, *18*(4), 1637–1755. https://doi.org/10.1063/1.555843

Xu, R., Qin, W., Tian, Z., He, Y., Wang, X., & Wen, X. 2020. Enhanced micropollutants removal by nanofiltration and their environmental risks in wastewater reclamation: A pilot-scale study. *Sci. Total Environ.*, *744*, 140954. https://doi.org/10.1016/j.scitotenv.2020.140954

Yang, Y., Jiang, J., Lu, X., Ma, J., & Liu, Y. 2015. Production of sulfate radical and hydroxyl radical by reaction of ozone with peroxymonosulfate: A novel advanced oxidation process. *Environ. Sci. Technol. 49,* 7330-7339*.* https://doi.org/10.1021/es506362e

Yusuf, A., Amusa, H. K., Eniola, J. O., Giwa, A., Pikuda, O., Dindi, A., & Bilad, M. R. 2023. Hazardous and emerging contaminants removal from water by plasma-based treatment: A review of recent advances. *Chem. Eng. J. Adv.*, *14*. https://doi.org/10.1016/j.ceja.2023.100443

Zuccato, E., Castiglioni, S., Bagnati, R., Melis, M., & Fanelli, R. 2010. Source, occurrence and fate of antibiotics in the Italian aquatic environment. *J. Hazard. Mater.*, *179*(1–3), 1042–1048. https://doi.org/10.1016/j.jhazmat.2010.03.110

Acknowledgements

Abstract

Development of oxidation technology in water treatment: pulsed corona discharge plasma combined with peroxocompounds

Advanced oxidation processes (AOPs) are actively studied as means of efficient removal of recalcitrant compounds in water treatment. These processes consist of *in-situ* generation and the use of strong oxidants, such as hydroxyl, sulfate, or chlorine radicals. Amongst the emerging AOPs, the application of persulfate and non-thermal plasma (NTP) processes possesses the most promising potential. Pulsed corona discharge (PCD) applied to the water dispersed in the discharge zone in droplets, jets and films outperforms other types of plasma, attracting interest also in the activation of persulfates. Some part of energy in plasma treatment is believed to be radiated without proper utilisation, resulting in a waste of energy. Thus, the active plasma species may activate extrinsic peroxocompounds, e.g., persulfates, resulting in additional or alternative reactive species with both strong oxidation potential and longer lifetimes.

The development of AOPs is necessary for the effective degradation of micropollutants in water due to their incomplete removal at conventional wastewater treatment plants. The work considers the degradation of anti-diabetic metformin (MTF), analgesic tramadol (TMD), antibiotic vancomycin (VMN), and imidazolium-based ionic liquids (ILs). These liquids include 1-ethyl-3-methylimidazolium chloride ([Emim][Cl]), 1-octyl-3-methylimidazolium chloride ([Omim][Cl]), and 1-ethyl-3-methylimidazolium bromide ([Emim][Br]). The release of these substances into the environment may have potential adverse effects on aquatic life.

The study aimed to evaluate the degradation of target compounds in unassisted PCD and in PCD/oxidant combinations. The effects of operating parameters, pH, high voltage pulse repetition frequency, and doses of extrinsic oxidants were evaluated. Peroxydisulfate (PDS), peroxymonosulfate (PMS), and hydrogen peroxide (HP) were used as extrinsic oxidants. The PCD/oxidant combinations were compared in their performance to conventional UV/oxidant combinations. The applicability of the studied methods was evaluated according to their energy efficiencies dependent on the oxidant dosing at their costs.

The application of unassisted PCD was effective for the degradation of aqueous pharmaceuticals and imidazolium-based ILs. The degradation rates followed the descending order VMN > MTF > TMD > [Emim][Cl] > [Omim][Cl] > [Emim][Br]. Similar degradation patterns were observed for MTF, TMD, VMN, and [Emim][Cl] suggesting a limitation in the amounts of reactive oxygen species (ROS) generated in PCD, which reacted fast with the target compounds. For all the compounds studied, except MTF, treatment at pH 11 significantly, by about 2-4 times increased the degradation rates due to the deprotonation of the molecules which is favourable for electrophilic hydroxyl radical attacks. However, MTF has a dissociation constant at higher pH values (pKa = 11.6–12.4), which resulted in a minor effect of alkaline pH on its degradation. Compared to [Emim][Cl], the long alkyl chain of [Omim][Cl] reduced the oxidation rate by 40%, making the imidazolium cation more recalcitrant to degradation. Bromide anions reduced the oxidation efficiency of [Emim]$^+$ by 2.8 times due to their noticeable reactivity.

A positive effect of oxidant addition in PCD/oxidant combinations was observed in MTF and VMN degradation. For instance, the energy-related reaction rate constant of MTF degradation increased from 3.1 to 7.9 m^3 kWh^{-1} at an MTF/PDS molar ratio of 1/10. In VMN oxidation, the addition of PDS and PMS also increased the oxidation rates by about 1.5 times. The difference in activation pathways of PDS and PMS, as well as in the types of resultant active species, provides better performance of PMS in combination with PCD in both the target compound oxidation rate and its mineralization. The activation of PMS is slower than that of PDS due to the higher O-O bond dissociation energy, which may play an important role in preventing radical recombination and scavenging.

The addition of PDS and PMS showed small to moderate negative effects (5−30%) in TMD and ILs degradation rates with some exceptions at low doses. Persulfate ions and sulfate radicals at elevated concentrations compete for the plasma-generated ROS capable of oxidizing TMD and ILs, thereby reducing the overall effectiveness of the treatment. The presence of sulfate radicals in PCD/persulfate combinations was confirmed by using ethanol and *tert*-butanol as radical scavengers. The presence of sulfate radicals in PCD/persulfate treated solutions together with the poor effect of persulfate on the ILs degradation rate confirms the hypothesis that PCD-generated ROS are consumed by persulfates producing sulfate radicals as substitutes with little change in ILs degradation rate. Therefore, the treatment of compounds with high reactivity with sulfate radicals may be enhanced by the addition of persulfate.

UV/oxidant combinations showed a pronounced dependence of the oxidation rate on the pollutant/oxidant molar ratio varying from 1/1 to 1/10: the reaction rate constants grew up to 8.0, 2.5, and 1.9 times for MTF, TMD, and VMN, respectively. Similarly, for ILs degradation, reaction rates increased up to 6-fold with PDS contributing to better oxidation at near-neutral conditions and PMS showing better performance at alkaline pH. However, complete degradation of ILs was only achieved at high doses of the oxidants. The degradation rates of ILs followed a pattern consistent with the one observed in PCD treatment, having the degradation of [Omim][Cl] and [Emim][Br] hindered by the long alkyl chain and the bromide anion, respectively.

For pharmaceuticals, the unassisted PCD surpassed UV/oxidant combinations in energy efficiency reaching 75, 81, and 126 $mmol$ kWh^{-1} for MTF, TMD, and VMN, respectively. In ILs degradation, unassisted PCD showed energy efficiencies comparable to or superior to UV/oxidant combinations. The addition of peroxocompounds verified the potential to improve the rates of oxidation and mineralization of target compounds, but not the energy efficiency. Moreover, the use of chemicals makes the combined treatment less convenient in terms of chemical delivery, storage, and handling.

The insights obtained from this doctoral research advance the ongoing development of pulsed corona discharge application and support its use as an energy-efficient approach to the treatment of persistent micropollutants in water.

Lühikokkuvõte

Oksüdatsioonitehnoloogia arendamine veepuhastuses: peroksoühenditega kombineeritud impulss koroona elektrilahendus

Süvaoksüdatsiooniprotsesse (ingl *Advanced oxidation processes*, AOPs) uuritakse aktiivselt kui lahendusi, mille abil saab veepuhastuses tõhusalt eemaldada raskesti lagundatavaid ühendeid. Need protsessid põhinevad tugevate oksüdantide, näiteks hüdroksüül-, sulfaat- või kloorradikaalide kohapealsel tekitamisel ja kasutamisel. Arenevate AOP-de hulgas on potentsiaalselt kõige paljulubavam persulfaadi ja mittetermilise plasma protsesside rakendamine. Impulss koroona elektrilahendus (ingl *Pulsed corona discharge*, PCD), mida rakendatakse veele, mis on hajutatud elektrilahenduse tsoonis tilkadeks, jugadeks ja kiledeks, ületab teisi plasmatüüpe energia efektiivsuses. Seetõttu PCD-töötlus äratab huvi ka persulfaatide aktiveerimisel. Arvatakse, et plasmakäitluses osa energiast kiirgub ilma otstarbeka kasutamiseta, mille tulemuseks on energia raiskamine. Seega võivad aktiivsed plasma osakesed aktiveerida peroksoühendeid, nt persulfaate, mille tulemuseks on täiendavad või alternatiivsed reaktiivsed osakesed, millel on nii tugev oksüdatsioonipotentsiaal kui ka pikem eluiga.

Süvaoksüdatsiooniprotsesside arendamine on vajalik vees sisalduvate mikrosaasteainete tõhusaks lagundamiseks, kuna nende eemaldamine tavapärastes reoveepuhastusjaamades on mittetäielik. Doktoritöös käsitletakse diabeedivastase metformiini (MTF), valuvaigistava tramadooli (TMD), antibiootilise vankomütsiini (VMN) ja imidasooliumipõhiste ioonsete vedelike (ingl *Ionic liquids*, ILs) lagundamist. Ioonsete vedelike hulka kuuluvad 1-etüül-3-metüüllimidasooliumkloriid ([Emim][Cl]), 1-oktüül-3-metüüllimidasooliumkloriid ([Omim][Cl]) ja 1-etüül-3-metüüllimidasooliumbromiid ([Emim][Br]). Nende ainete sattumine keskkonda võib avaldada potentsiaalselt kahjulikku mõju vee-elustikule.

Uuringu eesmärgiks oli hinnata sihtühendite lagundamist PCD-töötluse ja PCD/oksüdandi kombinatsioonide kasutamisel. Hinnati tööparameetrite, pH, kõrgepinge impulsside kordussageduse ja väliste oksüdantide dooside toimet. Väliste oksüdantidena kasutati peroksüdisulfaati (PDS), peroksümonosulfaati (PMS) ja vesinikperoksiidi (HP). PCD/oksüdandi kombinatsioone võrreldi nende efektiivsuse poolest tavaliste UV/oksüdandi kombinatsioonidega. Uuritud meetodite rakendatavust hinnati vastavalt nende energiatõhususele sõltuvalt oksüdeerija koguse kuludest.

PCD-töötluse rakendamine ilma peroksoühenditeta oli efektiivne ravimite ja imidasooliumipõhiste IL-de lagundamisel vees. Lagundamiskiirused kahanesid järgnevalt: VMN > MTF > TMD > [Emim][Cl] > [Omim][Cl] > [Emim][Br]. Metformiini, TMD-i, VMN-i ja [Emim][Cl]-i puhul täheldati sarnaseid lagundamismustreid, mis viitab reaktiivsete hapnikuosakeste (ingl *Reactive oxygen species*, ROS) koguste piiratusele sihtühenditega reageerimisel PCD-töötluses. Kõigi uuritud ühendite puhul, välja arvatud MTF, suurendas töötlemine pH 11 juures lagundamiskiirust umbes 2–4 korda. See oli tingitud molekulide deproteerimisest, mis soodustavad elektrofiilsete hüdroksüülradikaalide rünnakuid. Teisalt on MTF-i dissotsiatsioonikonstant (pKa = 11,6–12,4) kõrgem kui uuritud pH väärtus, mistõttu leeliseline pH mõjutas ühendi lagundamist vähe. Võrreldes [Emim][Cl]-ga, vähendas [Omim][Cl]-i pikk alküülahel oksüdatsioonikiirust 40% võrra, muutes [Omim]$^+$ lagundamise suhtes

vastupidavamaks. Bromiidi anioonid vähendasid [Emim]⁺ oksüdatsiooni tõhusust 2,8 korda nende märgatava reaktsioonivõime tõttu.

Oksüdandi lisamise positiivset mõju PCD/oksüdandi kombinatsioonides täheldati MTF-i ja VMN-i lagundamisel. Näiteks MTF/PDS molaarsuhtel 1/10 sihtühendi lagundamise reaktsioonikiiruse konstant suurenes $3,1~m^3~kWh^{-1}$ kuni $7,9~m^3~kWh^{-1}$. VMN-i oksüdeerimisel suurendas PDS-i ja PMS-i lisamine oksüdeerimiskiirust samuti umbes 1,5 korda. PDS ja PMS aktiveerimisviiside erinevus, kui ka saadud aktiivsete osakeste tüüpide erinevus, tagavad PMS-i parema tulemuslikkuse kombinatsioonis PCD-töötlusega nii sihtühendi oksüdatsioonikiiruse kui ka selle mineraliseerimise osas. PMS-i aktiveerimine on aeglasem kui PDS-i aktiveerimine kõrgema O-O sideme dissotsiatsioonienergia tõttu, mis võib mängida olulist rolli radikaalide rekombinatsiooni ja püüdmise vältimisel.

Välja arvatud mõned erandid väikeste dooside puhul, PDS-i ja PMS-i lisamine näitas väikest kuni mõõdukat negatiivset mõju (5–30%) TMD-i ja IL-de lagundamisele. Persulfaatioonid ja sulfaatradikaalid konkureerivad kõrgendatud kontsentratsioonidel plasmas tekkivate ROS-de pärast, mis on võimelised TMD-i ja IL-de oksüdeerima, vähendades seeläbi töötlemise üldist tõhusust. Sulfaatradikaalide olemasolu PCD/persulfaadi kombinatsioonides kinnitati, kasutades etanooli ja *tert*-butanooli radikaalide püüduritena. Sulfaatradikaalide esinemine PCD/persulfaadiga töödeldud lahustes koos persulfaadi vähese mõjuga ioonsete vedelike lagunemise kiirusele kinnitab hüpoteesi, et PCD-i poolt genereeritud ROS reageerivad persulfaatidega, tekitades asendajatena sulfaatradikaale, sealjuures IL-de lagunemise kiirus muutub vähe. Seetõttu võib persulfaadi lisamine tõhustada ühendite töötlemist, millel on kõrge reaktsioonivõime sulfaatradikaalidega.

UV/oksüdandi kombinatsioonid näitasid oksüdatsioonikiiruse tugevat sõltuvust sihtühendi ja oksüdandi molaarsest suhtest, kui suhe varieerus vahemikus 1/1 kuni 1/10. Metformiini, TMD-i ja VMN-i puhul reaktsioonikiiruse konstandid kasvasid vastavalt 8, 2,5 ja 1,9 korda. Samamoodi suurenesid reaktsioonikiirused ioonsete vedelike lagundamisel kuni kuus korda, kusjuures PDS aitas kaasa paremale oksüdeerimisele neutraalsetes tingimustes ja PMS näitas paremaid tulemusi leeliselise pH juures. Siiski saavutati IL-de täielik lagundamine ainult oksüdeerijate suurte dooside korral. Ioonsete vedelike lagundamiskiirused järgisid PCD-töötlusel täheldatud viisi, sealjuures [Omim][Cl]-i ja [Emim][Br]-i lagundamist takistasid vastavalt pikk alküülahel ja bromiidi anioon.

Uuritud ravimite puhul ületas PCD-töötlus UV/oksüdandi kombinatsioone energiatõhususe poolest, saavutades vastavalt 75, 81 ja 126 $mmol~kWh^{-1}$ MTF-i, TMD-i ja VMN-i puhul. Ioonsete vedelike lagundamisel näitas PCD-töötlus energiatõhusust, mis oli võrreldav või parem kui UV/oksüdandi kombinatsioonidel. Peroksoühendite lisamine tõestas potentsiaali parandada sihtühendite oksüdatsiooni ja mineraliseerimise kiirust, kuid mitte energiatõhusust. Lisaks muudab kemikaalide kasutamine kombineeritud töötluse vähem mugavaks kemikaalide manustamise, ladustamise ja käitlemise seisukohalt.

Doktoritöö tulemusena saadud teadmised aitavad edasi arendada impulss koroona elektrilahenduse rakendamist ning toetavad selle kasutamist energiatõhusa meetodina püsivate mikrosaasteainete lagundamisel veepuhastuses.

Appendix 1

ITIT

Persulfate contribution to photolytic and pulsed corona discharge oxidation of metformin and tramadol in water

Dmitri Nikitin [a], Balpreet Kaur [b], Sergei Preis [a], Niina Dulova [a],*

[a] Department of Materials and Environmental Technology, Tallinn University of Technology, Ehitajate tee 5, 19086 Tallinn, Estonia
[b] Department of Chemistry, University of Jyväskylä, P.O. Box 35, Survontie 9 B, FI-40014 Jyväskylä, Finland

ABSTRACT

Degradation and mineralization of antidiabetic metformin (MTF) and opioid tramadol (TMD) in water were studied in UV photolytic oxidation and pulsed corona discharge (PCD) combined with extrinsic persulfate (PS) as UV/PS and PCD/PS systems. The effect of PS dose variation on the oxidation rate and efficiency was assessed. The UV/PS combination showed considerable effect in MTF and TMD removal, enhancing the removal of TOC up to 60–65% at maximum applied PS dose, thus providing the highest cost efficiency. As for the PCD/PS oxidation, the synergy was noticed for MTF, moderately increasing the oxidation rate and mineralization at somewhat increased expense. The PS addition to PCD treatment, however, demonstrated no effect on TMD oxidation. The highest energy efficiency in MTF and TMD degradation was thus showed by non-assisted PCD treatment with an energy yield at 90% conversion of the target compound of 5.6 and 13 g kW^{-1} h^{-1}, respectively, confirming its practical applicability. The effective mineralization of the target compounds in persulfate photolysis makes it promising for use in advanced water purification. To assess the environmental safety of the studied oxidation processes, the acute toxicity of the treated MTF and TMD solutions to luminous bacteria (*Vibrio fischeri*) was examined.

1. Introduction

An increased production and consumption of pharmaceutical products results in their accumulation in surface and ground waters, as well as in soils, causing cumulative effects in aquatic organisms and humans (Patel et al., 2019). Metformin (MTF) and tramadol (TMD) are typical medicines commonly found in the environment (Lindim et al., 2016).

Metformin is the common drug used in the type 2 diabetes treatment with a global annual production of more than 30,000 tons (Global Metformin Hydrochloride Market, 2019). MTF has been detected worldwide in surface waters at ng L^{-1} to μg L^{-1} concentrations dependent on the burden on a water body (Scheurer et al., 2012; Blair et al., 2013; Houtman et al., 2014; Kong et al., 2015). For example, the median concentration of MTF in the influents to three wastewater treatment plants (WWTPs) in Germany comprised as high as 112 μg L^{-1} (Briones et al., 2016). Despite the low acute toxicity of MTF (Jacob et al., 2020), it acts as an endocrine-disruptor to non-target organisms at environmentally relevant concentrations (Niemuth and Klaper, 2015, 2018; Elizalde-Velázquez and Gómez-Oliván, 2020).

Tramadol is an opioid analgesic to treat moderate to severe acute or chronic pain. Worldwide consumption of medical tramadol increased from 290 tons in 2006 to 424 tons in 2012 (Radbruch et al., 2013), inducing, however, cytotoxic and genotoxic effects (Antonopoulou et al., 2020). Despite the low consumption, it is one of the most frequently detected compounds in concentrations ranging from ng L^{-1} to μg L^{-1} (Kostanjevecki et al., 2019; Golovko et al., 2021). Tramadol poorly degrades at WWTPs reaching only 40% removal (Lindim et al., 2016), having adverse effects on aquatic life (Sehonova et al., 2016; Ložek et al., 2019; Bachour et al., 2020; Plhalova et al., 2020).

Since WWTPs insufficiently remove MTF, TMD, their metabolites and by-products, the need for an effective and affordable treatment technology is obvious (Margot et al., 2015). Advanced oxidation processes (AOPs) removing recalcitrant contaminants by means of highly reactive non-selective hydroxyl radicals (HO$^•$) present a method of choice (Kulik et al., 2007; Homem and Santos, 2011; Ali et al., 2018.), differing in the way hydroxyl radicals are generated. Treatment methods using highly reactive sulfate radicals (SO$_4^{•-}$) also belong to AOPs having a longer lifespan than hydroxyl radical, therefore having more chances for useful utilization (Guerra-Rodríguez et al., 2018). In these processes, persulfate (PS) and peroxymonosulfate (PMS) anions are activated by

* Corresponding author.
E-mail address: niina.dulova@taltech.ee (N. Dulova).

heat, radiation, ultrasound, transition metal ions and oxides (Guerra-Rodríguez et al., 2018; Wang and Wang, 2018).
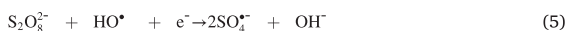
Little data are available on the oxidation efficiency of MTF and TMD in water with the UV/PS combination. Although high efficiency of MTF removal was shown by UV/H$_2$O$_2$ (Maćerak et al., 2018), UV/Fe^{2+} (Aseman-Bashiz and Sayyaf, 2020), UV/PMS (Karimian et al., 2020), UV/TiO$_2$ (Chinnaiyan et al., 2019), UV/TiO$_2$-ZrO$_2$ (Carbuloni et al., 2020), electro-Fenton system (Orata et al., 2019), and electrochemically activated PS (Aseman-Bashiz and Sayyaf, 2020). In the case of TMD, effective degradation was achieved by photocatalysis (Antonopoulou and Konstantinou, 2016; Majhi et al., 2019), Fenton process (Mackuľak et al., 2016), electro-Fenton system (Monteil et al., 2020), and electrochemical oxidation (Ghalwa et al., 2014; Lütke Eversloh et al., 2015). However, high energy consumption makes most of AOPs economically unfeasible (Taoufik et al., 2021).

Pulsed corona discharge (PCD) has shown promising results in removing recalcitrant contaminants with low energy consumption exceeding ozonation for up to three times in terms of energy efficiency (Preis et al., 2013). The short-time high-voltage electric discharge pulses are applied in air directly to water dispersed in the form of droplets, jets and films. This configuration has an advantage of high mass transfer due to the short distance reactive species need to travel in the gas phase before diffusion into the water phase, resulting in higher energy efficiency among other plasma types (Malik, 2010). Accordingly, hydroxyl radicals formed at the gas-liquid interface are utilized for direct oxidation of contaminants (Ajo et al., 2017). Other reactive oxygen species produced in the discharge, such as atomic oxygen, ozone, hydrogen peroxide and other reactive species, also contribute to the oxidation (Eqs. 1–3).

$$O_2 \ + \ e^- \rightarrow 2O^\bullet \ + \ e^- \tag{1}$$

$$O^\bullet \ + \ O_2 \ + \ O_2 \ (O_3 \ or \ N_2) \rightarrow O_3 \ + \ O_2 \ (O_3 \ or \ N_2) \tag{2}$$

$$H_2O \ + \ e^- \rightarrow HO^\bullet \ + \ H^\bullet \ + \ e^- \tag{3}$$
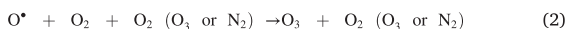
Previously, PCD showed high efficiency in the removal of pharmaceuticals (Derevshchikov et al., 2021), phenols and bisphenols (Wang et al., 2019), as well as an increased rate of oxalate oxidation when persulfate was added to the system (Tikker et al., 2021). Another plasma type, dielectric barrier discharge, is actively studied for activation of persulfates and it has shown increased removal rates for numerous aqueous pollutants including atrazine, benzotriazole, and phthalates (Ahmadi et al., 2020; Wu et al., 2020; Wang et al., 2021).

To the best of the authors' knowledge, PCD/PS oxidation has not yet been studied for its efficiency in the removal of aqueous micropollutants. Well-studied UV/PS systems showed the ability to effectively activate PS by the fission of O-O bond forming two sulfate radicals (Eq. 4) (Khan et al., 2014; Khan et al., 2017; Wang and Wang, 2018). While PCD has several potential ways to activate PS, including UV irradiation, reactions with active species, and interaction with discharge electrons (Eqs. 4–7) (Shang et al., 2019), their contribution to PS activation in PCD/PS system is currently unknown.

$$S_2O_8^{2-} \ \overset{h\nu}{\rightarrow} \ 2SO_4^{\bullet-} \tag{4}$$

$$S_2O_8^{2-} \ + \ HO^\bullet \ + \ e^- \rightarrow 2SO_4^{\bullet-} \ + \ OH^- \tag{5}$$

$$S_2O_8^{2-} \ + \ HO^\bullet \rightarrow SO_4^{\bullet-} \ + \ HSO_4^- \ + \ 0.5O_2 \tag{6}$$

$$S_2O_8^{2-} \ + \ e^- \rightarrow SO_4^{\bullet-} \ + \ SO_4^{2-} \tag{7}$$

Therefore, the present study aims to parallel, under comparable experimental conditions, the ability of UV photolysis, PCD, and especially UV/PS and PCD/PS combinations to degrade and mineralize contaminants of emerging concern. MTF and TMD were selected as target compounds in order to compare and analyze the effect of

Table 1
Technical parameters of the PCD reactor.

Parametr	Value
Reactor parameters	
Reactor full volume, L	110
Perforated plate size, mm × mm	500 × 30
Number of perforations	51
Diameter of perforations, mm	1
Water flow rate, L min^{-1}	2–28.5
Spray density, m s^{-1}	0.002–0.0243
Plasma zone volume, m^3	0.013
Contact surface area (at flow rate of 1 m^3 h^{-1}), m^{-1}	91.9
Electrode configuration	
High voltage wire length, m	20
Wire diameter, mm	0.5
Distance between electrodes and grounded plate, mm	18
Distance between high-voltage electrodes, mm	30
Generator characteristics	
Pulse repetition frequency, pps	50–880
Output power, W	9–123.2
Peak voltage, kV	18
Peak current, A	380
Current pulse duration, ns	100
Pulse energy, J	0.14–0.18

compound structure on the effectiveness of oxidation by the studied treatment methods. The effect of the operating parameters such as pH value and persulfate concentration on the efficiency of the oxidation processes was evaluated. In addition, the role of hydroxyl and sulfate radicals in the degradation of the target compounds in UV/PS and PCD/PS combinations was estimated. To assess the formation of toxic intermediates, the acute toxicity of treated solutions to luminous bacteria (*Vibrio fischeri*) was also examined.

2. Materials and methods

2.1. Chemicals

Metformin hydrochloride (C$_4$H$_{11}$N$_5$•HCl, >97%) was purchased from Alfa-Aesar. Tramadol hydrochloride (C$_{16}$H$_{25}$NO$_2$•HCl, ≥99%), potassium iodide (KI, ≥99%), sodium bicarbonate (NaHCO$_3$, 99%) and sodium sulfite (Na$_2$SO$_3$, ≥99%) were obtained from Sigma-Aldrich. Sodium persulfate (Na$_2$S$_2$O$_8$, ≥99%), tertbutyl alcohol ((CH$_3$)$_3$COH, *t*-BuOH, ≥ 99%) ethanol (C$_2$H$_6$O, EtOH, 99%), acetonitrile (CH$_3$CN, LiChrosolv®) and formic acid (CH$_2$O$_2$, 99%) were obtained from Merck KGaA.

2.2. Pulsed corona discharge equipment

The PCD experiments were conducted in a device made by Flowrox Oy (Finland) (Tikker et al., 2021) with characteristics given in Table 1. The device consists of PCD stainless steel reactor with the storage tank, pulse generator and circulation pump with the frequency regulator used to control the pump engine rotation rate (Fig. S1). The plasma reactor contains an electrode system consisting of high voltage wire electrodes, positioned horizontally between two grounded vertical parallel plates. Generator applies high voltage pulses to the electrode system at the pulse repetition frequencies regulated incrementally as shown in Table 1. The output-input ratio of pulse generator comprises 65%. Treated solution is dispersed through the perforated plate positioned above the wire electrodes at certain spray density determined as the flow rate divided by the planar cross-sectional area of the plasma zone, m s^{-1}. After passing the plasma zone, treated solution falls to a storage tank, from where it is circulated back to the top of reactor.

2.3. Photochemical equipment

Photochemical experiments were performed in batch mode in a 1-L

cylindrical glass reactor. A low-pressure mercury germicidal lamp (11 W, Philips TUV PL-S) placed in a quartz sleeve inside the reactor was used as a UVC source. According to datasheet, the input-output power of the lamp is approximately 32%. The incident photon flux at 254 nm of the lamp used in MTF and TMD oxidation comprised from 2.55×10^{-7} to 2.84×10^{-7} Einstein s^{-1} measured by ferrioxalate actinometry. The lamp was turned on at least 10 min prior to the trial to provide a constant radiation output. A water cooling jacket was used to keep the constant temperature in the reactor.

2.4. Experimental

The experiments were carried out at ambient room temperature of 22 ± 2 °C, at the initial concentration of MTF and TMD of 60.4 μM (7.8 mg L^{-1}) and 33.4 μM (8.8 mg L^{-1}), respectively, if not otherwise specified. The unadjusted pH value for MTF and TMD solutions was 6.4 $\pm$ 0.8 and 6.1 $\pm$ 0.5, respectively. For acidic (pH 3) or alkaline (pH 11) conditions, pH was regulated by adding 0.1–1 M H_2SO_4 or NaOH solutions. The effect of PS concentration in both photochemical and PCD experiments was studied varying it from 60.4 to 604 μM in MTF, and from 38 to 380 μM in TMD experiments, providing the PS to target compound molar ratio from 1 to about 11. In experiments with extrinsic PS, the oxidation reaction was quenched with ethanol added at the sample to EtOH volume ratio of 10 for HPLC-PDA and HPLC-MS analysis. For the TOC analysis, sodium sulfite was used at the Na_2SO_3 to PS molar ratio of 10.

In UV/PS oxidation trials, MTF and TMD solutions were prepared in bidistilled water and treated for 2 h with permanent stirring by means of magnetic stirrer. After dissolution of PS, the UVC-lamp inserted to the reactor initialized oxidation.

The stock solutions for PCD experiments were prepared in a 1-L volumetric flask using bidistilled water, followed by dilution to a total volume of 10 L by distilled water in the reactor tank. Pre-selected amounts of PS were dissolved in a 100-mL volumetric flask and added to the tank immediately before the start of treatment. All PCD experiments were performed at circulated water flow rate of 1 m^3 h^{-1}, and the pulse repetition frequency of 50 pps with the power input of 9 W. Plasma treatment time comprised 2 h with total energy dose of 1.8 kWh m^{-3} delivered to the treated sample. For proper sampling, the treated solutions were circulated in the reactor for four minutes after the pulse generator was turned off for equalizing the concentrations in the reactor's volume.

The energy efficiency E, g kW^{-1} h^{-1}, was calculated using equation (Eq. 8):

$$E = \frac{\Delta C \cdot V}{W} \qquad (8)$$

where ΔC – decrease of target compound concentration, g m^{-3}; V – volume of treated solution, m^3; W – energy consumption derived from the generator power output and the time of treatment, kWh.
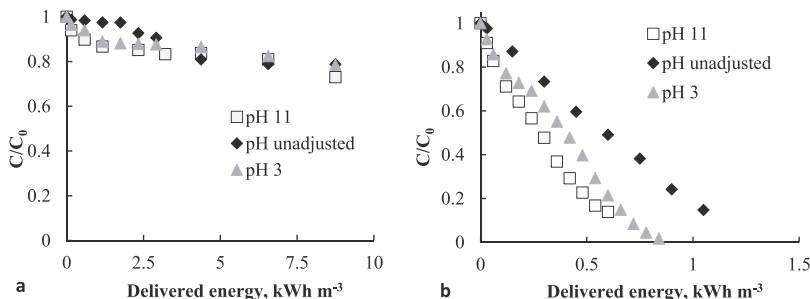
To evaluate the effect of oxidant addition on the degradation efficiency in the studied systems, a pseudo-first-order kinetics was used (Eq. 9). The apparent pseudo-first-order rate constants (k_1) were calculated from the slopes of the straight lines by plotting ln (C_t/C_0) as a function of delivered energy dose (P•t/V) through linear regression.

$$\frac{d[C]}{dt} = -\frac{k_1 \cdot P \cdot [C]}{V} \qquad (9)$$

where k_1 is the pseudo-first-order reaction rate constant, m^3 kW^{-1} h^{-1}; C is the concentration of target compound; P is the power applied in pulsed corona discharge or UV radiation, W; V is the volume of treated solution, m^3; t is the treatment time, h.

2.5. Analytical methods

Concentration of TMD was determined using a high performance liquid chromatography combined with a diode array detector (HPLC-PDA, Shimadzu, Japan) equipped with a Phenomenex Gemini (150 × 2.0 mm, 1.7 mm) NX-C18 (110 Å, 5 μm) column. The analysis was performed using an isocratic method with a mobile phase composed of 15% vol. of acetonitrile containing 0.3% of formic acid and 85% vol. of 0.3-% formic acid aqueous solution. The flow rate was kept at 0.2 mL min^{-1}. Metformin concentration was quantified using HPLC with the same eluent flow rate and chromatographic column combined with mass spectrometer (HPLC-MS, Shimadzu LC-MS, 2020). The isocratic eluent mixture was composed of 10% vol. of acetonitrile containing 0.3% of formic acid and 90% vol. of 0.3-% formic acid aqueous solution. Mass spectra were acquired in full-scan (scanning in the range of 50–500 m/z) and SIM (130 m/z) modes. The instrument was operated in positive ESI mode, and the results obtained with MS detector were handled using Shimadzu Lab Solutions software.

Total organic carbon was measured using a TOC analyzer multi N/C® 3100 (Analytik Jena, Germany) in 20-mL samples with an injection volume of 500 μL for each replicate. Solution pH was measured using a digital pH/Ion meter (Mettler Toledo S220). Utilization of persulfate was controlled by the quantification of residual PS concertation in the treated samples spectrophotometrically (Genesys 10 S, Thermo Scientific, USA) at λ = 352 nm by an excess KI reaction with residual persulfate towards the formation of I_2 (Liang et al., 2008).

The acute toxicity was examined using the Microtox® method (Model 500 Analyzer SDI) (ISO 11348–3:2007) (Kaur and Dulova, 2020). The reconstitution solution was prepared and used to activate freeze-dried *Vibrio fischeri*. To maintain the osmotic pressure of the test bacteria suspension, concentrated salt solution (2% NaCl) was used to achieve 2% salinity. The salt solution was used as control. Each toxicity test was performed in ten dilutions, and the luminescence was measured after 15 min of exposure. The bacterial luminescence inhibition (INH%) was calculated using Eqs. (10) and (11) (Jarque et al., 2016).
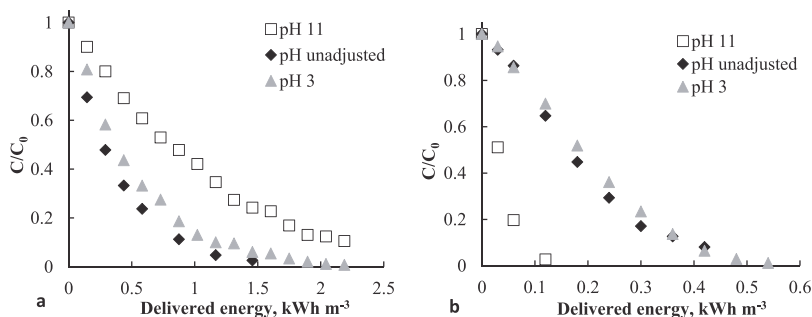

Fig. 1. UV photolysis (a) and PCD oxidation (b) of MTF at various pH ([MTF]$_0$ = 60.4 μM, UV output power 3.5 W, PCD output power 9 W).

Fig. 2. UV photolysis (a) and PCD oxidation (b) of TMD at various pH ($[TMD]_0 = 33.4$ μM, UV output power 3.5 W, PCD output power 9 W).

$$INH\% = 100 - \frac{IT_{15}}{KF \cdot IT_0} \cdot 100 \qquad (10)$$

$$KF = \frac{IC_{15}}{IC_0} \qquad (11)$$

where KF is the correction factor, IC_{15} is the luminescence intensity of control after contact time (15 min), IC_0 is the initial luminescence intensity of control sample, IT_{15} is the luminescence intensity of test sample after contact time (15 min), and IT_0 is the initial luminescence intensity of the test sample.

3. Results and discussion

3.1. Effect of pH on target compounds oxidation in UV photolysis and PCD

Oxidation experiments in UV photolysis and PCD oxidation were carried out with both target compounds in unbuffered solutions. During the UV photolysis, the pH values did not change along with all the experiments for 2 h. In contrast, the PCD oxidation resulted in noticeable, for more than two units, decrease in pH, at unadjusted initial pH conditions close to neutral. The latter can be explained by the atmospheric nitrogen oxidized to nitrates in plasma (Tikker et al., 2021). Acidic ($pH_0 = 3$) and alkaline ($pH_0 = 11$) PCD experiments showed only minor changes in pH.

The results of MTF degradation in unassisted UV photolysis at various pH are given in Fig. 1a: only 21% of MTF degraded within 2 h of treatment in acidic and unadjusted neutral media, having somewhat better, about 27%, efficacy achieved in alkaline solution. The latter is probably due to partial deprotonation of the amino moiety of MTF molecule ($pK_a = 11.6$) weakening its inductive effect (Scheurer et al., 2012). The obtained results are similar to the previously observed by Karimian et al. (2020) who found that MTF has low quantum yield (0.014 mol Einstein^{-1}) and molar absorption coefficient at 254 nm (940 M^{-1} cm^{-1}). In this study, the authors also noticed that the application of vacuum UV with 10% of photons emitted at 185 nm greatly improved the MTF removal and its mineralization efficiency explained by HO$^\bullet$ generation in water fission by high energy photons.

In PCD oxidation, MTF degraded in acidic and alkaline media faster than at unadjusted initial neutral to moderately acidic pH (Fig. 1b). At lower pH, an increase in oxidation efficiency may be explained by the oxidation potential of hydroxyl radicals being higher, $E^0 = 2.8$ V, than that in neutral media ($E^0 = 1.9$ V) (Wardman, 1989). An increase in oxidation rate in alkaline solutions may be attributed to the MTF partial deprotonation improving its nucleophilic potential in reactions with electrophilic radicals. Besides, ozone decomposition accelerates with hydroxyl radicals formation at higher pH (Umar et al., 2013).

One can see the energy efficiencies of TMD degradation by UV photolysis and PCD in Figs. 2a and 2b, respectively, in acidic, unadjusted
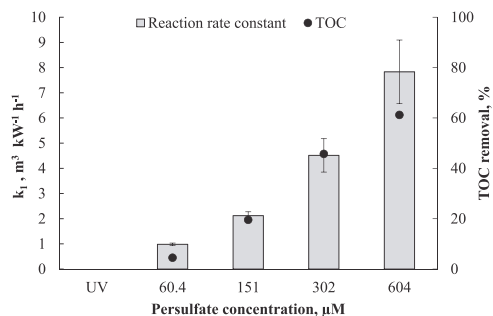

Fig. 3. Effect of PS dose on the k_1 and TOC removal in MTF oxidation by UV/PS combination ($[MTF]_0 = 60.4$ μM, UV output power 3.5 W, $t_{TOC} = 2$ h, unadjusted pH).

neutral-acidic and alkaline media. Almost completely ionized under alkaline conditions ($pK_a = 9.4$) (Derevshchikov et al., 2021), TMD decomposes slowly, reaching 90% conversion within 30 min of UV photolysis at the delivered energy dose of 0.34 kWh m^{-3}, whereas in acidic and unadjusted neutral media, similar result was achieved in 16 and 12 min, respectively, with higher energy efficiency. One can see that TMD degraded faster than MTF in UV photolysis, probably due to the aromatic ring in its structure providing better absorption of photons with further excitation of the substrate molecule.

In PCD experiments, acidic and unadjusted initial pH conditions have a negligible difference in the oxidation efficiency reaching 92–94% degradation of TMD at delivered energy dose of 0.42 kWh m^{-3} accumulated within 28 min of treatment. Significant growth of treatment efficiency was noticed at pH 11, where 98% of TMD was degraded at a delivered energy dose of 0.12 kWh m^{-3} or 8 min of treatment. The latter can be explained by the ionization of TMD molecules at pH 11, improving reactions with electrophilic hydroxyl radicals. Increased due to ozone decomposition amount of HO$^\bullet$ and decreased aqueous solubility of TMD (increased K_{ow}) also contribute to better oxidation of TMD in alkaline medium (Derevshchikov et al., 2021).

3.2. Effect of PS concentration on target compounds oxidation in UV/PS combination

UV photolysis and PCD oxidation experiments with PS added to the MTF and TMD solutions, i.e. treated with UV/PS and PCD/PS combinations, were carried out at unadjusted pH in order to study the treatment efficiency at minimum chemicals addition with possible minimum operation cost.

Addition of PS to the nonirradiated aqueous solutions of MTF at the PS concentration of 600 μM did not result in a notable decrease in MTF

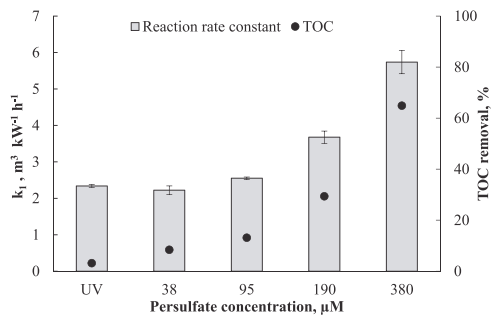**Fig. 4.** Effect of PS dose on the k_1 and TOC removal in TMD oxidation by UV/PS combination ([TMD]$_0$ = 33.4 µM, UV output power 3.5 W, t_{TOC} = 2 h, unadjusted pH).

Fig. 5. Effect of PS dose on the k_1 and TOC removal in MTF oxidation by PCD/PS combination ([MTF]$_0$ = 60.4 µM, PCD output power 9 W, t_{TOC} = 2 h, unadjusted pH).

concentration for 2 h of exposure. In turn, the addition of PS to the UV-irradiated MTF solution led to oxidation of the latter in a considerable degree (Fig. 3): at the PS concentration of 60.4 µM, 80% of MTF was degraded by the delivered radiant energy dose of 0.23 kWh m^{-3}, accumulated in 20 min of UV/PS treatment, demonstrating a dominant role of radicals in MTF oxidation.

Increasing the dose of PS showed a linear progression in the rate of MTF degradation (Fig. 3, Fig. S2). Thus, a ten-fold increase in the oxidant concentration from 60.4 to 604 µM led to an increase in the pseudo-first reaction rate constant by about 8 times from 0.98 to 7.83 m^3 kW^{-1} h^{-1} and the removal of TOC by almost 14 times from 4.5% to 61.2%, respectively.

The PS use was the most efficient at the highest studied oxidant concentration with its more than 87% decomposed after 2 h of UV/PS treatment. These observations allow a conclusion that the PS decomposition in photo-induced reaction, and the MTF oxidation and mineralization proceed with the rate proportional to the PS starting concentration, i.e., no self-scavenging or self-decomposition of PS was observed within the experimental conditions. It confirms the statement made earlier that the quantity of sulfate radicals generated in UV/PS process is proportional to the PS concentration, i.e., the greater the concentration of extrinsic oxidant, the greater the number of generated SO$_4^{\bullet-}$ (Karimian et al., 2020). As a result, sulfate radicals, which are more stable at low pH values, effectively oxidize MTF (Matzek and Carter, 2016; Xia et al., 2020).

Similarly to MTF, dark oxidation of TMD with PS at a concentration of 380 µM showed no degradation of the target compound. Oxidation of TMD by UV/PS combination was performed with the PS dose of 38 µM further increased 2.5, 5 and 10 times (Fig. 4 and Fig. S3). The highest oxidation rate was observed at the PS dose of 380 µM, with more than 99% of TMD decomposed within 10 min of treatment. The k_1 value increased about 2.5 times from 3.10 to 7.85 m^3 kW^{-1} h^{-1} with the PS dose increased from 0 to 380 µM. The TOC removal, comprising 3% under the unassisted UV-radiation within 2 h of treatment, reached 65% at the maximum PS dose under experimental conditions. Irrespective of the PS dose applied, the TMD degradation by-products oxidized more slowly than the parent compound.

It is worth to note that TMD shows negligible difference in reaction rates of UV oxidation and in the UV/PS combinations at PS concentrations up to 95 µM explained, presumably, by substitution of UV-photons decomposing TMD molecule with sulfate radicals producing further hydroxyl radicals (Eqs. 12 and 13) (Liang et al., 2008). Sulfate radicals, however, are prone to react with the more stable TMD oxidation by-products seen from the TOC removal in the UV/PS combinations (Fig. 4). Accordingly, TOC removal increased from 8.5% to 65%, i.e. 7.6 times with the growth of PS dose for an order of magnitude from 38 to 380 µM. Persulfate was mostly (90%+) utilized in the first hour of treatment, while for MTF oxidation, the PS utilization was slower and
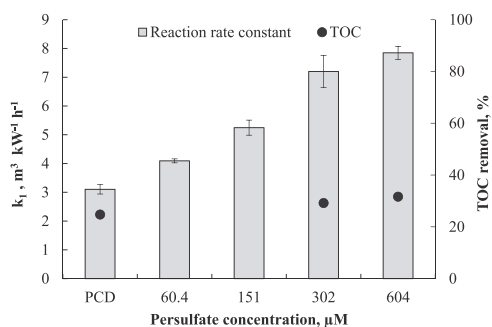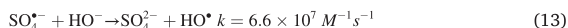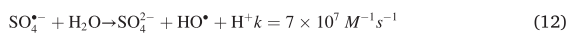
only about 60% of oxidant was consumed within the first hour. The latter can be explained by more complicated structure of TMD and the smaller amount of PS applied.

$$SO_4^{\bullet-} + H_2O \rightarrow SO_4^{2-} + HO^{\bullet} + H^+ \quad k = 7 \times 10^7 \ M^{-1}s^{-1} \quad (12)$$

$$SO_4^{\bullet-} + HO^- \rightarrow SO_4^{2-} + HO^{\bullet} \quad k = 6.6 \times 10^7 \ M^{-1}s^{-1} \quad (13)$$

3.3. Effect of PS concentration on target compounds oxidation in PCD/PS combination

The effect of PS dose on MTF degradation in PCD/PS combination is shown in Fig. 5 and Fig. S4. The results showed that the rate of MTF oxidation in the PCD/PS system steadily, albeit moderately, increased with the increasing PS dose. Accordingly, the PS dosage increased by an order of magnitude improved the reaction rate by about 1.7 times only; the pulsed energy dose necessary to reduce the MTF content by 90% decreased from 0.6 kWh m^{-3} in unassisted PCD to 0.3 kWh m^{-3} in the PCD/PS combination at the PS dose of 604 µM, i.e., two times.
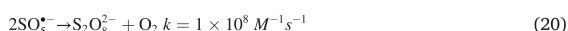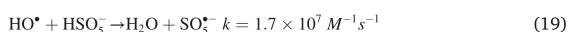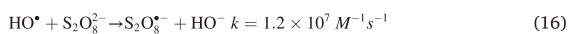
These observations clearly demonstrate PS activation with PCD. On the other hand, moderate contribution of extrinsic PS to the PCD oxidation of MTF differs substantially from the proportional growth in oxidation rate with the PS dose observed in UV/PS combination. Since PCD is known to form hydroxyl radicals at the gas-liquid interface (Ajo et al., 2017), one can presume HO$^{\bullet}$ interfering with the sulfate radicals. Tikker et al. (2021) suggested that sulfate radicals may react with hydroxyl radicals forming peroxymonosulfate ions (Eq. 14) thus wasting the reactive species:

$$SO_4^{\bullet-} + HO^{\bullet} \rightarrow HSO_5^- \quad k_{HSO_5^-} = 1 \times 10^{10} \ M^{-1}s^{-1} \quad (14)$$
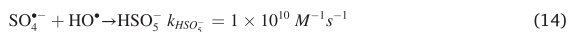
Besides the non-productive reactive species expense, sulfate radical may also prevent formation of hydrogen peroxide (Eq. 15):

$$HO^{\bullet} + HO^{\bullet} \rightarrow H_2O_2 \quad k_{H_2O_2} = 5.5 \times 10^9 \ M^{-1}s^{-1} \quad (15)$$
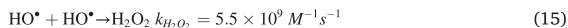
Other non-targeted recombination reactions may take place thus reducing effectiveness of PS addition to the treated solution (Eqs. 16–23) (Wang and Zhou, 2016):
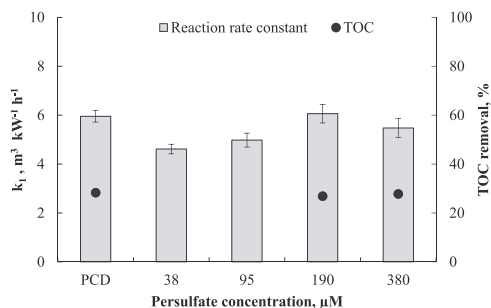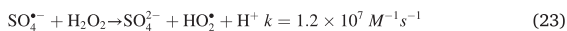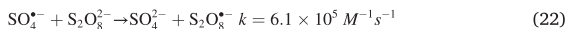
$$HO^{\bullet} + S_2O_8^{2-} \rightarrow S_2O_8^{\bullet-} + HO^- \quad k = 1.2 \times 10^7 \ M^{-1}s^{-1} \quad (16)$$

$$S_2O_8^{\bullet-} \ + \ 2e^- \rightarrow 2SO_4^{2-} \quad (17)$$

$$SO_4^{\bullet-} + HSO_5^- \rightarrow HSO_4^- + SO_5^{\bullet-} \quad k = 1 \times 10^5 \ M^{-1}s^{-1} \quad (18)$$

$$HO^{\bullet} + HSO_5^- \rightarrow H_2O + SO_5^{\bullet-} \quad k = 1.7 \times 10^7 \ M^{-1}s^{-1} \quad (19)$$

$$2SO_5^{\bullet-} \rightarrow S_2O_8^{2-} + O_2 \quad k = 1 \times 10^8 \ M^{-1}s^{-1} \quad (20)$$

Fig. 6. Effect of PS on the k_1 and TOC removal in TMD oxidation by PCD/PS combination ([TMD]$_0$ = 33.4 μM, PCD output power 9 W, t_{TOC} = 2 h, unadjusted pH).

Table 2
Degradation of target compounds by the UV/PS and PCD/PS combinations.

Target compound	Process	$(C_0 - C_t)/C_0$, %		
		Without scavenger	*t*-BuOH	EtOH
MTF[a]	UV/PS	93 %	82 %	61 %
	PCD/PS	96 %	55 %	51 %
TMD[b]	UV/PS	73 %	66 %	61 %
	PCD/PS	91 %	65 %	61 %

[a] Experimental conditions: [MTF]$_0$ = 60.4 μM, [PS]$_0$ = 302 μM, [*t*-BuOH]$_0$ = [EtOH]$_0$ = 15.1 mM, t_{UV} = 6 min, t_{PCD} = 40 min, unadjusted pH.
[b] Experimental conditions: [TMD]$_0$ = 33.4 μM, [PS]$_0$ = 190 μM, [*t*-BuOH]$_0$ = [EtOH]$_0$ = 8.4 mM, t_{UV} = 6 min, t_{PCD} = 40 min, unadjusted pH.

$$SO_4^{\bullet-} + SO_4^{\bullet-} \rightarrow S_2O_8^{2-} \quad k = 3.1 \times 10^8 \; M^{-1}s^{-1} \tag{21}$$

$$SO_4^{\bullet-} + S_2O_8^{2-} \rightarrow SO_4^{2-} + S_2O_8^{\bullet-} \quad k = 6.1 \times 10^5 \; M^{-1}s^{-1} \tag{22}$$

$$SO_4^{\bullet-} + H_2O_2 \rightarrow SO_4^{2-} + HO_2^{\bullet} + H^+ \quad k = 1.2 \times 10^7 \; M^{-1}s^{-1} \tag{23}$$

In contrast to UV-induced oxidation of TMD, PS added to the PCD-treated TMD solution did not accelerate TMD degradation. In opposite, oxidation rate decreased for about 18–19% at lower PS doses as shown in Fig. 6 and Fig. S5. The TMD mineralization also comprised approximately 30% as TOC removal within 2 h of treatment with or without PS additions.

As a matter of discussion, similar reaction rate constants and mineralization degrees shown in TMD oxidation may theoretically indicate a limited number of oxidants in PCD, when all oxidants generated in pulses are consumed. However, significantly increased efficiency of TMD oxidation at pH 11 (Fig. 2b) invalidates this hypothesis showing that the oxidants amount is not limited within the experimental conditions. Thus, the negative effect of PS addition on the oxidation rate of TMD shows the use of hydroxyl radicals being shifted towards reactions with sulfate radical species (Eqs. 14, 16 and 19), thereby, competing with the reactions of sulfate radicals with organics. Besides, the reaction rate constants of organic compounds oxidation with $SO_4^{\bullet-}$ were reported to be several orders of magnitude smaller than the ones of peroxymonosulfate ions formation (Eq. 14) (Lee et al., 2020).

3.4. Identification of active radical species in UV/PS and PCD/PS combinations

To identify the predominant radicals and better understand the reaction mechanism of MTF and TMD degradation by the UV/PS and PCD/PS combinations, scavenging studies were performed with the addition of two radical probes. The experiments were conducted with the addition of *t*-BuOH, which is a more effective scavenger for hydroxyl radicals (3.8 × 10^8 –

7.6 × 10^8 M^{-1} s^{-1}) than for sulfate radicals (4 × 10^5 – 9.1 × 10^5 M^{-1} s^{-1}), and EtOH, reacting at comparable rates with hydroxyl radicals (1.2 × 10^9 – 2.8 × 10^9 M^{-1} s^{-1}) and sulfate radicals (1.6 × 10^7 – 7.7 × 10^7 M^{-1} s^{-1}) (Anipsitakis and Dionysiou, 2004). Therefore, the presence of hydroxyl radicals was identified by adding an excess of *t*-BuOH to the studied combinations. The effect of sulfate radicals was assessed by comparing the efficiency of inhibition of the target compound degradation when an excess of *t*-BuOH and EtOH was added to the UV/PS and PCD/PS systems.

The results presented in Table 2 showed that the addition of *t*-BuOH reduced the MTF degradation efficiency by 11% and 41% in the UV/PS and PCD/PS combination, respectively, indicating the presence of hydroxyl radicals in both systems. A similar trend was observed for TMD degradation with 7% and 26% inhibition due to the addition of *t*-BuOH to the UV/PS and PCD/PS systems. For both target compounds, the role of hydroxyl radicals was more substantial in the PCD/PS combination.

The addition of excess EtOH substantially inhibited the decomposition of MTF in the UV/PS (32%) and PCD/PS (45%) combination, which, in turn, indicated the participation of sulfate radicals in the decomposition of the target compound. The remaining amount of MTF decomposition after adding excess EtOH was most likely due to the presence of other reactive oxygen species in the studied systems.

For TMD degradation in the UV/PS and PCD/PS combination, the reduction in the oxidation efficacy due to the addition of EtOH was 12% and 30%, respectively. It should be noted that in the case of the UV/PS combination, the addition of both scavengers led to insignificant inhibition in the decomposition of TMD (Fig. 4), most likely due to the high efficiency of direct UV photolysis in the decomposition of TMD (Fig. 4).

The findings of scavenging studies suggested that both hydroxyl and sulfate radicals contribute to the degradation of MTF and TMD in the UV/PS combination, while hydroxyl radicals turn out to be predominant oxidative species in the PCD/PS combination.

3.5. Ecotoxicity of target compounds oxidation intermediates

The results of this study showed that, regardless of the applied treatment process, complete mineralization of the target compounds could not be achieved, and thus all treated solutions contain a certain amount of by-products. For TMD oxidation by the studied systems, the primary transformation products (TPs) were identified by LC-MS analysis (ESI in positive mode). In the case of MTF, by-products could not be identified by means of the analytical tools used.

According to the results of the scavenging studied, the role of hydroxyl radicals was more prominent for the PCD/PS combination than for the UV/PS system (Table 2). Nevertheless, the identified TPs were similar for the studied activated PS systems. During the oxidation of TMD in PCD and both studied combinations, hydroxylated TPs were identified: mono-hydroxylated TP1 (m/z 280, $C_{16}H_{25}NO_3$), di-hydroxylated TP2 (m/z 296, $C_{16}H_{25}NO_4$) and tri-hydroxylated TP3 (m/z 312, $C_{16}H_{25}NO_4$) (Antonopoulou and Konstantinou, 2016; Gulde et al., 2021). Presumably, the observed hydroxylation of TMD occurred in the cyclohexane and/or aromatic ring. More specific for the UV/PS oxidation was the detection of N-demethylated TP4 (m/z 250, $C_{15}H_{23}NO_2$), while its hydroxylation product TP5 (m/z 266, $C_{15}H_{23}NO_3$) was found in PCD, PCD/PS and UV/PS treatment of TMD (Antonopoulou and Konstantinou, 2016; Gulde et al., 2021). Specific for PCD and PCD/PS systems was the detection of TP6 (m/z 278, $C_{16}H_{23}NO_3$), indicating the conversion of the methyl group in the amine moiety into an aldehyde group. This by-product has also been found in ozonation and photocatalytic oxidation of TMD (Zimmermann et al., 2012; Antonopoulou and Konstantinou, 2016).

During prolonged treatment, these primary TPs further decomposed into other low molecular weight conversion products, which could not be identified using the analytical instruments used. However, the observed removal of TOC (Figs. 4 and 6) confirmed the further degradation of by-products and the formation of final TPs, mainly carboxylic

Table 3

Bacterial luminescence inhibition (INH%) of 2-fold diluted MTF and TMD solutions after a 2-h oxidation in UV, UV/PS, PCD and PCD/PS.

Target compound	UV	UV/PS	PCD	PCD/PS
MTF[a]	0 %	98 %	37 %	51 %
TMD[b]	15 %	12 %	33 %	50 %

[a] Experimental conditions: $[MTF]_0 = 60.4$ µM, $[PS]_0 = 302$ µM, t = 2 h, unadjusted pH.

[b] Experimental conditions: $[TMD]_0 = 33.4$ µM, $[PS]_0 = 190$ µM; t = 2 h, unadjusted pH.

acids, which are common final by-products of phenolic-type derivatives oxidation (Ortiz-Gomez et al., 2008).

To evaluate the formation of toxic intermediates, the acute toxicity of MTF and TMD solutions treated with UV photolysis, PCD, UV/PS, and PCD/PS systems was studied. Accordingly, a *Vibrio fischeri* chemiluminescence inhibition assay was used to evaluate ecotoxicity and the results of INH% of 2-fold diluted treated MTF and TMD solutions are presented in Table 3.

The initial solutions of MTF and TMD were found to be non-toxic to *Vibrio fischeri*. In turn, the oxidation of the target compounds by the studied processes led to an increase in the toxicity of solutions (Table 3). Thus, the application of PCD process resulted in INH% of 33% and 37% for the treated solution of TMD and MTF, respectively, indicating the formation of toxic by-products. The use of PCD/PS oxidation resulted in INH% of ~50% for the by-products of both pharmaceuticals. Regarding the application of persulfate photolysis, this treatment method turned out to be more promising for the oxidation of TMD (with 5 µM unreacted PS and INH% of 12%) than for MTF (with 34 µM unreacted PS and INH% of 98%) in terms of lower residual ecotoxicity. The inhibition of *Vibrio fischeri* bioluminescence by persulfate solutions was also studied to evaluate the effect of residual PS concentration on the overall ecotoxicity of pretreated samples. Accordingly, PS solutions with a concentration of 5 and 34 µM showed INH% of ~0% and 52%. It should also be considered that the degradation of TMD by direct UV photolysis led to a slight inhibition of bacterial luminescence.

Overall, for persulfate-assisted treatment methods, the observed increased residual ecotoxicity can be explained to some extent by the toxic effect of residual PS concentration in these systems (Moreno-Andrés et al., 2019). Therefore, PS dose control is required to avoid secondary contamination of the water by unreacted oxidant, or, if necessary, unused PS must be removed from the treated water before being discharged into receiving water bodies.

3.6. Comparison of operating costs

To evaluate energy efficiencies of the treatment systems under the scope, energy yields E_{90} at 90% conversion (E_{90}, g kW^{-1} h^{-1}) of MFT and TMD were calculated taking into account the energies applied and consumed by UV radiation and PCD treatment together with the cost of extrinsic PS. The calculation results are shown in Table 4, Figs. S6 and S7. The PS cost of 1.5 EUR kg^{-1} is considered relevant including transportation and taxation based on average wholesale prices on market (per ton, 2021). The PS cost was converted to its energy expense of 12 kWh kg^{-1} considering the average European non-household electric energy price of 0.125 EUR kW^{-1} h^{-1} (Eurostat, 2020).

In the 90-% removal of MTF and TMD, the highest energy efficiency relative to the delivered energy was shown by unassisted PCD - 8.7 and 20 g kW^{-1} h^{-1}, respectively. These numbers exceed those observed in the UV photolysis for a few times (Table 4). The lower energy efficiencies observed in PCD/PS combinations are due to the additional cost of PS at minor treatment efficacy improvement. Also, the PS additions did not considerably affect the target pollutants mineralization thus being unable to compensate the energy efficiency loss from this side.

In the UV/PS system, the energy efficiency resulted in maximum 2.2 g kW^{-1} h^{-1} and 3.3 g kW^{-1} h^{-1} for MTF and TMD oxidation, respectively. Contrary to the PCD/PS combination, the oxidation rate demonstrated a substantial growth with the increasing PS dose. Moderate energy efficiency changes, however, shown in Table 4, indicate a substantial growth of expense on account of the PS additions. Notably, TOC removal increased greatly from around 3–5% to over 60% with the PS additions.

Summarizing, the non-assisted PCD process demonstrates high energy efficiency and reasonably efficient mineralization of the studied compounds without the addition of a supporting oxidant, which makes this process a promising alternative for the treatment of water contaminated with persistent micropollutants. As for the less efficient in target compounds removal UV/PS combination, its strength in mineralization of organic compounds offers an alternative under certain conditions.

4. Conclusions

The application of UV/PS and PCD/PS combinations was proven to be effective in degradation of aqueous metformin and tramadol pharmaceuticals. Certain synergism of persulfate addition was observed in the studied processes with exception of TMD treated by PCD/PS, where sulfate radicals most likely were not utilized on the TMD degradation due to the competing not-targeted reactions with hydroxyl radicals. This assumption was supported by the results of radical scavenging studies, which showed that both hydroxyl and sulfate radicals contribute to the degradation of target compounds in the UV/PS combination, while hydroxyl radicals appear to be the predominant oxidative species in the PCD/PS combination.

In the UV/PS combination, reaction rate constants and TOC removal increased linearly with the applied PS doses under experimental

Table 4

Comparison of energy efficiencies and TOC removal rates in MTF and TMD oxidation in UV/PS and PCD/PS combinations ($[MTF]_0 = 60.4$ µM, $[TMD]_0 = 33.4$ µM, t = 2 h, unadjusted pH).

Process	PS dose, µM		MTF			TMD		
	MTF	TMD	E_{90}, g kW^{-1} h^{-1}		TOC removal, %	E_{90}, g kW^{-1} h^{-1}		TOC removal, %
			Consumed[a]	Delivered		Consumed	Delivered	
UV/PS	0	0	_[b]	_[b]	4.5	2.5	7.9	3.2
	302	190	2.1	4.0	45.7	3	6.5	29.4
	604	380	2.2	2.9	61.2	3.3	5.3	64.9
PCD/PS	0	0	5.6	8.7	24.7	13	20	28.3
	302	190	3.9	4.6	29.2	8.2	9.7	26.9
	604	380	2.2	2.4	31.6	5.4	5.9	27.8

[a] Consumed UV energy takes into account the output-input ratio of the lamp 32%. Consumed energy in PCD treatment takes into account the output-input ratio of the pulse generator 65%.

[b] Removal of 90% of the main compound was not achieved, removal did not exceed 10%.

conditions studied for both MTF and TMD. Furthermore, the energy efficiencies were rising with PS dose increase indicating an improvement in the cost-effectiveness of this oxidation process.

As for the PCD/PS oxidation of MTF, the addition of PS noticeably reduced the overall energy efficiency of treatment, although having a positive but moderate effect on the degradation rate and mineralization of the target compound.

The highest energy efficiency in respect of MTF and TMD showed in PCD treatment achieved in terms of delivered pulsed energy 8.7 and 20.0 g kW^{-1} h^{-1}, respectively. From the standpoints of energy efficiency, chemical-free technology and the absence of secondary pollution, non-assisted PCD treatment of neutral aqueous media appears a reliable alternative to traditional water treatment methods. In turn, the high TOC removal in the UV/PS process at carefully adjusted PS dosages makes it highly promising in advanced water treatment.

Declaration of Competing Interest

The authors declare that they have no known competing financial interests or personal relationships that could have appeared to influence the work reported in this paper.

Acknowledgement

Appendix A. Supporting information

Supplementary data associated with this article can be found in the online version at doi:10.1016/j.psep.2022.07.002.

References

Ahmadi, E., Shokri, B., Mesdaghinia, A., Nabizadeh, R., Khani, M.R., Yousefzadeh, S., Salehi, M., Yaghmaeian, K., 2020. Synergistic effects of α-Fe2O3-TiO2 and Na2S2O8 on the performance of a non-thermal plasma reactor as a novel catalytic oxidation process for dimethyl phthalate degradation. Sep. Purif. Technol. 250, 117185 https://doi.org/10.1016/j.seppur.2020.117185.

Ajo, P., Kornev, I., Preis, S., 2017. Pulsed corona discharge induced hydroxyl radical transfer through the gas-liquid interface. Sci. Rep. 7, 16152. https://doi.org/10.1038/s41598-017-16333-1.

Ali, F., Khan, J.A., Shah, N.S., Sayed, M., Khan, H.M., 2018. Carbamazepine degradation by UV and UV-assisted AOPs: kinetics, mechanism and toxicity investigations. Process Saf. Environ. Prot. 117, 307–314. https://doi.org/10.1016/j.psep.2018.05.004.

Anipsitakis, G.P., Dionysiou, D.D., 2004. Radical generation by the interaction of transition metals with common oxidants. Environ. Sci. Technol. 38, 3705–3712. https://doi.org/10.1021/es035121o.

Antonopoulou, M., Konstantinou, I., 2016. Photo Degrad. Miner. Trama Pharm. aqueous TiO2 Suspens.: Eval. Kinet., Mech. ecotoxicity. Appl. Catal. A Gen., 515, pp. 136–143 doi: 10.1016/j.apcata.2016.02.005.

Aseman-Bashiz, E., Sayyaf, H., 2020. Metformin degradation in aqueous solutions by electro-activation of persulfate and hydrogen peroxide using natural and synthetic ferrous ion sources. J. Mol. Liq. 300, 112285 https://doi.org/10.1016/j.molliq.2019.112285.

Bachour, R.L., Golovko, O., Kellner, M., Pohl, J., 2020. Behavioral effects of citalopram, tramadol, and binary mixture in zebrafish (Danio rerio) larvae. Chemosphere 238, 124587. https://doi.org/10.1016/j.chemosphere.2019.124587.

Blair, B.D., Crago, J.P., Hedman, C.J., Klaper, R.D., 2013. Pharmaceuticals and personal care products found in the Great Lakes above concentrations of environmental concern. Chemosphere 93, 2116–2123. https://doi.org/10.1016/j.chemosphere.2013.07.057.

Briones, R.M., Sarmah, A.K., Padhye, L.P., 2016. A global perspective on the use, occurrence, fate and effects of anti-diabetic drug metformin in natural and engineered ecosystems. Environ. Pollut. 219, 1007–1020. https://doi.org/10.1016/j.envpol.2016.07.040.

Carbuloni, C.F., Savoia, J.E., Santos, J.S.P., Pereira, C.A.A., Marques, R.G., Ribeiro, V.A. S., Ferrari, A.M., 2020. Degradation of metformin in water by TiO2–ZrO2 photocatalysis. J. Environ. Manag. 262, 110347 https://doi.org/10.1016/j.jenvman.2020.110347.

Chinnaiyan, P., Thampi, S.G., Kumar, M., Balachandran, M., 2019. Photocatalytic degradation of metformin and amoxicillin in synthetic hospital wastewater: effect of

classical parameters. Int. J. Environ. Sci. Technol. 16, 5463–5474. https://doi.org/10.1007/s13762-018-1935-0.

Derevshchikov, V., Dulova, N., Preis, S., 2021. Oxidation of ubiquitous aqueous pharmaceuticals with pulsed corona discharge. J. Electro 110, 103567. https://doi.org/10.1016/j.elstat.2021.103567.

Elizalde-Velázquez, G.A., Gómez-Oliván, L.M., 2020. Occurrence, toxic effects and removal of metformin in the aquatic environments in the world: Recent trends and perspectives. Sci. Total Environ. 702, 134924 https://doi.org/10.1016/j.scitotenv.2019.134924.

Eurostat, 2020. Electricity price statistics - Statistics Explained. European Commission. https://ec.europa.eu/eurostat/statistics-explained/index.php/Electricity_price_statistics (accessed 12 December 2021).

Ghalwa, N.A., Abu-Shawish, H.M., Zaggout, F.R., Saadeh, S.M., Al-Dalou, A.R., Abou Assi, A.A., 2014. Electrochemical degradation of tramadol hydrochloride: Novel use of potentiometric carbon paste electrodes as a tracer. Arab. J. Chem. 7, 708–714. https://doi.org/10.1016/j.arabjc.2010.12.007.

Global Metformin Hydrochloride Market, 2019. Global metformin hydrochloride market 2019 by manufacturers, regions, type and application, forecast to 2024. https://www.absolutereports.com/global-metformin-hydrochloride-market-13813472 (accessed 12 December 2021).

Golovko, O., Örn, S., Sörengård, M., Frieberg, K., Nassazzi, W., Lai, F.Y., Ahrens, L., 2021. Occurrence and removal of chemicals of emerging concern in wastewater treatment plants and their impact on receiving water systems. Sci. Total Environ. 754, 142122 https://doi.org/10.1016/j.scitotenv.2020.142122.

Guerra-Rodríguez, S., Rodríguez, E., Singh, D.N., Rodríguez-Chueca, J., 2018. Assessment of sulfate radical-based advanced oxidation processes for water and wastewater treatment: a review. Water 10, 1828. https://doi.org/10.3390/w10121828.

Gulde, R., Clerc, B., Rutsch, M., Helbing, J., Salhi, E., McArdell, C.S., von Gunten, U., 2021. Oxidation of 51 micropollutants during drinking water ozonation: formation of transformation products and their fate during biological post-filtration. Water Res. 207, 117812 https://doi.org/10.1016/j.watres.2021.117812.

Homem, V., Santos, L., 2011. Degradation and removal methods of antibiotics from aqueous matrices - a review. J. Environ. Manag. 92, 2304–2347. https://doi.org/10.1016/j.jenvman.2011.05.023.

Houtman, C.J., Kroesbergen, J., Lekkerkerker-Teunissen, K., van der Hoek, J.P., 2014. Human health risk assessment of the mixture of pharmaceuticals in Dutch drinking water and its sources based on frequent monitoring data. Sci. Total Environ. 496, 54–62. https://doi.org/10.1016/j.scitotenv.2014.07.022.

Jacob, R.S., de Souza Santos, L.V., d'Auriol, M., Lebron, Y.A.R., Moreira, V.R., Lange, L. C., 2020. Diazepam, metformin, omeprazole and simvastatin: a full discussion of individual and mixture acute toxicity. Ecotoxicology 29, 1062–1071. https://doi.org/10.1007/s10646-020-02239-8.

Jarque, S., Masner, P., Klánová, J., Prokeš, R., Bláha, L., 2016. Bioluminescent vibrio fischeri assays in the assessment of seasonal and spatial patterns in toxicity of contaminated river sediments. Front. Microbiol. 7, 1738. https://doi.org/10.3389/fmicb.2016.01738.

Karimian, S., Moussavi, G., Fanaei, F., Mohammadi, S., Shekoohiyan, S., Giannakis, S., 2020. Shedding light on the catalytic synergies between Fe(II) and PMS in vacuum UV (VUV/Fe/PMS) photoreactors for accelerated elimination of pharmaceuticals: the case of metformin. Chem. Eng. J. 400, 125896 https://doi.org/10.1016/j.cej.2020.125896.

Kaur, B., Dulova, N., 2020. UV-assisted chemical oxidation of antihypertensive losartan in water. J. Environ. Manag. 261, 110170 https://doi.org/10.1016/j.jenvman.2020.110170.

Khan, J.A., He, X., Shah, N.S., Khan, H.M., Hapeshi, E., Fatta-Kassinos, D., Dionysiou, D. D., 2014. Kinetic and mechanism investigation on the photochemical degradation of atrazine with activated H2O2, S2O82- and HSO5-. Chem. Eng. J. 252, 393–403. https://doi.org/10.1016/j.cej.2014.04.104.

Khan, J.A., He, X., Shah, N.S., Sayed, M., Khan, H.M., Dionysiou, D.D., 2017. Degradation kinetics and mechanism of desethyl-atrazine and desisopropyl-atrazine in water with OH and SO4− based-AOPs. Chem. Eng. J. 325, 485–494. https://doi.org/10.1016/j.cej.2017.05.011.

Kong, L., Kadokami, K., Wang, S., Duong, H.T., Chau, H.T.C., 2015. Monitoring of 1300 organic micro-pollutants in surface waters from Tianjin, North China. Chemosphere 122, 125–130. https://doi.org/10.1016/j.chemosphere.2014.11.025.

Kostanjevecki, P., Petric, I., Loncar, J., Smital, T., Ahel, M., Terzic, S., 2019. Aerobic biodegradation of tramadol by pre-adapted activated sludge culture: Cometabolic transformations and bacterial community changes during enrichment. Sci. Total Environ. 687, 858–866. https://doi.org/10.1016/j.scitotenv.2019.06.118.

Kulik, N., Panova, Y., Trapido, M., 2007. The Fenton chemistry and its combination with coagulation for treatment of dye solutions. Sep. Sci. Technol. 42, 1521–1534. https://doi.org/10.1080/01496390701290185.

Lee, J., von Gunten, U., Kim, J.H., 2020. Persulfate-based advanced oxidation: critical assessment of opportunities and roadblocks. Environ. Sci. Technol. 54, 3064–3081. https://doi.org/10.1021/acs.est.9b07082.

Liang, C., Huang, C.F., Mohanty, N., Kurakalva, R.M., 2008. A rapid spectrophotometric determination of persulfate anion in ISCO. Chemosphere 73, 1540–1543. https://doi.org/10.1016/j.chemosphere.2008.08.043.

Lindim, C., van Gils, J., Georgieva, D., Mekenyan, O., Cousins, I.T., 2016. Evaluation of human pharmaceutical emissions and concentrations in Swedish river basins. Sci. Total Environ. 572, 508–519. https://doi.org/10.1016/j.scitotenv.2016.08.074.

Ložek, F., Kuklina, I., Grabicová, K., Kubec, J., Buřič, M., Grabic, R., Randák, T., Císař, P., Kozák, P., 2019. Behaviour and cardiac response to stress in signal crayfish exposed to environmental concentrations of tramadol. Aquat. Toxicol. 213, 105217 https://doi.org/10.1016/j.aquatox.2019.05.019.

Lütke Eversloh, C., Schulz, M., Wagner, M., Ternes, T.A., 2015. Electrochemical oxidation of tramadol in low-salinity reverse osmosis concentrates using boron-doped diamond anodes. Water Res. 72, 293–304. https://doi.org/10.1016/j.watres.2014.12.021.

Maćerak, A.L., Kerkez, Đ., Bečelić-Tomin, M., Pilipović, D.T., Kulić, A., Jokić, J., Dalmacija, B., 2018. Removal of Diclofenac and Metformin from Water in Laboratory Photo Reactor. Proceedings 2, 1288. https://doi.org/10.3390/proceedings2201288.

Mackuľak, T., Birošová, L., Bodík, I., Grabic, R., Takáčová, A., Smolinská, M., Hanusová, A., Híveš, J., Gál, M., 2016. Zerovalent iron and iron(VI): effective means for the removal of psychoactive pharmaceuticals and illicit drugs from wastewaters. Sci. Total Environ. 539, 420–426. https://doi.org/10.1016/j.scitotenv.2015.08.138.

Majhi, D., Samal, P.K., Das, K., Gouda, S.K., Bhoi, Y.P., Mishra, B.G., 2019. α-NiS/Bi2O3 nanocomposites for enhanced photocatalytic degradation of tramadol. ACS Appl. Nano Mater. 2, 395–407. https://doi.org/10.1021/acsanm.8b01974.

Malik, M.A., 2010. Water purification by plasmas: which reactors are most energy efficient. Plasma Chem. Plasma Process 30, 21–31. https://doi.org/10.1007/s11090-009-9202-2.

Margot, J., Rossi, L., Barry, D.A., Holliger, C., 2015. A review of the fate of micropollutants in wastewater treatment plants. WIREs Water 2, 457–487. https://doi.org/10.1002/wat2.1090.

Matzek, L.W., Carter, K.E., 2016. Activated persulfate for organic chemical degradation: a review. Chemosphere 151, 178–188. https://doi.org/10.1016/j.chemosphere.2016.02.055.

Monteil, H., Oturan, N., Péchaud, Y., Oturan, M.A., 2020. Electro-Fenton treatment of the analgesic tramadol: kinetics, mechanism and energetic evaluation. Chemosphere 247, 125939. https://doi.org/10.1016/j.chemosphere.2020.125939.

Moreno-Andrés, J., Farinango, G., Romero-Martínez, L., Acevedo-Merino, A., Nebot, E., 2019. Application of persulfate salts for enhancing UV disinfection in marine waters. Water Res. 163, 114866 https://doi.org/10.1016/j.watres.2019.114866.

Niemuth, N.J., Klaper, R.D., 2015. Emerging wastewater contaminant metformin causes intersex and reduced fecundity in fish. Chemosphere 135, 38–45. https://doi.org/10.1016/j.chemosphere.2015.03.060.

Niemuth, N.J., Klaper, R.D., 2018. Low-dose metformin exposure causes changes in expression of endocrine disruption-associated genes. Aquat. Toxicol. 195, 33–40. https://doi.org/10.1016/j.aquatox.2017.12.003.

Orata, E.D., De Leon, P.D.P., Doma, B.T., 2019. Degradation of metformin in water using electro-Fenton process. IOP Conf. Ser. Earth Environ. Sci. 344, 012007 https://doi.org/10.1088/1755-1315/344/1/012007.

Ortiz-Gomez, A., Serrano-Rosales, B., de Lasa, H., 2008. Enhanced mineralization of phenol and other hydroxylated compounds in a photocatalytic process assisted with ferric ions. Chem. Eng. Sci. 63, 520–557. https://doi.org/10.1016/j.ces.2007.04.053.

Patel, M., Kumar, R., Kishor, K., Mlsna, T., Pittman, C.U., Mohan, D., 2019. Pharmaceuticals of emerging concern in aquatic systems: Chemistry, occurrence, effects, and removal methods. Chem. Rev. 119, 3510–3673. https://doi.org/10.1021/acs.chemrev.8b00299.

Plhalova, L., Sehonova, P., Blahova, J., Doubkova, V., Tichy, F., Faggio, C., Berankova, P., Svobodova, Z., 2020. Evaluation of tramadol hydrochloride toxicity to juvenile zebrafish - morphological, antioxidant and histological responses. Appl. Sci. 10, 2349. https://doi.org/10.3390/app10072349.

Preis, S., Panorel, I.C., Kornev, I., Hatakka, H., Kallas, J., 2013. Pulsed corona discharge: the role of Ozone and hydroxyl radical in aqueous pollutants oxidation. Water Sci. Technol. 68, 1536–1542. https://doi.org/10.2166/wst.2013.399.

Radbruch, L., Glaeske, G., Grond, S., Münchberg, F., Scherbaum, N., Storz, E., Tholen, K., Zagermann-Muncke, P., Zieglgänsberger, W., Hoffmann-Menzel, H., Greve, H.,

Cremer-Schaeffer, P., 2013. Topical review on the abuse and misuse potential of tramadol and tilidine in Germany. Subst. Abus. 34, 313–320. https://doi.org/10.1080/08897077.2012.735216.

Scheurer, M., Michel, A., Brauch, H.J., Ruck, W., Sacher, F., 2012. Occurrence and fate of the antidiabetic drug metformin and its metabolite guanylurea in the environment and during drinking water treatment. Water Res. 46, 4790–4802. https://doi.org/10.1016/j.watres.2012.06.019.

Sehonova, P., Plhalova, L., Blahova, J., Berankova, P., Doubkova, V., Prokes, M., Tichy, F., Vecerek, V., Svobodova, Z., 2016. The effect of tramadol hydrochloride on early life stages of fish. Environ. Toxicol. Pharmacol. 44, 151–157. https://doi.org/10.1016/j.etap.2016.05.006.

Shang, K., Li, W., Wang, X., Lu, N., Jiang, N., Li, J., Wu, Y., 2019. Degradation of p-nitrophenol by DBD plasma/Fe2+/persulfate oxidation process. Sep. Purif. Technol. 218, 106–112. https://doi.org/10.1016/j.seppur.2019.02.046.

Taoufik, N., Boumya, W., Achak, M., Sillanpää, M., Barka, N., 2021. Comparative overview of advanced oxidation processes and biological approaches for the removal pharmaceuticals. J. Environ. Manag. 288, 112404 https://doi.org/10.1016/j.jenvman.2021.112404.

Tikker, P., Dulova, N., Kornev, I., Preis, S., 2021. Effects of persulfate and hydrogen peroxide on oxidation of oxalate by pulsed corona discharge. Chem. Eng. J. 411, 128586 https://doi.org/10.1016/j.cej.2021.128586.

Umar, M., Roddick, F., Fan, L., Aziz, H.A., 2013. Application of ozone for the removal of bisphenol A from water and wastewater - a review. Chemosphere 90, 2197–2207. https://doi.org/10.1016/j.chemosphere.2012.09.090.

Wang, J., Wang, S., 2018. Activation of persulfate (PS) and peroxymonosulfate (PMS) and application for the degradation of emerging contaminants. Chem. Eng. J. 334, 1502–1517. https://doi.org/10.1016/j.cej.2017.11.059.

Wang, Q., Zhang, A., Li, P., Héroux, P., Zhang, H., Yu, X., Liu, Y., 2021. Degradation of aqueous atrazine using persulfate activated by electrochemical plasma coupling with microbubbles: removal mechanisms and potential applications. J. Hazard. Mater. 403, 124087 https://doi.org/10.1016/j.jhazmat.2020.124087.

Wang, S., Zhou, N., 2016. Removal of carbamazepine from aqueous solution using sono-activated persulfate process. Ultrason. Sonochem. 29, 156–162. https://doi.org/10.1016/j.ultsonch.2015.09.008.

Wang, Y.X., Kornev, I., Wei, C.H., Preis, S., 2019. Surfactant and non-surfactant radical scavengers in aqueous reactions induced by pulsed corona discharge treatment. J. Electrochem. 98, 82–86. https://doi.org/10.1016/j.elstat.2019.03.001.

Wardman, P., 1989. Reduction potentials of one electron couples involving free radicals in aqueous solution. J. Phys. Chem. Ref. Data 18, 1637–1755. https://doi.org/10.1063/1.555843.

Wu, J., Xiong, Q., Liang, J., He, Q., Yang, D., Deng, R., Chen, Y., 2020. Degradation of benzotriazole by DBD plasma and peroxymonosulfate: Mechanism, degradation pathway and potential toxicity. Chem. Eng. J. 384, 123300 https://doi.org/10.1016/j.cej.2019.123300.

Xia, X., Zhu, F., Li, J., Yang, H., Wei, L., Li, Q., Jiang, J., Zhang, G., Zhao, Q., 2020. A review study on sulfate-radical-based advanced oxidation processes for domestic/industrial wastewater treatment: degradation, efficiency, and mechanism. Front. Chem. 8, 592056 https://doi.org/10.3389/fchem.2020.592056.

Zimmermann, S.G., Schmukat, A., Schulz, M., Benner, J., von Gunten, U., Ternes, T.A., 2012. Kinetic and mechanistic investigations of the oxidation of tramadol by ferrate and ozone. Environ. Sci. Technol. 46, 876–884. https://doi.org/10.1021/es203348q.

Antonopoulou, M, Thoma, A., Konstantinou, F., Vlastos, D., Hela, D., 2020. Assessing the human risk and the environmental fate of pharmaceutical Tramadol. Sci. Total Environ. 710, 135396 https://doi.org/10.1016/j.scitotenv.2019.135396.

Appendix 2

catalysts

Article

Degradation of Antibiotic Vancomycin by UV Photolysis and Pulsed Corona Discharge Combined with Extrinsic Oxidants

Dmitri Nikitin [1], Balpreet Kaur [2], Sergei Preis [1] and Niina Dulova [1,*]

1   Department of Materials and Environmental Technology, Tallinn University of Technology, Ehitajate tee 5, 19086 Tallinn, Estonia
2   Department of Chemistry, University of Jyväskylä, Survontie 9 B, P.O. Box 35, FI-40014 Jyväskylä, Finland
*   Correspondence: niina.dulova@taltech.ee

Abstract: Antibiotics are the most frequently detected pharmaceuticals in the environment creating conditions for the development of resistant genes in bacteria. Degradation and mineralization of glycopeptide antibiotic vancomycin (VMN) were examined by UV photolysis, pulsed corona discharge (PCD), and their combinations with extrinsic oxidants, hydrogen peroxide (HP), peroxydisulfate (PDS), and peroxymonosulfate (PMS). Both combinations were effective in VMN degradation and faster at pH 11 than in acidic or neutral media. Combined with the UV photolysis, HP showed a higher oxidation rate than other oxidants, whereas PMS and PDS proved to be more efficient in combinations with PCD. In contrast to low-to-moderate mineralization of VMN in the UV/oxidant combinations, PCD and PCD/oxidant combinations appeared to be more effective, reaching up to 90% of TOC removal in acidic/neutral solutions. Application of extrinsic oxidants resulted in an energy efficiency of VMN 90% oxidation improved from 36 to 61 g kW^{-1} h^{-1} in HP-assisted photolysis, and from 195 to 250 g kW^{-1} h^{-1} in PCD with additions of HP and PDS, thus showing the promising character of the combined treatment.

Keywords: advanced oxidation; energy efficiency; non-thermal plasma; persulfate

1. Introduction

In recent years, antibiotics, becoming the most frequently detected pharmaceutical compounds in the environment [1], have created conditions for the development of resistant genes in bacteria [2,3]. The resistant bacteria are of increasing concern due to their eco-toxicological effects [4,5]. Vancomycin (VMN) is an amphoteric glycopeptide antibiotic used to treat infections caused by Gram-positive organisms [6]. This antibiotic and its modifications are considered as drugs of last resort, i.e., the world's last line of defense against resistant pathogens, making these of extreme importance from the environmental point of view [7]. Vancomycin was detected in French rivers in concentrations reaching up to 90 ng L^{-1} [8], and in the effluents of the wastewater treatment plants (WWTPs) of Milan and Varese, Italy, as high as 17.4 $\pm$ 1.7 ng L^{-1} and 24.4 $\pm$ 31 ng L^{-1}, respectively [9].

Incomplete removal of antibiotics and other drugs from wastewaters at WWTPs requires alternative or supplementary approaches, such as, e.g., advanced oxidation processes (AOPs) using reactive oxygen species (ROS), including atomic oxygen, hydroxyl, and other radicals, able to degrade organic contaminants in water [3,10]. For example, the application of UV/TiO$_2$ combination showed 89.5% degradation of VMN in 36 min at the initial concentration of 58 mg L^{-1}, TiO$_2$ dosage of 55 mg L^{-1}, and temperature 40 °C [11].

Advanced oxidation methods include, among others, UV-induced oxidation and non-thermal electric discharge plasma. Photolysis is used for the activation of extrinsic oxidants such as hydrogen peroxide (HP), peroxydisulfate (PDS), and peroxymonosulfate (PMS) to produce hydroxyl (HO$^{\bullet}$) or sulfate radicals (SO$_4^{\bullet-}$) [12]. Compared with HO$^{\bullet}$, SO$_4^{\bullet-}$ possess equal or even higher redox potential of 2.5–3.1 V and exhibits higher selectivity at longer

half-life [13]. Numerous studies showed high efficacy in degradation and mineralization of contaminants of emerging concern by UV/HP, UV/PDS, and UV/PMS processes [3,13–15].

Non-thermal plasma generates hydroxyl radicals in a variety of electric discharge types [16]. The gas-phase pulsed corona discharge (PCD) is applied to the water dispersed in the form of droplets, jets, and films in the discharge zone. This discharge surpasses other plasma types in energy efficiency due to the formation of hydroxyl radicals at the surface of the treated aqueous solution, i.e., in close vicinity of the target pollutants experiencing negligible resistance in diffusion into the aqueous phase [17]. Except for hydroxyl radicals, atomic oxygen, ozone, hydrogen peroxide, and other reactive species participate in PCD oxidation. Previously, it showed high removal efficiency for pharmaceuticals such as metformin, tramadol, and dexamethasone [18,19], as well as improved oxidation rates with persulfate addition [20]. The use of persulfate additives is actively studied for other plasma types, for example, double barrier discharge, achieving increased degradation rates for different organic pollutants [21–23].

The current study aimed to evaluate the effect of extrinsic oxidants on the degradation and mineralization of VMN in combination with UV photolysis and PCD. To the best of the authors' knowledge, no similar research has been performed, both in terms of the target compound and the use of combinations. Operation parameters, pH, and extrinsic oxidant dose were evaluated for cost efficiency according to the delivered energy and the cost of extrinsic oxidants.

2. Results and Discussion

2.1. Effect of pH on VMN Oxidation in UV Photolysis and PCD Treatment

In blank VMN hydrolysis experiments at unadjusted pH without applying UV or PCD, no significant changes ($\leq$5%) in concentration of VMN were observed in 2 h. In turn, the application of direct UV photolysis and PCD treatment resulted in 90% removal at about 0.53 kWh m^{-3} and 0.09 kWh m^{-3} of delivered energy (Figure 1). Thus, the PCD oxidation of VMN was a few times more energy efficient than in UV photolysis.
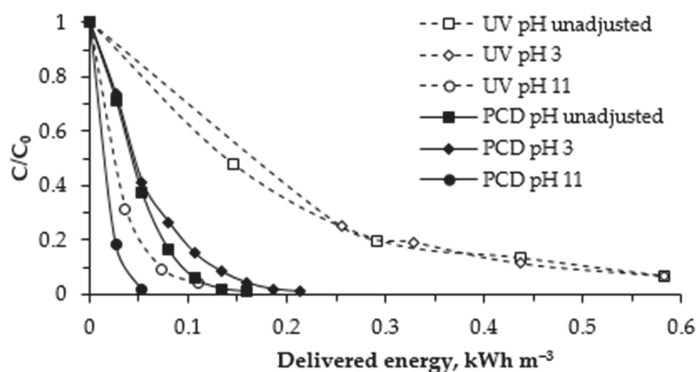

Figure 1. Degradation of VMN at different pH values in UV photolysis and PCD treatment ([VMN]$_0$ = 13.5 μM).

The effect of pH on the oxidation of organic molecules is often associated with their dissociation or protonation. Due to its molecular structure containing numerous deprotonated moieties available for the electrophilic attack [24], the VMN molecule has several dissociation constants making the increase in pH from 2.9 to 11.7, greatly improving its oxidation rate. As shown in Figure 1, the effect of pH on VMN oxidation within acidic to circum-neutral, i.e., the unadjusted conditions interval was negligible for both PCD and UV photolysis processes. However, in alkaline solutions, both processes showed increased oxidation efficacy providing >90% VMN degradation at energy doses lower than in acidic media for 2.5 and 6.0 times in PCD and UV photolysis, respectively. The results of PCD

oxidation are consistent with the study by Dodd et al. [24] where VMN degradation rates in ozonation increased at alkaline pH. This may be also explained with decomposition of ozone-forming hydroxyl radicals at faster rates. The change in pH may also affect the light absorbance properties of the compound, improving it with increasing pH and thus explaining the increased efficiency of UV photolysis at pH 11 [25].

Due to the negligible difference in oxidation rates between acidic and circum-neutral pH, UV/oxidant and PCD/oxidant combinations were studied only in alkaline and neutral solutions. In addition, unadjusted circum-neutral pH decreases during the treatment of VMN solutions due to acidic by-products formation. In PCD treatment, nitrates are formed with nitrogen oxidation [26].

2.2. VMN Oxidation in UV/Oxidant and PCD/Oxidant Combinations

Experiments with oxidants without application of UV irradiation and PCD showed no effect on VMN. Figure 2, Figures S1 and S2 from Supplementary Materials demonstrate the kinetics of VMN degradation in the pseudo-first-order reaction for UV and PCD treatment with and without extrinsic oxidants ($R^2 > 0.98$).
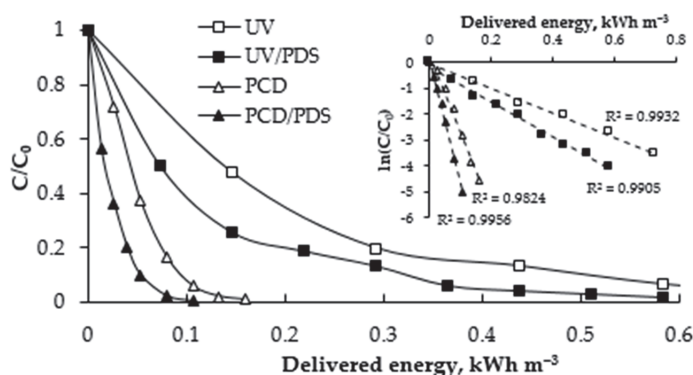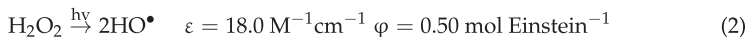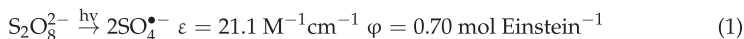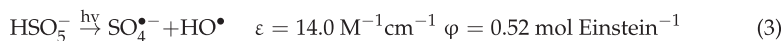

Figure 2. Degradation of VMN in UV photolysis, PCD treatment, UV/PDS, and PCD/PDS combinations ($[VMN]_0 = 13.5$ μM, $[PDS]_0 = 67.5$ μM, unadjusted pH).

For example, the addition of PDS in the amount of 67.5 μM, i.e., in the VMN/PDS molar ratio of 1/5 to UV-irradiated VMN solution, showed synergetic growth of k_1 value 1.43 times from 4.7 to 6.7 $m^3 kW^{-1} h^{-1}$. For the PCD treatment, the addition of PDS in the same amount improved the reaction rate constant 1.57 times from 30.3 to 47.7 $m^3 kW^{-1} h^{-1}$. The enhanced VMN degradation may be attributed to the activation of PDS to strong reactive species, $HO^\bullet$ and $SO_4^{\bullet-}$.

Similar VMN degradation enhancement was observed with extrinsic HP and PMS in combinations with UV and PCD (Figures S1 and S2 from Supplementary Materials), showing, however, certain quantitative difference: in the UV photolysis, the addition of 67.5 μM of hydrogen peroxide resulted in $k_1 = 8.8$ $m^3 kW^{-1} h^{-1}$ surpassing the combination with PDS (6.7 $m^3 kW^{-1} h^{-1}$) and PMS (5.3 $m^3 kW^{-1} h^{-1}$). The effect of PMS additions on the UV photolysis was of minor importance (Figure S2 from Supplementary Materials), although both oxidants, HP and PMS, exhibited a noticeable yet moderate synergy effect on PCD oxidation (Figure S1 from Supplementary Materials). The reason for this difference is most likely related to the different extrinsic oxidants' activation mechanisms: UV photolysis activates the oxidants by the fission of the O-O bond providing a mixture of sulfate and hydroxyl radicals (Equations (1)–(3)) [13,27]:

$$S_2O_8^{2-} \xrightarrow{h\nu} 2SO_4^{\bullet-} \quad \varepsilon = 21.1 \text{ M}^{-1}\text{cm}^{-1} \quad \varphi = 0.70 \text{ mol Einstein}^{-1} \tag{1}$$

$$H_2O_2 \xrightarrow{h\nu} 2HO^\bullet \quad \varepsilon = 18.0 \text{ M}^{-1}\text{cm}^{-1} \quad \varphi = 0.50 \text{ mol Einstein}^{-1} \tag{2}$$

$$HSO_5^- \xrightarrow{h\gamma} SO_4^{\bullet-} + HO^\bullet \quad \varepsilon = 14.0\ M^{-1}cm^{-1}\ \varphi = 0.52\ mol\ Einstein^{-1} \tag{3}$$

where ε is the molar extinction coefficient at a wavelength of 254 nm, and φ is the quantum yield for UV photolysis.
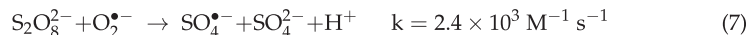
Activation of extrinsic oxidants in PCD proceeds via a complex action of electromagnetic field, UV radiation, and formation of hydroxyl radicals and other reactive species acting as activators. Contrary to UV photolysis, the activation in PCD occurs at the plasma–liquid interface with a minor contribution of reactions in the bulk solution [28].

In PCD, UV light is emitted by the $C^3\Pi_u \rightarrow B^3\Pi_g$ electronic transition in the N_2 molecule and the reported wavelengths for pulsed corona discharge of point-to-plane configuration are above 300 nm [29]. Considering the effective wavelengths activating extrinsic oxidants from 200 to 310 nm, the radiation emitted by PCD most probably plays a negligible role in their activation [13,30].
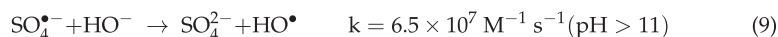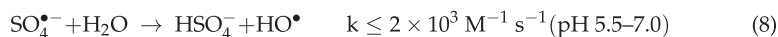
In water radiolysis experiments, a solvated electron (e_{aq}^-) rapidly activates peroxydisulfate anion (Equation (4)) [31]:

$$S_2O_8^{2-} + e_{aq}^- \rightarrow SO_4^{2-} + SO_4^{\bullet-} \qquad k = 1.1 \times 10^{10}\ M^{-1}\ s^{-1} \tag{4}$$
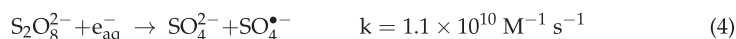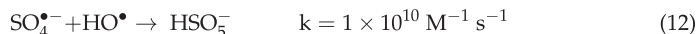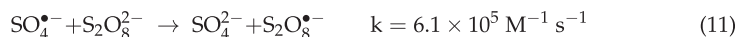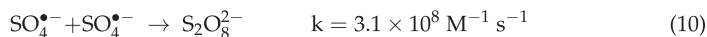
The presence of solvated electrons in atmospheric-pressure plasmas was confirmed by Rumbach et al. [32]. They found an average penetration depth of electrons to water of 2.5 ± 1.0 nm and noted that the kinetics of electron scavenging is similar, although not identical, to the solvated electrons formed in water radiolysis. The extrinsic oxidants' activation mechanism with solvated electrons is presumably the most important one since the rate of PDS activation by ROS (Equations (5)–(7)) is several orders of magnitude lower [22]:

$$S_2O_8^{2-} + HO^\bullet \rightarrow SO_4^{\bullet-} + HSO_4^- + 0.5O_2 \quad k = 8 \times 10^4\ M^{-1}\ s^{-1} \tag{5}$$

$$S_2O_8^{2-} + H^\bullet \rightarrow SO_4^{\bullet-} + SO_4^{2-} + H^+ \qquad k = 2.5 \times 10^7\ M^{-1}\ s^{-1} \tag{6}$$

$$S_2O_8^{2-} + O_2^{\bullet-} \rightarrow SO_4^{\bullet-} + SO_4^{2-} + H^+ \qquad k = 2.4 \times 10^3\ M^{-1}\ s^{-1} \tag{7}$$

The reaction described in Equation (6) is less probable for hydrogen radicals being scavenged at the gas–liquid interface by abundant oxygen. Sulfate radicals formed this or that way, however, are more selective than hydroxyl radicals and may not be utilized in reactions with organic compounds. Instead, sulfate radicals react with water molecules forming hydroxyl radicals in reactions strongly dependent on pH (Equations (8)–(9)) [33,34]:

$$SO_4^{\bullet-} + H_2O \rightarrow HSO_4^- + HO^\bullet \qquad k \leq 2 \times 10^3\ M^{-1}\ s^{-1}(pH\ 5.5–7.0) \tag{8}$$

$$SO_4^{\bullet-} + HO^- \rightarrow SO_4^{2-} + HO^\bullet \qquad k = 6.5 \times 10^7\ M^{-1}\ s^{-1}(pH > 11) \tag{9}$$

The recombination of sulfate radicals and their reactions with other radicals are faster (Equations (10)–(12)) making these more probable [35,36], hindering the actions of sulfate and hydroxyl radicals:

$$SO_4^{\bullet-} + SO_4^{\bullet-} \rightarrow S_2O_8^{2-} \qquad k = 3.1 \times 10^8\ M^{-1}\ s^{-1} \tag{10}$$

$$SO_4^{\bullet-} + S_2O_8^{2-} \rightarrow SO_4^{2-} + S_2O_8^{\bullet-} \qquad k = 6.1 \times 10^5\ M^{-1}\ s^{-1} \tag{11}$$

$$SO_4^{\bullet-} + HO^\bullet \rightarrow HSO_5^- \qquad k = 1 \times 10^{10}\ M^{-1}\ s^{-1} \tag{12}$$

The activation of peroxymonosulfate anions introduced with PMS or formed from PDS in PCD presents another concern. The anion HSO_5^- has an asymmetrical structure with the O-O bond having the dissociation energy of 377 kJ mol^{-1} vs. 92 kJ mol^{-1} of peroxydisulfate anion [37], making the HSO_5^- activation via direct cleavage of O-O less probable than that of $S_2O_8^{2-}$ (Equation (13)):

$$HSO_5^- + e_{aq}^- \rightarrow HO^\bullet + SO_4^{2-}\ /\ SO_4^{\bullet-} + HO^-\ k = 8.4 \times 10^8\ M^{-1}\ s^{-1} \tag{13}$$
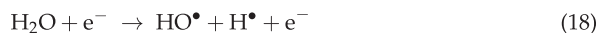
Nevertheless, Shang et al. [37] showed performance of PMS surpassing that of PDS in accelerating oxidation of sulfamethoxazole by dielectric barrier discharge (DBD). They supposed faster oxidation was contributed by the activation of PMS with dissolved ozone (Equations (14)–(16)) [38]:
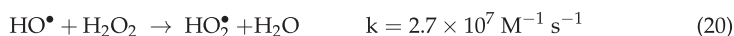
$$-O_3SOO^- + O_3(aq) \rightarrow -O_3SO_5^- \rightarrow SO_5^{\bullet-} + O_3^{\bullet-} \quad k = 2.2 \times 10^4 \text{ M}^{-1} \text{ s}^{-1} \quad (14)$$

$$2SO_5^{\bullet-} \rightarrow 2SO_4^{\bullet-} + O_2 \quad (15)$$

$$SO_5^{\bullet-} + O_3 \rightarrow SO_4^{\bullet-} + 2O_2 \quad (16)$$

Due to a relatively slow rate (Equation (14)), the reaction with dissolved ozone formed in PCD [28] likely takes place in the bulk solution.

Concerning hydrogen peroxide, Tikker et al. [20] showed that PCD results in H_2O_2 formation in concentrations of up to 0.11 mM in acidic solutions in 1 h of treatment at the pulsed power of 32 W. The H_2O_2 formation is associated with the hydroxyl radicals' recombination (Equation (17)), which is produced from water molecules (Equation (18)) [37]:
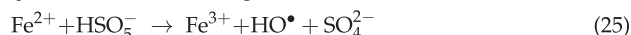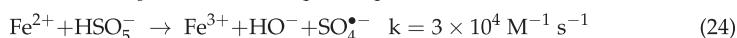
$$HO^\bullet + HO^\bullet \rightarrow H_2O_2 \qquad k = 5.5 \times 10^9 \text{ M}^{-1} \text{ s}^{-1} \quad (17)$$

$$H_2O + e^- \rightarrow HO^\bullet + H^\bullet + e^- \quad (18)$$

Sulfate and hydroxyl radicals may also react with HP producing hydroperoxyl radicals ($HO_2^\bullet$) able to activate persulfate anion (Equations (19)–(21)) [33]:

$$SO_4^{\bullet-} + H_2O_2 \rightarrow SO_4^{2-} + HO_2^\bullet + H^+ \qquad k = 1.2 \times 10^7 \text{ M}^{-1} \text{ s}^{-1} \quad (19)$$

$$HO^\bullet + H_2O_2 \rightarrow HO_2^\bullet + H_2O \qquad k = 2.7 \times 10^7 \text{ M}^{-1} \text{ s}^{-1} \quad (20)$$

$$S_2O_8^{2-} + HO_2^\bullet \rightarrow SO_4^{\bullet-} + SO_4^{2-} + O_2 + H^+ \quad k = 2.2 \times 10^4 \text{ M}^{-1} \text{ s}^{-1} \quad (21)$$

Notably, moderate amounts of ferrous cations form in the stainless steel PCD reactor reaching Fe^{2+} concentrations of up to 0.2 mg L^{-1} within 2 h of treatment. It makes the Fenton reaction (Equation (22)) play a part, presumably minor, in the oxidation mechanism of the target compound in the PCD process.

$$Fe^{2+} + H_2O_2 \rightarrow Fe^{3+} + HO^- + HO^\bullet \qquad k = 53 \text{ M}^{-1} \text{ s}^{-1} \quad (22)$$
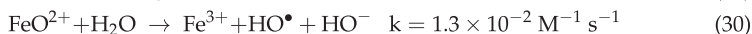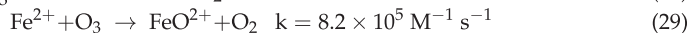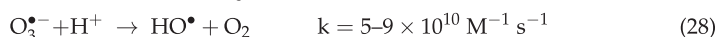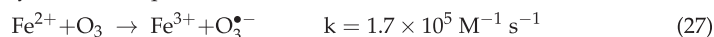
Activation of PDS and PMS with ferrous ions is actively studied (Equations (23)–(25)) [39]:

$$Fe^{2+} + S_2O_8^{2-} \rightarrow Fe^{3+} + SO_4^{2-} + SO_4^{\bullet-} \quad k = 30 \text{ M}^{-1} \text{ s}^{-1} \quad (23)$$

$$Fe^{2+} + HSO_5^- \rightarrow Fe^{3+} + HO^- + SO_4^{\bullet-} \quad k = 3 \times 10^4 \text{ M}^{-1} \text{ s}^{-1} \quad (24)$$

$$Fe^{2+} + HSO_5^- \rightarrow Fe^{3+} + HO^\bullet + SO_4^{2-} \quad (25)$$

Shang et al. [22] reported somewhat accelerated *p*-nitrophenol (2.5 mM) oxidation in the combination of DBD/PDS with the addition of 3.6 μM of Fe^{2+}. A tenfold increase in Fe^{2+} dose modestly accelerated oxidation rate, which may be explained by rapid scavenging of sulfate radicals with excessive ferrous ions (Equations (26)) [22]:

$$SO_4^{\bullet-} + Fe^{2+} \rightarrow Fe^{3+} + SO_4^{2-} \qquad k = 4.6 \times 10^9 \text{ M}^{-1} \text{ s}^{-1} \quad (26)$$
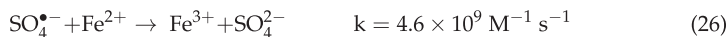
Besides Fenton-like reactions, leaching iron may also catalyze ozone decomposition, producing hydroxyl radicals (Equations (27)–(30)) [40]:

$$Fe^{2+} + O_3 \rightarrow Fe^{3+} + O_3^{\bullet-} \qquad k = 1.7 \times 10^5 \text{ M}^{-1} \text{ s}^{-1} \quad (27)$$

$$O_3^{\bullet-} + H^+ \rightarrow HO^\bullet + O_2 \qquad k = 5\text{–}9 \times 10^{10} \text{ M}^{-1} \text{ s}^{-1} \quad (28)$$

$$Fe^{2+} + O_3 \rightarrow FeO^{2+} + O_2 \quad k = 8.2 \times 10^5 \text{ M}^{-1} \text{ s}^{-1} \quad (29)$$

$$FeO^{2+} + H_2O \rightarrow Fe^{3+} + HO^\bullet + HO^- \quad k = 1.3 \times 10^{-2} \text{ M}^{-1} \text{ s}^{-1} \quad (30)$$

2.2.1. Effect of Extrinsic Oxidant Dose on VMN Oxidation in UV/Oxidant Combinations

Figure 3 presents the effect of extrinsic oxidant dose, expressed as VMN/oxidant molar ratio, and pH on the reaction rate constant k_1 and TOC removal in VMN oxidation

by unassisted UV photolysis and the UV/oxidant combinations. In the UV photolysis, the k_1 values in circum-neutral and acidic solutions were similarly low, while having TOC elimination slightly increased with decreasing pH. At alkaline pH, the k_1 and TOC degradation achieved the highest values of 29.8 m^3 kW^{-1} h^{-1} and 24.1%, respectively.
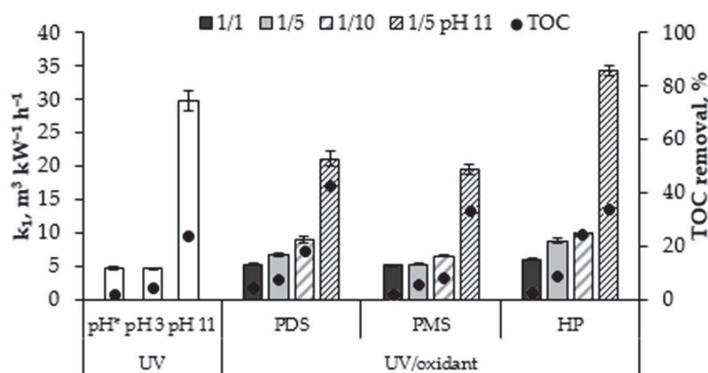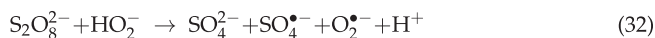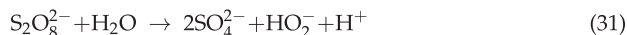

Figure 3. Effects of pH and VMN/oxidant molar ratio on the target compound UV photolytic oxidation rate constant k_1 and TOC removal ($[VMN]_0$ = 13.5 μM, unadjusted pH*, treatment time for TOC removal 2 h).

The performance of the combined treatment in unadjusted pH conditions was moderately enhanced with the increasing extrinsic oxidant concentrations. For instance, the PDS addition in the molar VMN/oxidant ratios of 1/1 (13.5 μM), 1/5 (67.5 μM), and 1/10 (135.0 μM) resulted in the k_1 value increased by 12.2%, 41.3%, and 89.2%, respectively, compared with the unassisted UV photolysis. A similar trend was observed with the UV/HP combination, while the addition of PMS showed low performance achieving only 37.8% in the best k_1 improvement at the 1/10 VMN/PMS molar ratio. These results are consistent with the different molar extinction coefficients presumably resulting in different amounts of produced radicals (Equations (1)–(3)): slower activation of PMS at the fast degradation of VMN by unassisted UV photolysis resulted in a smaller effect of PMS addition.
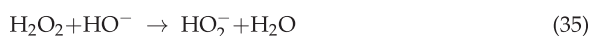
The VMN mineralization was also improved with extrinsic oxidants (Figure 3). The UV/oxidant combinations showed an increase in TOC removal from 1.7% in unassisted UV photolysis in circum-neutral solutions to 18.1%, 24.2%, and 7.9%, respectively, in UV/PDS, UV/HP, and UV/PMS combinations at the oxidant concentrations of 135.0 μM. These observations suggest hydroxyl radicals produced from H_2O_2 are utilized in the oxidation of degradation by-products more effectively for their unselective reactions.

At pH 11, the VMN degradation rate constant k_1 in the unassisted UV photolysis, and UV/PDS and UV/PMS combinations at the VMN/oxidant molar ratio of 1/5 comprised 29.8 m^3 kW^{-1} h^{-1}, 21.1 m^3 kW^{-1} h^{-1}, and 19.5 m^3 kW^{-1} h^{-1}, respectively (Figure 3). The reason for lower oxidation rates in UV/PDS and UV/PMS combinations may be the absorption of the photons by persulfate or peroxymonosulfate anions preventing deprotonated VMN direct photolytic degradation, which is faster than that proceeding via formation of sulfate radicals. The use of the UV/HP combination resulted in k_1 being increased to 34.3 m^3 kW^{-1} h^{-1}, which was probably due to the faster degradation of hydrogen peroxide and production of hydroxyl radicals, thus overpowering their lower oxidation potential in alkaline media [41]. The TOC removal also rose from 24.1% to 33.9% in UV-irradiated alkaline VMN solution with HP addition, which is similar to the improvement at unadjusted circum-neutral pH. The UV/PDS combination showed better performance in TOC removal than UV/PMS, 42.6% vs. 33.0%, due to faster synergism of both VMN photolysis (Figure 1) and PDS decomposition (Equation (5)) in alkaline conditions. The synergy is supported by the persulfate anion activation with hydroperoxide anion-producing sulfate radicals

contributing to the mineralization of VMN oxidation products (Equations (31) and (32)) [13]. Further transformation of sulfate radicals to hydroxyl radicals through Equation (9) may also somewhat change the balance between ionic and molecular forms of VMN and its oxidation by-products affecting further oxidation.

$$S_2O_8^{2-}+H_2O \rightarrow 2SO_4^{2-}+HO_2^-+H^+ \tag{31}$$

$$S_2O_8^{2-}+HO_2^- \rightarrow SO_4^{2-}+SO_4^{\bullet-}+O_2^{\bullet-}+H^+ \tag{32}$$

The activation of PMS in alkaline solutions can also take place, producing hydroxyl radicals, singlet ozone, and superoxide radicals. For example, the degradation of Acid Orange 7 was observed for the alkali/PMS combination but not for the alkali/PDS [42]. One of the important steps of PMS activation at alkaline pH is the formation of hydrogen peroxide and its hydrolysis to hydroperoxide anion, which further produces other ROS (Equations (33)–(35)) [42]:

$$HSO_5^-+H_2O \rightarrow H_2O_2+HSO_4^- \tag{33}$$

$$H_2O_2 \rightarrow HO_2^-+H^+ \tag{34}$$

$$H_2O_2+HO^- \rightarrow HO_2^-+H_2O \tag{35}$$

For example, hydrogen peroxide formed in the reaction described by Equation (33) may also be degraded by UV radiation forming hydroxyl radicals (Equation (2)), thus oxidizing VMN and its degradation products. This hypothesis may be evidenced by mineralization with UV/HP proceeding with efficiency similar to the one of PMS in alkaline solutions (Figure 3).

2.2.2. Effect of Extrinsic Oxidant Dose on VMN Oxidation in PCD/Oxidant Combinations

In acidic media, the unassisted PCD treatment showed a somewhat decreased VMN degradation reaction rate constant compared with the unadjusted circum-neutral pH, although the TOC removal increased from 76.9% to 85.7% with decreasing pH (Figure 4). The higher oxidational potential of hydroxyl radicals in acidic media [41] most probably contributed to more effective oxidation, whereas selective reactions of more stable molecular ozone may be attributed to the lower oxidation rate of VMN in acidic solutions. These contrary phenomena resulted in a decreased VMN oxidation rate, although the reaction products, such as oxalate, are easier oxidized in acidic medium providing deeper mineralization [20]. At alkaline pH, similarly to unassisted UV photolysis, the value of k_1 increased to 75.8 m^3 kW^{-1} h^{-1}, while TOC removal decreased by almost half to 48.8%. Similar results were obtained by Tikker et al. [20] for oxalate mineralization in unassisted PCD treatment, and the decreased TOC removal was explained by (i) the decreased hydroxyl radical oxidation potential [41], (ii) scavenging of hydroxyl radicals by carbonates and/or bicarbonates, and (iii) possible scavenging of hydroxyl radicals by ozone. Carbonates/bicarbonates are accumulated in alkaline solutions due to absorption from the air (Equations (36) and (37)) and mineralization of by-products.
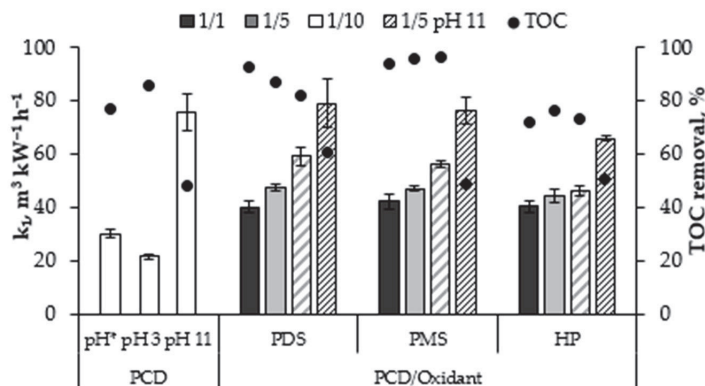
$$CO_2+HO^- \rightarrow HCO_3^- \tag{36}$$

$$HCO_3^-+HO^- \rightarrow CO_3^{2-}+H_2O \tag{37}$$
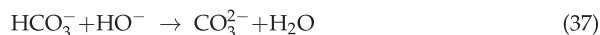
Figure 4. Effect of pH and VMN/oxidant molar ratio on the target compound PCD oxidation rate constant k_1 and TOC removal ($[VMN]_0 = 13.5$ μM, unadjusted pH*, treatment time for TOC removal 2 h).

Table 1 shows the TIC concentration after 2 h of treatment in acidic/circum-neutral and alkaline conditions. In alkaline media, the total inorganic carbon changed during the treatment from around $TIC_0 = 7 \pm 1.4$ to 14 ± 0.7 mg C L^{-1} corresponding to 35 ± 7.0 and 70 ± 3.5 mg L^{-1} of bicarbonate/carbonate, while at the starting circum-neutral pH, the final concentration of bicarbonates did not exceed 4 mg L^{-1} since the pH was reduced during the treatment. The second-order reaction rate constants of radical scavenging reactions with bicarbonates/carbonates are high enough to reduce the number of available hydroxyl radicals and, also, interrupt the formation of ozonide ion radicals from superoxide radicals responsible for the generation of hydroxyl radicals (Equations (38)–(41)) [34]:
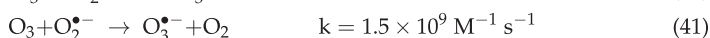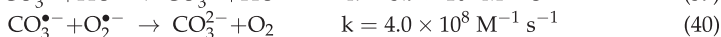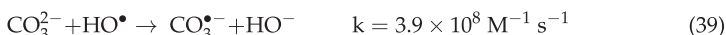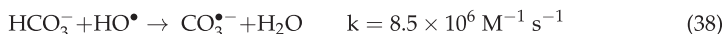
$$HCO_3^- + HO^\bullet \rightarrow CO_3^{\bullet-} + H_2O \qquad k = 8.5 \times 10^6 \text{ M}^{-1}\text{ s}^{-1} \qquad (38)$$

$$CO_3^{2-} + HO^\bullet \rightarrow CO_3^{\bullet-} + HO^- \qquad k = 3.9 \times 10^8 \text{ M}^{-1}\text{ s}^{-1} \qquad (39)$$

$$CO_3^{\bullet-} + O_2^{\bullet-} \rightarrow CO_3^{2-} + O_2 \qquad k = 4.0 \times 10^8 \text{ M}^{-1}\text{ s}^{-1} \qquad (40)$$

$$O_3 + O_2^{\bullet-} \rightarrow O_3^{\bullet-} + O_2 \qquad k = 1.5 \times 10^9 \text{ M}^{-1}\text{ s}^{-1} \qquad (41)$$

**Table 1.** Concentration of TIC in VMN solutions in 2 h of treatment dependent on pH values ($[VMN]_0 = 13.5$ μM, $[oxidant]_0 = 67.5$ μM).

Combination	TIC, mg C L^{-1}	
	pH 3/Unadjusted pH	pH 11
UV	0.5	3.6
UV/PDS	0.8	5.8
UV/HP	1.3	4.3
UV/PMS	0.7	4.7
PCD	0.6	14.3
PCD/PDS	0.6	12.9
PCD/HP	0.6	14.6
PCD/PMS	0.5	13.5

At alkaline pH, ozone may react with hydroxyl radicals forming less reactive hydroperoxyl radicals (Equation (42)) [34]:

$$O_3 + HO^\bullet \rightarrow HO_2^\bullet + O_2 \qquad k = 1.0 \times 10^8 \text{ M}^{-1}\text{ s}^{-1} \qquad (42)$$
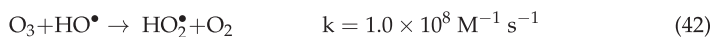
The dose of added oxidants directly affects the oxidation performance in tested combinations, with excessive concentrations exhibiting a self-scavenging effect, whereas a lack of oxidant shows a negligible effect. Previously, the optimum target compound-to-oxidant molar ratio in DBD treatment of benzotriazole and sulfamethoxazole solutions was found to fit into a 1/30–1/40 interval [23,43]. For oxalate, however, oxidation in PCD showed the optimal molar ratio with PDS of 1/0.5, improving the energy efficiency of mineralization for 1.7 times.

In this study, the performance of PCD/oxidant combinations in circum-neutral solutions moderately improved with increased concentrations of extrinsic oxidants following the descending order PCD/PDS > PCD/PMS > PCD/HP (Figure 4), suggesting more effective production of radicals in the PCD/PDS combination. The moderate character of oxidation enhancement is seen from, for example, a less than twofold increase in VMN degradation rate when PDS was added in the amount of tenfold the VMN content: the k_1 value at its maximum of 59.3 m^3 kW^{-1} h^{-1} was achieved at the PDS dose of 135.0 μM at the VMN/PDS molar ratio of 1/10 compared with 30.3 m^3 kW^{-1} h^{-1} for unassisted PCD treatment. The required time to degrade VMN decreased 2-fold from 4 to 2 min indicating that contact with electrical discharges (Equation (4)) is the main mechanism of PDS activation because long-living oxidants, i.e., ozone, were at low concentrations [26]. The disproportional but direct connection between the extrinsic oxidant dose and the reaction rate indicates that sulfate radicals formed by PCD activation from PDS contribute to VMN oxidation. Further oxidation of the VMN degradation products with sulfate radicals also showed an effect compared with unassisted PCD; thus, TOC removal at the lowest PDS dose of 13.5 μM comprised 92.5%, whereas unassisted PCD removed TOC for 76.9% in circum-neutral solutions (Figure 4). The increased PDS dose showed a negative trend in VMN mineralization with decreasing the TOC removal to 82.1% at the maximum VMN/PDS ratio of 1/10, indicating a scavenging effect of sulfate radicals (Equations (10) and (11)) and/or hydrogen peroxide (Equation (19)).

Contrary to the PCD/PDS process, the PCD/PMS combination demonstrated improvement with growing PMS dose in both the pseudo-first-order VMN degradation reaction constant k_1 and mineralization of VMN oxidation products, reaching 56.4 m^3 kW^{-1} h^{-1} and 96.4%, respectively. The difference in activation pathways of PDS and PMS, as well as in the types of active species, provides better performance of PMS in combination with PCD. Furthermore, the activation of PMS with ozone (Equations (14)–(16)) and ferrous ions (Equations (24) and (25)) may also play an important role in changing the tendency in the oxidation rate and mineralization dependent on the extrinsic oxidant dosing. The activation of PMS with aqueous electrons is two orders of magnitude slower than that of PDS due to the higher O-O bond dissociation energy (Equations (4) and (13)), which makes the number of radical species smaller, thus helping to avoid scavenging associated with sulfate radical recombination seen for PDS (Equations (10) and (11)). Somewhat similar results were reported by Shang et al. [37] for the degradation of sulfamethoxazole in DBD/oxidant combinations: the increase in the reaction rate constant with PMS additions was higher than that with PDS compared with unassisted DBD.

The use of PCD/HP combination resulted in the lowest effect on the k_1 value amongst the studied extrinsic oxidants resulting in 46.1 m^3 kW^{-1} h^{-1} at the highest dose of HP (Figure 4). Since there is an accumulation of HP in PCD, its activation is slow, meaning that PCD is a weak hydrogen peroxide activator. This is consistent with the rather low VMN mineralization degree fluctuating from 71.8% to 76.5%. A large dose of HP did not improve oxidation, which was most likely the consequence of radical self-scavenging reactions.

In alkaline solutions, the PCD/oxidant combinations demonstrated accelerated VMN decomposition and decelerated mineralization compared with circum-neutral and acidic media (Figure 4). The accumulation of TIC (Table 1), supposedly as carbonates at pH 11, and associated oxidant-scavenging reactions were the reason for the lower VMN mineralization. The PMS and HP additions showed neutral effect in mineralization compared with unassisted PCD. In the PCD/PDS combination, however, the TOC removal increased from

47.9% in unassisted PCD to 60.9%, which may be determined by the TIC content decrease from 14.3 to 12.9 mg C L^{-1} in the PCD and PCD/PDS combination, respectively, and the increase in the number of reactive species possibly overpowering the scavenging effect of carbonates.

2.3. Identification of VMN Transformation Products

In addition to the efficiency of degradation and mineralization of the target compound, transformation products (TPs) were identified during the oxidation of VMN by the studied UV- and PCD-based systems using LC-MS analysis.

The results obtained showed that in the case of UV-based systems, the predominant transformation product was TP1 with m/z 716, most likely formed during the dehydroxylation of the VMN molecule (proposed elemental composition $C_{66}H_{73}Cl_2N_9O_{23}$), which was also previously identified by Furia et al. [44] in the oxidation of VMN with a Fenton-based system. In addition, the formation of TP2 with m/z 733 ($C_{66}H_{75}Cl_2N_9O_{25}$) and TP4 with m/z 741 ($C_{66}H_{75}Cl_2N_9O_{26}$) was observed, which suggests the hydroxylation of the VMN molecule. For PCD-based oxidation, traces of TP1, TP2, and TP3 were also found, but TP4 with m/z 758 turned out to be specific and more abundant, which most likely indicates the formation of a polyhydroxylated VMN molecule ($C_{66}H_{77}Cl_2N_9O_{28}$).

2.4. Comparison of Operating Costs

To evaluate energy efficiencies of the treatment systems under the scope, energy yields at 90% conversion of VMN (E_{90}, g kW^{-1} h^{-1}) were calculated as the ratio of the oxidized VMN quantity to the energies consumed by the UV irradiation and PCD treatment together with the cost of extrinsic oxidants [20]. The cost of oxidants was considered as EUR 1.0 kg^{-1}, EUR 1.5 kg^{-1}, and EUR 2.5 kg^{-1} for HP, PDS, and PMS, respectively, including transportation and taxation based on average wholesale prices on the market in 2022. The cost of oxidants was converted to the equivalent energy expense considering the average European non-household electric energy price of EUR 0.125 kW^{-1} h^{-1} [45] dependently on the dose, and added to the total energy expenditure. The calculation results are shown in Table 2.

Table 2. Energy efficiencies of VMN oxidation in UV/oxidant and PCD/oxidant combinations ($[VMN]_0$ = 13.5 μM, unadjusted pH).

	E_{90}, g kW^{-1} h^{-1}					
	UV			**PCD**		
pH 3	36			146		
Unadjusted pH	36			195		
pH 11	228			540		
Molar ratio	UV/PDS	UV/HP	UV/PMS	PCD/PDS	PCD/HP	PCD/PMS
1/1	37	44	34	250	256	126
1/5	34	52	23	187	196	39
1/10	28	61	18	143	136	21
1/5, pH 11	58	173	40	243	248	40

In the unassisted processes at unadjusted circum-neutral pH, the PCD treatment showed more than five times higher energy efficiency than UV photolysis. At pH 11, PCD and UV processes achieved their highest energy efficiencies of 228 g kW^{-1} h^{-1} and 540 g kW^{-1} h^{-1}, respectively.

The addition of extrinsic oxidants without substantial improvement in the oxidation rate negatively affects the energy efficiency while also making the combined treatment less convenient in terms of chemicals delivery, storing, and handling. However, some combinations with PDS and HP demonstrated considerably increased E_{90} values dependent on the applied oxidant dose; thus, at the lowest PDS and HP doses, combinations with PCD

showed cost efficiencies exceeding the unassisted process for about 1.3 times, decreasing with further extrinsic oxidant additions (Table 2).

The UV/PDS combination at the VMN/PDS molar ratio of 1/1 showed the VMN degradation result similar to the unassisted UV photolysis, although noticeably improving TOC removal (Figure 3). Interestingly, in the UV/HP combination, the trend in the treatment energy efficiency dependent on the HP dose is positive, showing the efficiency increased from 44 g kW^{-1} h^{-1} to 61 g kW^{-1} h^{-1} (Table 2). Showing the k_1 values similar to the ones in the UV/PDS process, the UV/HP combination was more effective due to the hydrogen peroxide cost being 1.5 times smaller than PDS.

Finally, being the most expensive and heaviest extrinsic oxidant (MW = 304 g mol^{-1}), PMS yields to other oxidants in energy efficiency compared with direct photolysis and unassisted PCD (Table 2).

3. Materials and Methods

3.1. Chemicals

Vancomycin hydrochloride ($C_{66}H_{75}Cl_2N_9O_{24}$·xHCl, ≥99%), sodium persulfate ($Na_2S_2O_8$, ≥99%), potassium peroxymonosulfate (Oxone®, $KHSO_5$·$0.5KHSO_4$·$0.5K_2SO_4$), hydrogen peroxide (H_2O_2, PERDROGEN™, ≥30%), potassium iodide (KI, ≥ 99%), sodium bicarbonate ($NaHCO_3$, 99%), and sodium sulfite (Na_2SO_3, ≥99%) were obtained from Sigma-Aldrich, St. Louis, MO, USA and used without further treatment. Methanol (CH_3OH, ≥99%), acetonitrile (CH_3CN, LiChrosolv®), and formic acid (CH_2O_2, 99%) used as eluents were obtained from Merck KGaA, Darmstadt, Germany.

3.2. Pulsed Corona Discharge Equipment

The PCD experiments were conducted in a device made by Flowrox Oy (Finland) with characteristics given in Table 3. The device consists of a PCD stainless steel reactor with the storage tank, pulse generator, and circulation pump with the frequency regulator used to control the pump rotation rate (Figure S3 from Supplementary Materials). The plasma reactor contains an electrode system consisting of high voltage wire electrodes positioned horizontally between two grounded vertical parallel plates. The generator applies high voltage pulses to the electrode system at the pulse repetition frequencies in pulses per second (pps) controlled incrementally as shown in Table 3. The output–input ratio of the pulse generator comprises 65%. Treated solution is dispersed through the perforated plate positioned above the wire electrodes at a certain spray density determined as the flow rate divided by the planar cross-sectional area of the plasma zone, m s^{-1}. After passing the plasma zone, treated solution falls to a storage tank, from where it is circulated back to the top of the reactor.

3.3. Photochemical Equipment

Photochemical experiments were performed in batch mode in a 1 L cylindrical glass reactor. A low-pressure mercury germicidal lamp (11 W, TUV PL-S, Philips, Netherlands) placed in a quartz sleeve inside the reactor was used as a UVC source. The input–output power of the lamp is approximately 32%. The incident photon flux at 254 nm of the lamp used in VMN oxidation comprised 2.55×10^{-7} Einstein s^{-1} measured by ferrioxalate actinometry. The lamp was turned on for 10 min before the trial to provide a constant radiation output. A water-cooling jacket was used to maintain constant temperature in the reactor.

3.4. Experimental Procedures

Experiments were carried out at an ambient room temperature of 21 ± 1 °C at the VMN initial concentration of 20 mg L^{-1} or 13.5 μM. The unadjusted water pH values were 5.8 ± 0.2 and 6.8 ± 0.2 for UV and PCD experiments, respectively. For acidic (pH 3) and alkaline (pH 11) conditions, pH was regulated by adding H_2SO_4 or NaOH in 0.1 to 5.0 M solutions. The effect of PDS, PMS, and HP additions in both photochemical and PCD

experiments were studied at concentrations of 13.5 µM, 67.5 µM, and 135.0 µM, providing the oxidant-to-target compound molar ratio equal to 1, 5, and 10. In experiments with the oxidant additions, the oxidation reaction in samples taken for HPLC-PDA analysis was quenched by adding methanol at the sample-to-CH_3OH volume ratio of 10. For the TOC analysis, sodium sulfite was used at the Na_2SO_3-to-oxidant molar ratio of 10. In the UV/oxidant trials, the VMN solution in the amount of 0.8 L was prepared in bi-distilled water and treated for 2 h with permanent stirring by means of a magnetic stirrer. After the dissolution of the added oxidant, the preheated UVC lamp inserted into the reactor initiated the oxidation.

Table 3. Technical parameters of PCD device.

Parameter	Value
Reactor parameters	
Reactor full volume, L	80
Perforated plate size, mm × mm	565 × 97
Number of perforations	24
Diameter of perforations, mm	3
Water flow rate, L min^{-1}	2–18
Spray density, m s^{-1}	0.002–0.0177
Plasma zone volume, m^3	0.011
Contact surface area at flow rate of 1 m^3 h^{-1}, m^{-1}	130 *
Electrode configuration	
High voltage wire length, m	12
Wire diameter, mm	0.6
Distance between electrodes and grounded plate, mm	17
Distance between high-voltage electrodes, mm	30
Generator characteristics	
Pulse repetition frequency, pps	25, 50, 100, 200, 500, and 800
Output power, W	8–112
Peak voltage, kV	22
Peak current, A	290
Current pulse duration, ns	70
Pulse energy, J	0.14–0.16

* The gas–liquid contact surface was measured using a classical method of sulfite oxidation by air oxygen in the presence of cobalt sulfate catalyst [46].

The stock solutions for PCD experiments were prepared in a 1 L volumetric flask using bi-distilled water, followed by dilution to a total volume of 5 L by distilled water in the reactor tank. Pre-selected amounts of the extrinsic oxidant were dissolved in a 100 mL volumetric flask and mixed with the treated solution in the tank before the start of treatment. All PCD experiments were performed at a circulated water flow rate of 1 m^3 h^{-1} corresponding to the gas–liquid contact surface area of 130 m^{-1} and the pulse repetition frequency of 50 pps with the pulsed power input of 8 W. The plasma treatment time comprised 2 h with a total energy dose of 2.4 kWh m^{-3} delivered to the treated sample. For proper sampling, the treated solutions were circulated in the reactor for four minutes after the pulse generator was turned off for equalizing the concentrations in the reactor's volume.

3.5. Analytical Methods

The concentration of VMN was determined using high-performance liquid chromatography combined with a diode array detector (HPLC-PDA, Shimadzu SPD-M20A, Shimadzu, Kyoto, Japan) equipped with a Phenomenex Gemini (150 × 2.0 mm, 1.7 mm) NX-C18 (110 Å, 5 µm) column. The analysis was performed using an isocratic method with a mobile phase composed of 9% vol. of acetonitrile containing 0.3% of formic acid and

91% vol. of 0.3% formic acid aqueous solution. The flow rate was kept at 0.25 mL min^{-1}. Samples injected in 75 μL volume were analyzed at a wavelength of 220 nm.

Samples from selected experiments were analyzed by high-performance liquid chromatography coupled with a mass spectrometer (HPLC-MS, Shimadzu LC-MS 2020, Shimadzu, Japan). Mass spectra were acquired in the full scan mode (scanning in the range of 100–1500 m/z). The instrument was operated in positive ESI mode and the results obtained with the MS detector were processed using Shimadzu Lab Solutions software.

Total carbon (TC) and total inorganic carbon (TIC) were measured using a TOC analyzer multi N/C$^{\circledR}$ 3100 (Analytik Jena, Jena, Germany) in 20 mL samples with an injection volume of 500 μL for each replicate. Solution pH was measured using a digital pH/Ion meter (Mettler Toledo S220, Mettler Toledo, Greifensee, Switzerland).

Utilization of persulfates was quantified iodometrically measuring residual concentrations in the treated samples by adding an excess KI and using a spectrophotometer (Genesys 10S, Thermo Scientific, Waltham, MA, USA) at λ = 352 nm [47]. The residual H_2O_2 concentration was measured spectrophotometrically at λ = 410 nm with titanyl sulfate by a H_2O_2-Ti^{4+} complex formation [48].

Due to different volumes of treated water and power input, photolytic and PCD oxidation processes cannot be compared by observing the decrease in VMN concentration over time, but only by the delivered energy doses calculated for the water volumes and the delivered power in the time of treatment.

To evaluate the effect of extrinsic oxidant addition on the VNM degradation efficiency, a pseudo-first-order reaction rate constant k_1 was calculated (Equation (43)) using slopes of the straight lines by plotting ln (C_t/C_0) as a function of delivered energy dose D (Equation (44)) through linear regression:

$$\frac{d[C]}{dD} = -k_1 \cdot [C] \tag{43}$$

$$D = \frac{P \cdot t}{V} \tag{44}$$

where k_1—pseudo-first-order reaction rate constant, m^3 kW^{-1} h^{-1}; C—concentration of target compound; D—delivered energy dose, kWh m^{-3}, P—power delivered in PCD or UV treatment, kW; and V—volume of treated solution, m^3.

The energy efficiency E_{90}, g kW^{-1} h^{-1}, was calculated for 90% VMN degradation using Equation (45):

$$E_{90} = \frac{\Delta C \cdot V}{W} \tag{45}$$

where ΔC—a decrease in target compound concentration, g m^{-3}; V—volume of treated solution, m^3; and W—energy consumption derived from the generator power output and the time of treatment, kWh.

4. Conclusions

The UV photolysis, PCD, UV/oxidant, and PCD/oxidant processes were found to be effective in decomposing the aqueous pharmaceutical vancomycin. All studied extrinsic oxidants demonstrated certain synergism with PCD and UV, accelerating oxidation. For all combinations, with a minor exception for UV/PMS showing negligible improvement, an increase in the dose of extrinsic oxidant resulted in a noticeable increase in the pseudo-first-order rate constant. In the UV/oxidant combination, TOC removal increased mostly linearly with the applied oxidant dose, although in the PCD/oxidant combination, the effect of the oxidant dose on TOC removal showed variable deviations, with only the PCD/PMS combination showing a positive trend at the highest removals. The TOC removal in the PCD/oxidant combinations remarkably exceeds the one in the UV/oxidant treatment.

The direct UV photolysis and unassisted PCD demonstrated relatively high energy efficiency of 36 g kW^{-1} h^{-1} and 195 g kW^{-1} h^{-1}, respectively. For all combinations, a positive effect on the energy efficiency was observed only at the lowest oxidants doses,

except for the UV/HP combination which almost doubled the energy efficiency at the VMN/oxidant molar ratio of 1/10 compared with unassisted UV photolysis. In conclusion, the application of UV/HP at higher oxidant doses and PCD/HP and PCD/PDS combinations at moderate oxidant doses provide advantageous VMN degradation and mineralization. On the other hand, the unassisted PCD treatment provides sufficiently high energy efficiency as a chemical-free method.

Supplementary Materials: The following supporting information can be downloaded at: https://www.mdpi.com/xxx/s1. Figure S1. Degradation of VMN in UV photolysis, PCD treatment, UV/HP and PCD/HP combinations ($[VMN]_0 = 13.5$ μM, $[HP]_0 = 67.5$ μM, unadjusted pH); Figure S2. Degradation of VMN in UV photolysis, PCD treatment, UV/PMS and PCD/PMS combinations ($[VMN]_0 = 13.5$ μM, $[PMS]_0 = 67.5$ μM, unadjusted pH); Figure S3. Scheme of pulsed corona discharge device.

Author Contributions: Conceptualization, N.D.; data curation, D.N. and B.K.; formal analysis, D.N., B.K. and N.D.; funding acquisition, S.P.; investigation, D.N. and B.K.; methodology, N.D.; resources, N.D.; supervision, N.D.; validation, D.N. and B.K.; writing—original draft, D.N. and N.D.; writing—review and editing, S.P. and N.D. All authors have read and agreed to the published version of the manuscript.

Data Availability Statement: Data supporting the results presented can be provided upon request to the respective author.

Conflicts of Interest: The authors declare no conflict of interest.

References

1. Patel, M.; Kumar, R.; Kishor, K.; Mlsna, T.; Pittman, C.U.; Mohan, D. Pharmaceuticals of emerging concern in aquatic systems: Chemistry, occurrence, effects, and removal methods. *Chem. Rev.* **2019**, *119*, 3510–3673. [CrossRef] [PubMed]
2. Larsson, D.G.J. Antibiotics in the environment. *Ups. J. Med. Sci.* **2014**, *119*, 108–112. [CrossRef]
3. Wang, J.; Zhuan, R. Degradation of antibiotics by advanced oxidation processes: An overview. *Sci. Total Environ.* **2020**, *701*, 135023. [CrossRef] [PubMed]
4. Carvalho, I.T.; Santos, L. Antibiotics in the aquatic environments: A review of the European scenario. *Environ. Int.* **2016**, *94*, 736–757. [CrossRef]
5. Cycon, M.; Borymski, S.; Orlewska, K.; Wasik, T.J.; Piotrowska-Seget, Z. An analysis of the effects of vancomycin and/or vancomycin-resistant citrobacter freundii exposure on the microbial community structure in soil. *Front. Microbiol.* **2016**, *7*, 1015. [CrossRef]
6. Gotvajn, A.Ž.; Rozman, U.; Antončič, T.; Urbanc, T.; Vrabel, M.; Derco, J. Fe^{2+} and UV catalytically enhanced ozonation of selected environmentally persistent antibiotics. *Processes* **2021**, *9*, 521. [CrossRef]
7. Okano, A.; Isley, N.A.; Boger, D.L. Peripheral modifications of [Ψ[CH2NH]Tpg4]vancomycin with added synergistic mechanisms of action provide durable and potent antibiotics. *Proc. Natl. Acad. Sci. USA* **2017**, *114*, E5052–E5061. [CrossRef] [PubMed]
8. Tuc Dinh, Q.; Alliot, F.; Moreau-Guigon, E.; Eurin, J.; Chevreuil, M.; Labadie, P. Measurement of trace levels of antibiotics in river water using on-line enrichment and triple-quadrupole LC-MS/MS. *Talanta* **2011**, *85*, 1238–1245. [CrossRef]
9. Zuccato, E.; Castiglioni, S.; Bagnati, R.; Melis, M.; Fanelli, R. Source, occurrence and fate of antibiotics in the Italian aquatic environment. *J. Hazard. Mater.* **2010**, *179*, 1042–1048. [CrossRef] [PubMed]
10. Dulova, N.; Kattel, E.; Trapido, M. Activated Persulfate and Hydrogen Peroxide Treatment of Highly Contaminated Water Matrices: A Comparative Study. *Int. J. Environ. Sci. Develop.* **2020**, *11*, 549–554. [CrossRef]
11. Dehghani, F.; Yousefinejad, S.; Dehghani, M.; Borghei, S.M.; Javid, A.H. Photocatalytic degradation of vancomycin using titanium dioxide and optimization by central composite design. *Int. J. Environ. Sci. Technol.* **2022**, *19*, 8957–8968. [CrossRef]
12. Lee, J.; Von Gunten, U.; Kim, J.H. Persulfate-based advanced oxidation: Critical assessment of opportunities and roadblocks. *Environ. Sci. Technol.* **2020**, *54*, 3064–3081. [CrossRef]
13. Wang, J.; Wang, S. Activation of persulfate (PS) and peroxymonosulfate (PMS) and application for the degradation of emerging contaminants. *Chem. Eng. J.* **2018**, *334*, 1502–1517. [CrossRef]
14. Kaur, B.; Kattel, E.; Dulova, N. Insights into nonylphenol degradation by UV-activated persulfate and persulfate/hydrogen peroxide systems in aqueous matrices: A comparative study. *Environ. Sci. Pollut. Res.* **2020**, *27*, 22499–22510. [CrossRef] [PubMed]
15. Wols, B.A.; Harmsen, D.J.H.; Wanders-Dijk, J.; Beerendonk, E.F.; Hofman-Caris, C.H.M. Degradation of pharmaceuticals in UV (LP)/H$_2$O$_2$ reactors simulated by means of kinetic modeling and computational fluid dynamics (CFD). *Water Res.* **2015**, *75*, 11–24. [CrossRef]

16. Malik, M.A. Water purification by plasmas: Which reactors are most energy efficient? *Plasma Chem. Plasma Process.* **2010**, *30*, 21–31. [CrossRef]
17. Ajo, P.; Kornev, I.; Preis, S. Pulsed corona discharge induced hydroxyl radical transfer through the gas-liquid interface. *Sci. Rep.* **2017**, *7*, 16152. [CrossRef] [PubMed]
18. Derevshchikov, V.; Dulova, N.; Preis, S. Oxidation of ubiquitous aqueous pharmaceuticals with pulsed corona discharge. *J. Electrostat.* **2021**, *110*, 103567. [CrossRef]
19. Onga, L.; Kattel-Salusoo, E.; Preis, S.; Dulova, N. Deegradation of anti-inflammatory drug dexamethasone by pulsed corona discharge: The effect of peroxycompounds addition. *J. Environ. Chem. Eng.* **2022**, *10*, 108042. [CrossRef]
20. Tikker, P.; Dulova, N.; Kornev, I.; Preis, S. Effects of persulfate and hydrogen peroxide on oxidation of oxalate by pulsed corona discharge. *Chem. Eng. J.* **2021**, *411*, 128586. [CrossRef]
21. Shang, K.; Wang, X.; Li, J.; Wang, H.; Lu, N.; Jiang, N.; Wu, Y. Synergetic degradation of Acid Orange 7 (AO7) dye by DBD plasma and persulfate. *Chem. Eng. J.* **2017**, *311*, 378–384. [CrossRef]
22. Shang, K.; Li, W.; Wang, X.; Lu, N.; Jiang, N.; Li, J.; Wu, Y. Degradation of p-nitrophenol by DBD plasma/Fe^{2+}/persulfate oxidation process. *Sep. Purif. Technol.* **2019**, *218*, 106–112. [CrossRef]
23. Wu, J.; Xiong, Q.; Liang, J.; He, Q.; Yang, D.; Deng, R.; Chen, Y. Degradation of benzotriazole by DBD plasma and peroxymonosulfate: Mechanism, degradation pathway and potential toxicity. *Chem. Eng. J.* **2020**, *384*, 123300. [CrossRef]
24. Dodd, M.C.; Buffle, M.O.; Von Gunten, U. Oxidation of antibacterial molecules by aqueous ozone: Moiety-specific reaction kinetics and application to ozone-based wastewater treatment. *Environ. Sci. Technol.* **2006**, *40*, 1969–1977. [CrossRef] [PubMed]
25. Shen, Y.-S.; Lin, C.-C. The Effect of pH on the Decomposition of hydrophenols in aqueous solutions by ultraviolet direct photolysis and the ultraviolet-hydrogen peroxide process. *Water Environ. Res.* **2003**, *75*, 54–60. [CrossRef] [PubMed]
26. Kornev, I.; Osokin, G.; Galanov, A.; Yavorovskiy, N.; Preis, S. Formation of nitrite- and nitrate-ions in aqueous solutions treated with pulsed electric discharges. *Ozone Sci. Eng.* **2013**, *35*, 22–30. [CrossRef]
27. Luo, C.; Ma, J.; Jiang, J.; Liu, Y.; Song, Y.; Yang, Y.; Guan, Y.; Wu, D. Simulation and comparative study on the oxidation kinetics of atrazine by UV/H_2O_2, UV/HSO_5^- and $UV/S_2O_8^{2-}$. *Water Res.* **2015**, *80*, 99–108. [CrossRef] [PubMed]
28. Preis, S.; Panorel, I.C.; Kornev, I.; Hatakka, H.; Kallas, J. Pulsed corona discharge: The role of ozone and hydroxyl radical in aqueous pollutants oxidation. *Water Sci. Technol.* **2013**, *68*, 1536–1542. [CrossRef]
29. Mraihi, A.; Merbahi, N.; Yousfi, M.; Abahazem, A.; Eichwald, O. Electrical and spectroscopic analysis of mono- and multi-tip pulsed corona discharges in air at atmospheric pressure. *Plasma Sources Sci. Technol.* **2011**, *20*, 065002. [CrossRef]
30. Sizykh, M.; Batoeva, A.; Tsydenova, O. UV-activated persulfate oxidation of Orange III dye using KrCl excilamp. *Clean Soil Air Water* **2018**, *46*, 1700187. [CrossRef]
31. Neta, P.; Madhavan, V.; Zemel, H.; Fessenden, R.W. Rate constants and mechanism of reaction of SO_4 with aromatic compounds. *J. Am. Chem. Soc.* **1977**, *99*, 163–164. [CrossRef]
32. Rumbach, P.; Bartels, D.M.; Sankaran, R.M.; Go, D.B. The solvation of electrons by an atmospheric-pressure plasma. *Nat. Commun.* **2015**, *6*, 7248. [CrossRef] [PubMed]
33. Chen, N.; Lee, D.; Kang, H.; Cha, D.; Lee, J.; Lee, C. Catalytic persulfate activation for oxidation of organic pollutants: A critical review on mechanisms and controversies. *J. Environ. Chem. Eng.* **2022**, *10*, 107654. [CrossRef]
34. Neta, P.; Huie, R.E.; Ross, A.B. Rate constants for reactions of inorganic radicals in aqueous solution. *J. Phys. Chem. Ref. Data* **1988**, *17*, 1027–1284. [CrossRef]
35. Wang, S.; Zhou, N. Removal of carbamazepine from aqueous solution using sono-activated persulfate process. *Ultrason. Sonochem.* **2016**, *29*, 156–162. [CrossRef] [PubMed]
36. Xie, P.; Ma, J.; Liu, W.; Zou, J.; Yue, S.; Li, X.; Wiesner, M.R.; Fang, J. Removal of 2-MIB and geosmin using UV/persulfate: Contributions of hydroxyl and sulfate radicals. *Water Res.* **2015**, *69*, 223–233. [CrossRef]
37. Shang, K.; Morent, R.; Wang, N.; Wang, Y.; Peng, B.; Jiang, N.; Lu, N.; Li, J. Degradation of sulfamethoxazole (SMX) by water falling film DBD plasma/persulfate: Reactive species identification and their role in SMX degradation. *Chem. Eng. J.* **2022**, *431*, 133916. [CrossRef]
38. Deniere, E.; Van Hulle, S.; Van Langenhove, H.; Demeestere, K. Advanced oxidation of pharmaceuticals by the ozone-activated peroxymonosulfate process: The role of different oxidative species. *J. Hazard. Mater.* **2018**, *360*, 204–213. [CrossRef]
39. Xiao, S.; Cheng, M.; Zhong, H.; Liu, Z.; Liu, Y.; Yang, X.; Liang, Q. Iron-mediated activation of persulfate and peroxymonosulfate in both homogeneous and heterogeneous ways: A review. *Chem. Eng. J.* **2020**, *384*, 123265. [CrossRef]
40. Zeng, Z.; Zou, H.; Li, X.; Arowo, M.; Sun, B.; Chen, J.; Chu, G.; Shao, L. Degradation of phenol by ozone in the presence of Fenton reagent in a rotating packed bed. *Chem. Eng. J.* **2013**, *229*, 404–411. [CrossRef]
41. Wardman, P. Reduction potentials of one electron couples involving free radicals in aqueous solution. *J. Phys. Chem. Ref. Data* **1989**, *18*, 1637–1755. [CrossRef]
42. Qi, C.; Liu, X.; Ma, J.; Lin, C.; Li, X.; Zhang, H. Activation of peroxymonosulfate by base: Implications for the degradation of organic pollutants. *Chemosphere* **2016**, *151*, 280–288. [CrossRef] [PubMed]
43. Wang, Y.; Huang, J.; Guo, H.; Puyang, C.; Han, J.; Li, Y.; Ruan, Y. Mechanism and process of sulfamethoxazole decomposition with persulfate activated by pulse dielectric barrier discharge plasma. *Sep. Purif. Technol.* **2022**, *287*, 120540. [CrossRef]

44. Furia, F.; Minella, M.; Gosetti, M.; Turci, F.; Sabatino, R.; Di Cesare, A.; Corno, G.; Vione, D. Elimination from wastewater of antibiotics reserved for hospital settings, with a Fenton process based on zero-valent iron. *Chemosphere* **2021**, *283*, 131170. [CrossRef] [PubMed]
45. European Commission Eurostat. Electricity Price Statistics-Statistics Explained 2022. Available online: https://ec.europa.eu/eurostat/statistics-explained/index.php/Electricity_price_statistics (accessed on 22 December 2022).
46. Danckwerts, P.V. *Gas-Liquid Reactions*; McGraw-Hill Book Co.: New York, NY, USA, 1970.
47. Liang, C.; Huang, C.F.; Mohanty, N.; Kurakalva, R.M. A rapid spectrophotometric determination of persulfate anion in ISCO. *Chemosphere* **2008**, *73*, 1540–1543. [CrossRef] [PubMed]
48. Eisenberg, G.M. Colorimetric determination of hydrogen peroxide. *Ind. Eng. Chem. Anal. Ed.* **1943**, *15*, 327–328. [CrossRef]

Appendix 3

Degradation of imidazolium-based ionic liquids by UV photolysis and pulsed corona discharge: The effect of persulfates addition

Dmitri Nikitin, Sergei Preis, Niina Dulova [*]

Department of Materials and Environmental Technology, Tallinn University of Technology, Ehitajate tee 5, 19086 Tallinn, Estonia

ABSTRACT

Ionic liquids (ILs) are salts with exceptional properties important for future development, although potentially hazardous for humans and aquatic life due to their high aqueous solubility and toxicity. Biodegradation of ILs depends on the anion nature and cation structure: many ILs are not readily degraded during conventional wastewater treatment, thus requiring alternative cost-effective and energy-efficient solutions. In this research, the degradation of aqueous imidazolium-based ILs by pulsed corona discharge (PCD) and UV photolysis combined with persulfates was studied, using peroxymonosulfate (PMS) and peroxydisulfate (PDS) as extrinsic oxidants. 1-Ethyl-3-methylimidazolium chloride ([Emim][Cl]), 1-methyl-3-octylimidazolium chloride ([Omim][Cl]), and 1-ethyl-3-methylimidazolium bromide ([Emim][Br]) were chosen as imidazolium-based ILs with different alkyl chain lengths and anions in oxidation experiments under variable operation factors - pH, concentrations of persulfates, pulse repetition frequency in PCD. Pulsed corona discharge has previously shown high energy efficiency in the degradation of micropollutants but has not yet been applied to ionic liquids. The experimental results showed the ability of PCD, PCD/oxidant and UV/oxidant combinations to completely degrade the ILs with the degradation rates in descending order [Emim][Cl] > [Omim][Cl] > [Emim][Br], indicating an impact of both the alkyl chain length and the type of anion on the oxidation rate. The strong activation of persulfates was observed in UV/oxidant combinations, whereas PCD demonstrated the effect of persulfates addition between slight acceleration and moderate deceleration of oxidation dependent on the concentration of extrinsic oxidants. The addition of the sulfate radicals' scavenger, however, showed the presence of those in all combinations indicating a certain replacement of PCD-generated reactive oxygen species with secondary reactants formed from persulfates. The unassisted PCD and UV/PDS combination demonstrated similar energy efficiencies of about 54 and 26 mmol kWh^{-1} for [Emim][Cl] and [Emim][Br] degradation, respectively, while for [Omim][Cl] the UV/PDS combination showed energy efficiency 1.42 times higher than unassisted PCD.

1. Introduction

Ionic liquids (ILs) are organic salts with melting points below 100 °C, composed of inorganic/organic anions and organic cations. Due to their exceptional properties such as low vapour pressure, high thermal and chemical stability, and tunability, ILs are becoming widespread in industry [1]. Although ILs do not evaporate and cannot cause atmospheric pollution, they, being hygroscopic and water-soluble, may cause adverse environmental effects if spilt or leaked [2]. At the beginning of their development and usage, they were considered as 'green chemicals', but further investigations of ILs' life cycle revealed their toxic character when released into the environment [3], several studies reported their

bacterial toxicity and slow biodegradability [4–6].

Among the ionic liquids, imidazolium-based compounds have gained attention becoming the most studied ionic liquids [7]. They are applicable in numerous fields including extraction and separation processes, including biomass and wood dissolution, electrochemistry (batteries, fuel cells, supercapacitors), as plasticizers in the manufacture of plastics, biodiesel production, advanced materials, carbon capture, and even water treatment [1,7–9].

The toxicity of imidazolium-based ILs is of great concern being mainly attributed to the alkyl chain, the length of which positively correlates with toxicity [4,10]. For example, [Omim][Cl] and [Omim][Br] show acute toxicity to *Vibrio fischeri* (logEC$_{50}$, μM) of 0.94 ± 0.14

and 0.63 ± 0.06, whereas [Emim][Cl] is less toxic with $\log EC_{50}$ of 4.02 $\pm$ 0.14 [4]. Moreover, 1-octyl-3-methylimidazolium cation [Omim]$^+$ shows acute toxicity LD_{50} on mice at concentrations of 35 mg kg^{-1} body weight [11], whereas the 1-ethyl-3-methyl imidazolium cation [Emim]$^+$ shows negative impact on mice at an exposure concentration of 10 mg mL^{-1} [12].

The degradation of ILs by conventional wastewater treatment methods is inefficient due to their poor biodegradability [13]. This makes more potent methods, such as advanced oxidation processes (AOPs) utilizing hydroxyl radicals (HO$^{\bullet}$), actively studied for different recalcitrant compounds, including ionic liquids. The Fenton-based process, electro- and photo-assisted combinations of oxidants have been demonstrating their performance in the degradation of various ILs [14–18]. Amongst AOPs, non-thermal plasma technology is getting more interest in water purification due to its energy-efficient character and rapid performance [19]. Previous studies showed the non-thermal gas-phase pulsed corona discharge (PCD) being of higher energy efficiency than other plasma types [19,20]: since PCD applicable to water dispersed in droplets, jets and films forms the reactive oxidant species (ROS) predominantly at the surface of the treated aqueous solution, these meet little resistance diffusing into the aqueous phase thus utilizing the short-living oxidants in reactions with aqueous pollutants [21]. Except for hydroxyl radicals, atomic oxygen, ozone, hydrogen peroxide and other reactive species participate in reactions. Besides, enhancement of PCD energy efficiency is possible by partial utilization of the discharge energy and a uselessly decomposing ROS in reactions with extrinsic oxidants, like persulfate salts, added to the treated solutions. This approach is actively studied for non-thermal plasma technologies [22]. Activated persulfate produces sulfate radical (SO$_4^{\bullet-}$) that has a longer half-life (30–40 μs) than hydroxyl radical (0.2 ns) [23]. Extending the lifetime of the ROS may enhance the efficient utilization of oxidants in reaction with organic pollutants.

The authors failed to find a description of non-thermal plasma used for ILs degradation [14]. This makes the study aimed at the evaluation of the degradation of imidazolium-based ILs in unassisted PCD and UV photolysis and in PCD/oxidant and UV/oxidant combinations. Peroxymonosulfate (PMS) and peroxydisulfate (PDS) were chosen as extrinsic oxidants. The experiments were performed on 1-ethyl-3-methylimidazolium chloride ([Emim][Cl]), 1-methyl-3-octylimidazolium chloride ([Omim][Cl]), and 1-ethyl-3-methylimidazolium bromide ([Emim][Br]) as model compounds with different alkyl chain and counter anion. The impacts of the alkyl chain length and the type of anion on the ILs degradation efficiency and rates were examined, together with the effect of persulfate dosages. The applicability of the methods under the scope was compared in their energy efficiencies (mmol kWh^{-1}) at 90 % degradation extent dependent on the oxidant dosing at its current cost.

2. Materials and methods

2.1. Chemicals

1-Ethyl-3-methylimidazolium chloride ([Emim][Cl], $\geq$ 98 %) and 1-ethyl-3-methylimidazolium bromide ([Emim][Br], $\geq$ 98 %) were obtained from Arcos Organics. 1-Octyl-3-methylimidazolium chloride ([Omim][Cl], $\geq$ 97 %) was purschased from Alfa Aesar. Sodium persulfate (Na$_2$S$_2$O$_8$, $\geq$ 99 %), potassium peroxymonosulfate (Oxone®, KHSO$_5$·0.5KHSO$_4$·0.5K$_2$SO$_4$), ethanol (C$_2$H$_5$OH, $\geq$ 96 %), and tertbutyl alcohol ((CH$_3$)$_3$COH, *t*-BuOH, $\geq$ 99 %) were obtained from Sigma-Aldrich. Acetonitrile (CH$_3$CN, LiChrosolv®) and formic acid (CH$_2$O$_2$, 99 %) were obtained from Merck KGaA.

2.2. Pulsed corona discharge equipment

The PCD experiments were conducted in a device made by Flowrox Oy (Finland) with characteristics given in Table 1. The device consists of a PCD stainless steel reactor with a storage tank, pulse generator and

Table 1
Technical parameters of PCD reactor.

Reactor parameters	Value
Reactor full volume, L	110
Perforated plate size for water distribution, mm	500×30
Number of perforations	51
Diameter of perforations, mm	1
Water flow rate, L min^{-1}	2–28.5
Spray density, m s^{-1}	0.002–0.0243
Plasma zone volume, m^3	0.013
Contact surface area (at flow rate of 1 m^3 h^{-1}), m^{-1}	91.9
Electrode configuration	
High voltage wire length, m	20
Wire diameter, mm	0.5
Distance between high-voltage electrodes and grounded plate, mm	18
Distance between high-voltage electrodes, mm	30
Voltage pulse generator's characteristics	
Pulse repetition frequency, pps	50–880
Output power, W	9–123.2
Peak voltage, kV	18
Peak current, A	380
Current pulse duration, ns	100
Pulse energy, J	0.14–0.18

circulation pump with the frequency regulator used to control the pump engine rotation rate (Figure S1). The plasma reactor contains an electrode system consisting of high voltage wire electrodes, positioned horizontally between two grounded vertical parallel plates. The generator applies high voltage pulses to the electrode system at the pulse repetition frequencies regulated incrementally as shown in Table 1.

The output-input ratio of the pulse generator comprises 65 %. The treated solution is dispersed through the perforated plate positioned above the wire electrodes at a certain spray density determined as the flow rate divided by the planar cross-sectional area of the plasma zone. After passing the plasma zone, the treated solution returns to a storage tank, from where it is circulated back to the top of the reactor.

2.3. Photochemical equipment

Photochemical experiments were performed in batch mode in a 1-L cylindrical glass reactor. A low-pressure mercury germicidal lamp (11 W, Philips TUV PL-S) placed in a quartz sleeve inside the reactor was used as a UVC source. The input–output power of the lamp is approximately 32 %. The incident photon flux at 254 nm of the lamp used in oxidation comprised 2.55×10^{-7} Einstein s^{-1} measured by ferrioxalate actinometry. The lamp was turned on at least 10 min before the trial to provide a constant radiation output. A water-cooling jacket was used to keep the constant temperature in the reactor.

2.4. Experimental part

Experiments were carried out at ambient room temperature of 21 $\pm$ 1 °C, at the initial concentration of ionic liquids of 100 μM. The unadjusted pH values of [Emim][Cl], [Omim][Cl], and [Emim][Br] were 6.9 $\pm$ 0.7, 6.2 $\pm$ 0.8, and 6.0 $\pm$ 0.7 (average for UV and PCD), respectively. For acidic (pH 3) or alkaline (pH 11) conditions, pH was regulated by adding H$_2$SO$_4$ or NaOH 0.1- to 5.0-M solutions. The effects of PMS and PDS in both photochemical and PCD experiments were studied at concentrations of 50, 100, 250, and 500 μM, providing the oxidant-to-substrate molar ratio from 0.5 to 5. In experiments with oxidants, the oxidation reaction was quenched with ethanol added at the sample-to-EtOH volume ratio of 10 for HPLC analysis.

In UV/oxidant trials, a solution with an IL (0.8 L) was prepared in bidistilled water and treated for 2 h with permanent stirring using a magnetic stirrer. After the dissolution of persulfate salt, the UVC-lamp inserted into the reactor initialized oxidation.

The stock solutions for PCD experiments were prepared in a 100-mL volumetric flask using bidistilled water, followed by dilution to a total

volume of 10 L by distilled water in the reactor tank constantly stirred with the circulation pump. Pre-selected amounts of persulfate salts were dissolved in a 100-mL volumetric flask and added to the tank immediately before the start of the treatment. PCD experiments were performed at a circulated water flow rate of 1 m^3 h^{-1} corresponding to the gas–liquid contact surface area of 91.9 m^{-1} and the pulse repetition frequency of 50, 200, and 880 pulses per second (pps) with the power input of 9, 32 and 123.2 W, respectively. For proper sampling and calculation of the energy efficiency relative to the volume of the treated solution, the solutions were circulated in the reactor for four minutes after the pulse generator was turned off to equalize the concentrations in the reactor's volume.

2.5. Analytical methods

The concentration of [Emim]$^+$ was determined using high-performance liquid chromatography combined with a mass spectrometer (HPLC-MS, Shimadzu LC-MS, 2020) equipped with a Phenomenex Gemini (150 × 2 mm, 1.7 mm) NX-C18 (110 Å, 5 μm) column. The analysis was performed using an isocratic method with a mobile phase composed of 10 % vol. of acetonitrile and 90 % vol. of 0.3-% formic acid aqueous solution. The flow rate was kept at 0.2 mL min^{-1} and the injected sample volume was 20 μL. Mass spectra were acquired in full-scan (scanning in the range of 50–500 m/z) and SIM (111 m/z) modes. The instrument was operated in positive ESI mode, and the results obtained with the MS detector were handled using Shimadzu Lab Solutions software. The concentration of [Omim]$^+$ was determined using HPLC with the same eluent flow rate and chromatographic column combined with a diode array detector (HPLC-PDA, Shimadzu, Japan). The isocratic eluent mixture was composed of 25 % vol. of acetonitrile containing 0.3 % of formic acid and 75 % vol. of 0.3-% formic acid aqueous solution. Samples injected in 60 μL volume were analyzed at a wavelength of 205 nm.

Solution pH was measured using a digital pH/Ion meter (Mettler Toledo S220). The residual hydrogen peroxide concentration in the treated samples was measured spectrophotometrically at λ = 410 nm with titanium sulfate by a H$_2$O$_2$-Ti^{4+} complex formation [24].

Due to the different treated water volumes and applied powers, the UV- and PCD-based oxidation may not be compared by the decrease of an IL concentration in time. Delivered energy dose relative to the treated solution volume and treatment time was implemented to compare the IL removal results by the different treatment methods. To evaluate the effect of oxidant addition on the removal efficiency, an energy-related pseudo-first-order reaction rate coefficient k_1 was implemented (Eq. (1) being calculated using slopes k_1 of the straight lines by plotting ln (C_t/C_0) as a function of delivered energy dose D (Eq. (2) through linear regression:

$$\frac{d[C]}{dD} = -k_1 \bullet [C] \tag{1}$$

$$D = \frac{P \bullet t}{V} \tag{2}$$

where k_1 is the pseudo-first-order reaction rate coefficient, m^3 kWh^{-1}; C is the concentration of target compound; D is the delivered energy dose, kWh m^{-3}, P is the power applied in pulsed corona discharge or UV photolysis, kW; V is the volume of treated solution, m^3.

The energy efficiency E, mmol kWh^{-1}, was calculated using the equation Eq. (3):

$$E = \frac{\Delta C \bullet V}{W} \tag{3}$$

where ΔC – a decrease of target compound concentration, mmol m^{-3}; V – the volume of treated solution, m^3; W – energy consumption derived from the generator power output and the time of treatment, kWh.

3. Results and discussion

3.1. Degradation of ionic liquids in PCD-based treatment

Ionic liquids were degraded in PCD at pulse repetition frequencies of 50, 200 and 880 pps (Figures S2-S4): comparisons of ILs' degradation are shown in Fig. 1. Degradation of 90 % of [Emim][Cl] in PCD treatment at a pulse repetition frequency of 200 pps was 1.54 and 2.4 times faster than the degradation of [Omim][Cl] and [Emim][Br], respectively (Fig. 1a), showing noticeable effects of the length of alkyl chain and the character of anion on the oxidation.

Fig. 2 demonstrates the energy-related pseudo-first order reaction rate constants of ILs' PCD-degradation in aqueous solutions of 100-μM starting concentration and unadjusted circum-neutral pH dependent on the pulse repetition frequency. The reaction rate constants at 200 pps were found to be 1.72, 1.03, and 0.68 m^3 kWh^{-1} for [Emim][Cl], [Omim][Cl], and [Emim][Br], respectively.

The difference in reaction rates of ILs of different structures may find an explanation in the side-chain length and the nature of the anion. The size of the octyl alkyl chain hinders the oxidation of the imidazolium ring by screening off a part of the hydroxyl radicals utilized inefficiently due to low reactivity towards saturated side-chains: these chains provide certain surfactant properties to ILs, being oriented towards the gas phase at the gas–liquid interface [25]. The longer side-chain of [Omim]$^+$ provides its slower degradation compared to [Emim]$^+$ paired with chloride.

Bromide anion affected the oxidation of imidazolium cations even stronger: [Emim][Cl] is oxidized more than two times faster than [Emim][Br] (Fig. 1). This observation may be explained by using information available in the literature. Accordingly, Grebel et al. [26] reported that both anions may participate in reactions forming chlorine
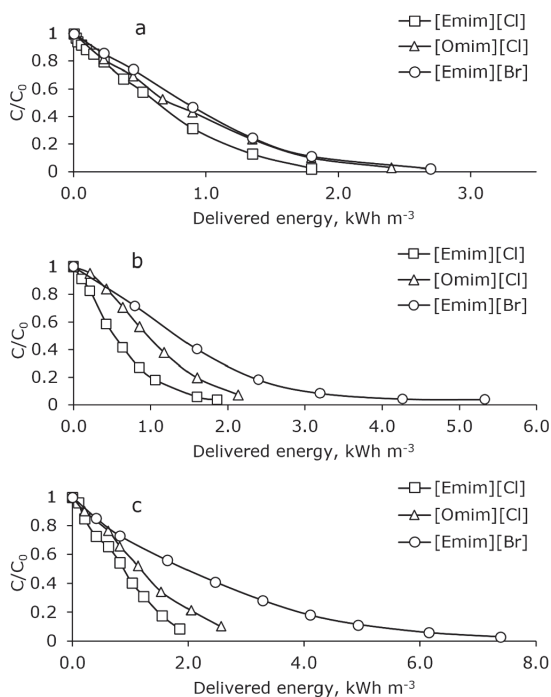

Fig. 1. Degradation of imidazolium-based ILs in PCD oxidation ([IL]$_0$ = 100 μM, pH unadjusted, pulse repetition frequency: 50 pps (a), 200 pps (b), 880 pps (c)).
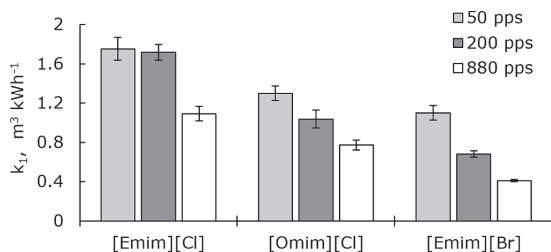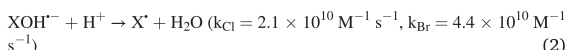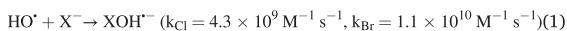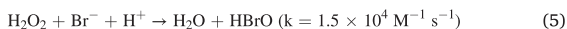
Fig. 2. Effect of pulse repetition frequency on the ILs energy-related degradation rate constant k_1 in PCD oxidation ($[IL]_0 = 100$ μM, pH unadjusted).

and bromine radicals (R1-R3):

$$HO^{\bullet} + X^- \rightarrow XOH^{\bullet-} \quad (k_{Cl} = 4.3 \times 10^9 \text{ M}^{-1} \text{ s}^{-1}, k_{Br} = 1.1 \times 10^{10} \text{ M}^{-1} \text{ s}^{-1}) \quad (1)$$

$$XOH^{\bullet-} + H^+ \rightarrow X^{\bullet} + H_2O \quad (k_{Cl} = 2.1 \times 10^{10} \text{ M}^{-1} \text{ s}^{-1}, k_{Br} = 4.4 \times 10^{10} \text{ M}^{-1} \text{ s}^{-1}) \quad (2)$$

$$X^{\bullet} + X^- \rightarrow X_2^{\bullet-} \quad (3)$$

Chlorine radical (Cl$^{\bullet}$) ($E_0 = 2.55$ V) and dichlorine radical-anion (Cl$_2^{\bullet-}$) ($E_0 = 2.13$ V) are highly reactive towards organic compounds, while bromine radical (Br$^{\bullet}$) ($E_0 = 1.93$ V) and dibromine radical-anion (Br$_2^{\bullet-}$) ($E_0 = 1.62$ V) have lower redox potentials [26,27], thus not contributing to the imidazole oxidation. However, the author's previous study did not observe acceleration of PCD oxidation reactions in the presence of sodium chloride: salts addition only reduced the target pollution oxidation rate due to a partial loss of the discharge energy in conductive media showing no difference between chloride or sulphate [28].

Differently from chloride, bromide is known to be oxidized by ROS in acidic and neutral media to bromate via hypobromite [29,30]. Bromide oxidation rate is fast enough to compete with the target reaction scavenging a substantial part of oxidants. Competitive oxidation of bromide may thus contribute to the reduced [Emim]$^+$ oxidation. Supporting this observation, there are data pointing to the oxidation of bromide to hypobromite (R5) with subsequent reduction in reverse reaction (R6) with hydrogen peroxide formed by recombination of hydroxyl radicals (R4) [31]:

$$HO^{\bullet} + HO^{\bullet} \rightarrow H_2O_2 \quad (k = 5.5 \times 10^9 \text{ M}^{-1} \text{ s}^{-1}) \quad (4)$$

$$H_2O_2 + Br^- + H^+ \rightarrow H_2O + HBrO \quad (k = 1.5 \times 10^4 \text{ M}^{-1} \text{ s}^{-1}) \quad (5)$$

$$H_2O_2 + HBrO \rightarrow H_2O + O_2 + H^+ + Br^- \quad (k = 2.3 \times 10^4 \text{ M}^{-1} \text{ s}^{-1}) \quad (6)$$

Bromide thus degrades hydrogen peroxide possibly formed in reactions involving hydroxyl radicals contributing to all the oxidants' waste [32]. The authors' previous results showed the accumulation of hydrogen peroxide in water during PCD treatment [33]. In this study, the concentration of hydrogen peroxide reached 0.07 mM after a half-hour treatment of [Emim][Cl], whereas no accumulation of hydrogen peroxide was observed even after one hour of [Emim][Br] oxidation. This provides indirect evidence of bromide playing a competitive role in ILs' PCD oxidation.

At a pulse repetition frequency of 880 pps, the degradation of ILs showed similar trends with respect to the character of the hydrocarbon chains and the nature of anions (Fig. 1c): the degradation of [Emim][Cl] was 1.41 and 2.86 times faster than of the [Omim][Cl] and [Emim][Br], respectively, with the k_1 values 1.09, 0.77, and 0.41 m^3 kWh^{-1}. Compared to 50 and/or 200 pps (Fig. 2), the reaction rate constants expectedly decreased with the pulse repetition frequency as observed with other aqueous pollutants [33]. Given the similar energy-related reaction rate constant values for the oxidation of target compounds at 50 and 200 pps, but faster reactions in the case of the latter conditions

(Figures S2-S4), 200 pps was chosen for further studies.

3.1.1. Effect of pH in unassisted PCD oxidation

The experiments on the degradation of ILs affected by pH were conducted in acidic (pH 3), circum-neutral (pH unadjusted), and alkaline (pH 11) media with detailed results given in Figures S5-S7. Fig. 3 shows the effect of pH on the energy-related reaction rate constant in PCD treatment at 200 pps. Notably, the non-thermal plasma oxidation resulted in noticeable decrease in pH at unadjusted initial pH conditions. The latter can be explained by atmospheric nitrogen being oxidized to nitrate in plasma [34].

One can see that higher reaction rate constants are observed at pH 11 for all ILs under consideration with k_1 comprising 2.71, 2.61, and 1.08 m^3 kWh^{-1} for [Emim][Cl], [Omim][Cl], and [Emim][Br], respectively. The noticeable effect of alkaline pH can be explained by the fact that the organic cation is a desirable target for nucleophiles such as hydroxide, transforming the imidazolium cation to a neutral molecule with the hydroxyl group. Further deprotonation of the molecule in the alkaline medium enhances its reactivity with electrophilic hydroxyl radicals improving degradation efficiency (Fig. 4).

The impact of pH on [Emim][Cl] and [Emim][Br] oxidation appeared similar, improving it, if compared to the circum-neutral solution, by the factor of 1.58 for both, although absolute k_1 values remain remarkably different. The difference may point to a difference in charge neutralization and deprotonation of the cation bond with different inorganic anions. A stronger pH impact on the [Omim][Cl] oxidation may indicate better charge neutralization of the long-chain cation in an alkaline solution. Acidic media had a negligible effect on ILs PCD oxidation.

It should be noted that hydrogen peroxide in alkaline solutions was not detected indicating its possible fast decomposition (R7, R8) [35].

$$H_2O_2 + HO^- \rightarrow H_2O + HO_2^- \quad (7)$$

$$2H_2O_2 \rightarrow 2H_2O + O_2 \quad (8)$$

3.1.2. Effect of pH in PCD/oxidant combinations

The results of ILs oxidation at different pH values in the PCD/oxidant combinations are shown in Fig. 5, where the energy-related reaction rate constants are compared with the ones of unassisted PCD. The addition of extrinsic oxidants at the IL/oxidant molar ratio of 1/1 inhibited oxidation in more than half of the experiments due to, possibly, wasting active oxidants in recombination and other reactions between each other forming less reactive species.

No improvement was observed in the degradation of [Emim][Cl] with additions of PDS and PMS, while the [Omim][Cl] with longer alkyl chain degraded faster at pH 3 with additions of both PDS and PMS, having k_1 increased from 1.12 m^3 kWh^{-1} in the unassisted PCD oxidation to 1.57 and 1.44 m^3 kWh^{-1}, respectively. This observation may be explained by longer-living sulfate radicals having higher redox potential

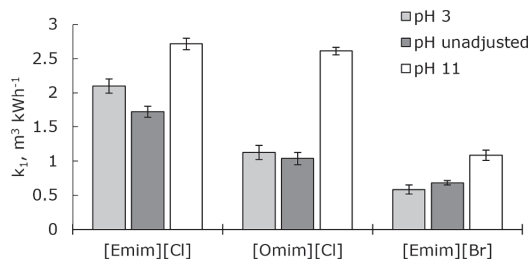**Fig. 3.** Effect of pH on the ILs energy-related degradation rate constant k_1 in PCD oxidation ($[IL]_0 = 100$ μM, pulse repetition frequency 200 pps).
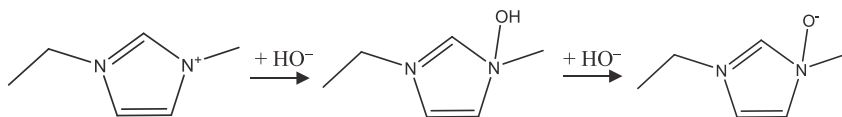
Fig. 4. Transformation of 1-ethyl-3-methylimidazolium cation in alkaline solution.
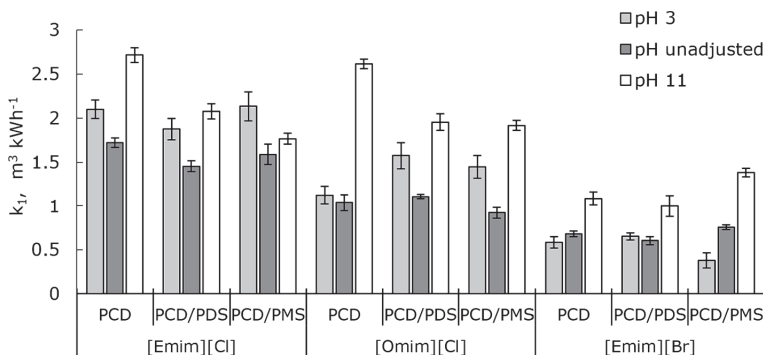

Fig. 5. Effect of pH on the ILs energy-related degradation rate constant k_1 in PCD and PCD/oxidant combinations ($[IL]_0 = [PDS]_0 = [PMS]_0 = 100$ μM, pulse repetition frequency 200 pps).

in the acidic media thus contributing to a better oxidation. This, however, was observed only for the longer alkyl chain cation, having a stronger inductive effect on the imidazolium moiety. With [Emim][Br], in contrast to the other ILs under consideration, the addition of PMS moderately improved the degradation at alkaline pH, and k_1 increased from 1.08 to 1.38 m^3 kWh^{-1}. This observation requires a more detailed study for explanation: bromide is known not to be oxidized in an alkaline medium thus having little impact on PCD reactions in the presence of extrinsic oxidants [36].

3.1.3. Effect of persulfates dosage in PCD/oxidant combinations

Fig. 6 demonstrates the results of ILs degradation in the PCD/oxidant treatment at unadjusted circum-neutral pH dependent on the IL/oxidant molar ratio. The addition of persulfates at small molar ratios showed, for example, for [Emim][Cl], a minor positive effect decreased with the increased oxidant dosage. Persulfate ions and sulfate radicals in increased concentrations compete for the plasma-generated ROS able to oxidize [Emim][Cl], thereby reducing the overall effectiveness of treatment [34,37]. The performance of the PCD/PDS combination for [Omim][Cl] and [Emim][Br], in general, remained at the level of unassisted PCD. This also may point to the nearly equal substitution of the discharge-generated ROS with sulfate radicals. The use of PCD/PMS
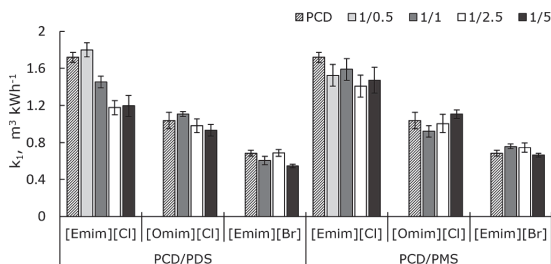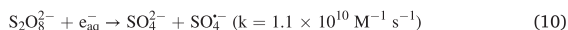
combination resulted in k_1 values for [Emim][Cl] fluctuating from 1.4 to 1.58 m^3 kWh^{-1}, i.e., being noticeably lower than that of unassisted PCD. The activation of PMS (R9) may produce hydroxyl radicals, making it different from the PDS one (R10). This may explain why PCD/PMS shows better results compared to PDS at high PMS dosages [31,38]. Possibly, the formation of hydroxyl radicals from PMS prevails in reactions with [Emim][Cl], reducing the scavenging effect of the extrinsic oxidant.

$$HSO_5^- + e_{aq}^- \rightarrow HO^\bullet + SO_4^{2-}/SO_4^{\bullet-} + HO^- \ (k = 8.4 \times 10^8 \ M^{-1} \ s^{-1}) \quad (9)$$

$$S_2O_8^{2-} + e_{aq}^- \rightarrow SO_4^{2-} + SO_4^{\bullet-} \ (k = 1.1 \times 10^{10} \ M^{-1} \ s^{-1}) \quad (10)$$

The increased PMS dose showed a small positive effect on the oxidation efficiency of [Omim][Cl], the reaction rate constant k_1 achieved 1.1 m^3 kWh^{-1} at the IL/oxidant molar ratio of 1/5, exceeding the value observed at the unassisted PCD oxidation. For the [Emim][Br], the addition of PMS had no effect on the oxidation, only slightly reducing the one at the highest IL/oxidant molar ratio of 1/5. The absence of noticeable change in degradation may point to a compensatory oxidation mechanism, in which PMS-derived secondary oxidation species equally replace ROS reacted with PMS.

3.2. Degradation of ionic liquids in UV-based treatment

The UV photolysis of ILs was studied in the UVC light at a wavelength of 254 nm. In 2-h irradiation, a near-zero removal of ILs was observed in acidic and unadjusted circum-neutral pH, imidazolium cation showed high stability to photodegradation. At alkaline pH, 2-h UV photolysis resulted in 25 %, 5 %, and 30 % decomposition of [Emim][Cl], [Omim] [Cl], and [Emim][Br], respectively. Faster degradation of [Emim]$^+$ cations in an alkaline medium might be explained similarly to the PCD oxidation, i.e., cations transformed to molecular form are more reactive. Being degraded either by direct photolysis or oxidation with hydroxyl radicals formed from water dissociation, ILs show different reactivity dependent on their structure. The difference in removal of [Emim]$^+$ and [Omim]$^+$ suggests the prevalation of photonic oxidation, since electrophilic hydroxyl radicals should faster oxidize [Omim]-moieties for a stronger inductive effect of longer side-chain.

Fig. 6. Effect of the IL/oxidant molar ratio on the ILs energy-related degradation rate constant k_1 in PCD and PCD/oxidant combinations ($[IL]_0 = 100$ μM, pH unadjusted, pulse repetition frequency 200 pps).

3.2.1. Effect of pH in UV/oxidant combinations

Contrary to PCD/persulfate combined treatment, the UV/persulfate combination is a well-known process with prompt activation of persulfate salts by the fission of O-O bond with high-energy photons creating sulfate and hydroxyl radicals (R11, R12). Activation of PDS is easier than PMS for different dissociation energy of the O-O bond in these molecules, 92 and 372 kJ mol^{-1}, respectively. The difference originates from the asymmetrical structure of peroxymonosulfate anion (HSO$_5^-$) [31].

$$S_2O_8^{2-} + hv \rightarrow 2SO_4^{\cdot-} \tag{11}$$

$$HSO_5^- + hv \rightarrow SO_4^{\cdot-} + HO^{\cdot} \tag{12}$$

Fig. 7 shows the effect of pH on the energy-related degradation rate constant k_1 at the IL/persulfate molar ratio of 1/2.5 oxidizing ILs with UV-generated sulfate and hydroxyl radicals. At unadjusted circum-neutral pH, [Emim][Cl] and [Omim][Cl] showed similar degradation rates with k_1 values of 2.35 and 2.04 m^3 kWh^{-1}, respectively. For [Emim][Br], the PDS concentration necessary to achieve 90 % degradation was twice as high as the PDS concentration in experiments with [Emim][Cl] and [Omim][Cl], i.e., 500 μM, thus showing k_1 value as low as 1.46 m^3 kWh^{-1} indicating the presence of bromide hindering oxidation of the target cation. Additions of PMS demonstrated expectedly lower oxidation rate with reaction rate constants of 0.86, 1.02, and 0.45 m^3 kWh^{-1} for [Emim][Cl], [Omim][Cl], and [Emim][Br], respectively. Besides higher O-O-bond dissociation energy, PMS is a triple-salt introducing more ions participating in scavenging reactions. The difference between oxidative species formed from PDS and PMS may also make a difference in reactivity: the formation of long-living sulfate radicals from PDS may provide more efficient oxidation of ILs as compared to sulfate and hydroxyl radicals from PMS. It is worth noting that regardless of the UV/persulfate system studied, the unadjusted initial pH value decreases during the oxidation process due to the formation of acidic by-products and a certain acidity associated with persulfates.

Compared to the circum-neutral medium, the acidic one showed slightly increased oxidation efficiency with PDS for [Emim]$^+$, while a negative effect was observed with respect to [Omim]$^+$. This observation points to the relative importance of the IL's cation structure compared to the sulfate radicals' redox potential strengthened in an acidic medium. Alkaline pH is known to activate persulfate salts enhancing the oxidized pollutants removal (R13-R17, R7) [39,40]: oxidation proceeds in a two-stage reaction with rapid full use of persulfate at the beginning with a subsequent slow stage of the direct UV photolysis.
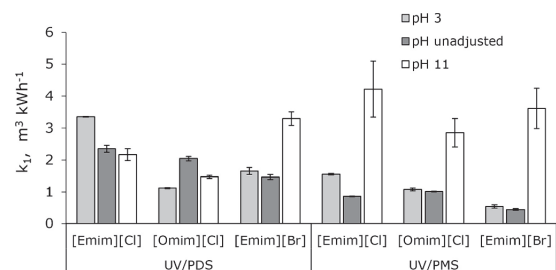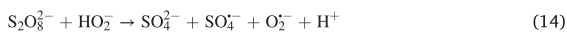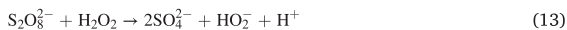
$$S_2O_8^{2-} + H_2O \rightarrow 2SO_4^{2-} + HO_2^- + H^+ \tag{13}$$

$$S_2O_8^{2-} + HO_2^- \rightarrow SO_4^{2-} + SO_4^{\cdot-} + O_2^{\cdot-} + H^+ \tag{14}$$

$$SO_4^{\cdot-} + HO^- \rightarrow SO_4^{2-} + HO^{\cdot} \tag{15}$$

$$HSO_5^- + H_2O \rightarrow H_2O_2 + HSO_4^- \tag{16}$$

$$H_2O_2 \rightarrow HO_2^- + H^+ \tag{17}$$

In the ILs UV/PDS oxidation, the enhancement of reactions in an alkaline medium was observed only for [Emim][Br] with no effect for others. This observation is difficult to explain since neutralized ILs' cations in alkaline solutions should present a desirable target for electrophilic oxidants, sulfate and hydroxyl radicals. Possibly, reactions scavenging active species, weakened radicals' oxidation potential, or the shift in oxidation stoichiometry may need a closer look in the UV/PDS treatment. Showing low oxidizability compared to [Emim][Cl] in acidic and circum-neutral media, [Emim][Br] may be oxidized faster due to bromide indifference towards oxidation in alkaline media [36], thus alleviating its impact on the reactions observed in acidic and neutral media.

At the same time, PMS used in alkaline conditions greatly increased the removal rate of all ILs compared to acidic and circum-neutral conditions. The amounts of PMS, however, were not sufficient for the complete degradation of ILs: PMS consumed within the first 10 min of combined treatment, achieving around 90 % of ILs' elimination; further treatment was the slow direct photolysis. One more circumstance may enhance the photoproduction of HO$^{\cdot}$ and SO$_4^{\cdot-}$ in alkaline media – the molar absorption coefficient of PMS increasing from 14.3 to 146.4 M^{-1} cm^{-1} at pH 7 and 11, respectively, thus activating PMS at a greater rate [41]. To explain the difference with the PDS behaviour, one can pay attention to its molar absorption coefficient remaining in alkaline media close to it at neutral pH ($\varepsilon = 20.07$ M^{-1} cm^{-1}) [42].

3.2.2. Effect of persulfates dosage in UV/oxidant combinations

The use of increased dosages of persulfates in the UV/oxidation combination resulted in a pronounced impact on the energy-related reaction rate constants (Fig. 8).

For example, additions of PDS at the [Emim][Cl]/PDS molar ratios from 1/1 to 1/5 at circum-neutral unadjusted pH increased k_1 value from 0.76 to 4.48 m^3 kWh^{-1}, i.e., for about six times. The UV/PDS combination showed similar results in [Omim][Cl] oxidation resulting in k_1 values increased more than seven times up to 5.40 m^3 kWh^{-1}. Degradation of [Emim][Br] was inhibited by the presence of bromide ions with k_1 reaching only 1.46 m^3 kWh^{-1} at the highest PDS dosage, although the effect of the increased PDS dosage was also big exceeding five times. However, the addition of PDS at an IL/oxidant molar ratio of 1/1 was insufficient for the 90-% [Emim][Br] degradation; persulfate degraded faster than [Emim][Br] indicating disproportion in the reaction stoichiometry.

Similar disproportion was observed in UV/PMS combinations at the molar ratio of 1/1 for all ILs and even at the molar ratio of 1/2.5 for [Emim][Br] (Figure S8). The addition of PMS at a concentration of 500 μM, i.e. in an IL/oxidant molar ratio of 1/5, showed about 2.5-fold lower reaction rate constants than PDS addition, reaching 1.96, 2.1, and 0.44 m^3 kWh^{-1} for [Emim][Cl], [Omim][Cl], and [Emim][Br], respectively.

Fig. 7. Effect of pH on the ILs energy-related degradation rate constant k_1 in UV/oxidant combinations ([IL]$_0$ = 100 μM, [PDS]$_0$ = [PMS]$_0$ = 250 μM for [Emim][Cl] and [Omim][Cl], [PDS]$_0$ = [PMS]$_0$ = 500 μM for [Emim][Br]).
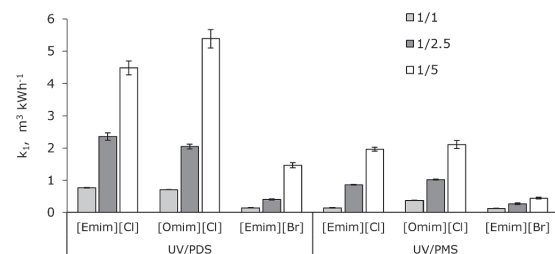

Fig. 8. Effect of the IL/oxidant molar ratio on the ILs energy-related degradation rate constant k_1 in UV/oxidant combinations ([IL]$_0$ = 100 μM, pH unadjusted).

Consistently with PCD experiments, the degradation of [Emim][Br] at maximum PMS dose was four times slower than that of [Emim][Cl], indicating the negative impact of bromide ions interacting with PMS and oxidative species.

3.3. Comparison of UV- and PCD-based treatment

The rate of degradation of target ILs in oxidant-assisted photolysis and PCD combinations follows the descending order: [Emim][Cl] > [Omim][Cl] > [Emim][Br], clearly indicating the long alkyl chain and bromide anion as moieties with decelerating impact on the oxidation. The PCD-based treatment showed k_1 values up to 1.80 (PCD/PDS, IL/oxidant molar ratio of 1/0.5), 1.10 (PCD/PDS, IL/oxidant molar ratio of 1/1), and 0.68 (unassisted PCD) m³ kWh^{-1}, respectively for [Emim][Cl], [Omim][Cl], [Emim][Br]. In turn, the UV/oxidant combinations showed a pronounced dependence of the oxidation rate on the oxidant dose achieving k_1 up to 4.48, 5.39, and 1.46 m³ kWh^{-1}, respectively, with PDS addition at an IL/oxidant molar ratio of 1/5. It is worth noting that unassisted PCD was also able to effectively degrade ILs, having the addition of extrinsic oxidants in optimized quantities only slightly improving the ILs' degradation. Amongst factors reducing the oxidation rate, recombination of hydroxyl radicals with subsequent degradation of hydrogen peroxide in PCD should be mentioned. The negative effect of bromide anion is seen in both studied oxidation methods, indicating its involvement in competing reactions with oxidants and the interference with ILs ionic dissociation reactions.

While the energy-related reaction rate constant k_1 takes into account the energy dose required for oxidation, it does not count the cost of extrinsic oxidant participating in the reaction, bringing certain incompleteness to the methods' comparison from an economic point of view. Energy efficiency or energy yield E_{90}, mmol kWh^{-1}, helping in the applicability assessment, considers the energies consumed by the UV irradiation and PCD treatment needed for 90 % conversion of ILs together with the cost of extrinsic oxidants. The latter was considered as EUR 1.5 kg^{-1} and EUR 2.5 kg^{-1} for PDS and PMS, respectively, as average wholesale prices on the market in 2023. The cost of oxidant dose was then converted to the equivalent energy expense considering the average European non-household electric energy price of EUR 0.21 kWh^{-1} and added to the energy expense [43].

The addition of extrinsic oxidant to the PCD-treated ILs solutions resulted in a small increase in the degradation rate at best, thus, the added oxidant will inevitably make the process more expensive (Table S1). Table 2 shows energy efficiencies of realizable unassisted PCD at three pulse repetition frequencies and UV/oxidant combinations at circum-neutral unadjusted pH. Energy efficiencies of PCD treatment at 50 pps were similar to 200 pps and comprised about 51 and 40 mmol kWh^{-1} for [Emim][Cl] and [Omim][Cl] degradation, respectively. However, the E_{90} of [Emim][Br] at 50 pps were 1.6 times higher than that of 200 pps, but almost 2 times lower than [Emim][Cl] at 50 pps: the long time between pulses contributed to the action of long-living oxidants improving energy usage. Compared to 200 pps, PCD treatment at 880 pps proceeds about four times faster, although with a respective decrease in energy efficiency for 28.5 %, 21.6 %, and 40.1 %. In the UV-based treatment, the energy efficiency increases with the dosages of

persulfates (Table S1). Compared to PCD, a similar result was obtained for the [Emim][Cl] and [Emim][Br] degradation in the UV/PDS combination with E_{90} of 54.2 and 24.5 mmol kWh^{-1}. In turn, the energy efficiency of [Omim][Cl] surpassed PCD treatment by 29.7 %, making the UV/PDS combination more energy efficient. Application of a more expensive PMS oxidant with a small improvement in the oxidation rate negatively affects the energy efficiency with approximately two- to three-fold lower results. Unassisted PCD treatment thus provides sufficiently high energy efficiency in the oxidation of recalcitrant ILs using only electric energy without added extrinsic oxidants, i.e., being free from chemicals delivery, storage, and handling. Overall, PCD presents a viable alternative to other AOPs, such as highly effective persulfate photolysis [44].

3.4. Hydroxyl and sulfate radicals contribution to ILs oxidation

To estimate the contribution of radicals in the ILs oxidation, the study using ethanol (EtOH) and *tert*-butanol (*t*-BuOH) as radical scavengers was performed. EtOH reacts with hydroxyl radicals at the second-order reaction rate constant from $1.2 \bullet 10^9$ to $2.8 \bullet 10^9$ M^{-1} s^{-1} and sulfate radicals at $1.6 \bullet 10^7$ to $7.7 \bullet 10^7$ M^{-1} s^{-1}, while *t*-BuOH is a more effective scavenger for hydroxyl radicals with the reaction rate constant from $3.8 \bullet 10^8$ to $7.6 \bullet 10^8$ M^{-1} s^{-1} than for sulfate radicals with much smaller reaction rate, $4.0 \bullet 10^5$ to $9.1 \bullet 10^5$ M^{-1} s^{-1} [45]. Thus, the application of both radical scavengers may allow distinguishing the inhibition extent in ILs' degradation: in the presence of an excess amount of *t*-BuOH, the effect of hydroxyl radicals is seen, while the effect of sulfate radicals is visible from the difference in inhibition caused with alternating excess amounts of EtOH and *t*-BuOH.

For the PCD/oxidant combination, the results presented in Table 3 showed that the 25-mM addition of *t*-BuOH inhibited PCD oxidation of all ILs compared to the absence of *t*-BuOH indicated as a reference experiment. Slower oxidation of target compounds thus indicates the scavenging of hydroxyl radicals. The strongest inhibition was observed for [Omim][Cl] in PCD/PDS oxidation with the IL degraded for 32 % against 86 % in the reference experiment. The experiment with [Emim][Br] showed the weakest effect of *t*-BuOH reducing degradation of the IL in PCD/PDS combination only from 87 % to 70 %. Considering the substantial inhibition of [Emim][Cl] oxidation with the PCD/PDS combination from 83 % to 44 %, the weak effect of *t*-BuOH on the [Emim][Br] oxidation may be explained by the substantial part of hydroxyl radicals consumed in reactions with easily oxidizable bromide ions. This observation is consistent with the poor oxidation efficiency of the brominated IL observed in the experiments (Fig. 5). The formation of a smaller amount of hydroxyl radicals in the oxidation of [Emim][Br] is less probable for their predominant formation at the gas-plasma interface confirmed earlier, thus being consumed in the bulk of liquid [20].

Interestingly, the addition of EtOH dramatically, three to four times inhibited the oxidation of all ILs (Table 3), pointing to the key role of sulfate radicals. The contribution of sulfate radicals to the ILs' degradation is seen from the difference between the inhibition effects of *t*-BuOH and EtOH and follows the descending order: [Emim][Br] >

Table 2
Energy efficiencies of unassisted PCD and UV/oxidant combinations in ILs oxidation ([ILs]$_0$ = 100 μM, pH unadjusted, [PDS]$_0$ = [PMS]$_0$ = 500 μM).

Process	Conditions	E_{90}, mmol kWh^{-1}		
		[Emim][Cl]	[Omim][Cl]	[Emim][Br]
PCD	50 pps	48.3	41.9	27.8
	200 pps	53.5	38.7	17.2
	880 pps	38.2	30.3	10.3
UV/oxidant	PDS	54.2	59.6	24.5
	PMS	23.1	26.2	6.8

Table 3
Results of hydroxyl and sulfate radical scavenging study in PCD/oxidant combinations ([ILs]$_0$ = [PDS]$_0$ = [PMS]$_0$ = 100 μM, [EtOH]$_0$ = [*t*-BuOH]$_0$ = 25 mM, pH unadjusted, pulse repetition frequency 200 pps).

Ionic liquid	Extrinsic oxidant		Ionic liquid degradation, %		
		Time, min	Reference	EtOH	*t*-BuOH
[Emim][Cl]	PDS	30	83	24	44
	PMS	30	85	16	48
[Omim][Cl]	PDS	40	86	26	32
	PMS	40	87	11	38
[Emim][Br]	PDS	60	87	23	70
	PMS	60	89	25	65

[Emim][Cl] > [Omim][Cl] for both persulfates. The fact of substantial presence of sulfate radicals in PCD/persulfate-treated solutions together with the poor persulfate effect on the ILs degradation rate confirms the hypothesis of the PCD-generated ROS consumed by persulfates producing sulfate radicals as substitutes with little change in ILs degradation rate.

In the UV/oxidant combination, the addition of *t*-BuOH inhibited the ILs degradation with a big difference in performance dependent on the oxidant (Table 4).

In oxidation with PDS, the weaker inhibition was observed indicating only a small amount of hydroxyl radicals being formed (R15) and, thus, scavenged with *t*-BuOH. Accordingly, the UV/PDS combination demonstrated a predominance of sulfate radicals in the oxidation of ILs: the addition of EtOH dramatically inhibited the oxidation of all ILs compared to both reference experiments and the oxidation with the *t*-BuOH scavenger. Additions of *t*-BuOH to ILs solutions treated with the UV/PMS combination resulted in a stronger inhibition of oxidation, than with PDS confirming larger amounts of hydroxyl radicals produced by the decomposition of PMS (R11 and R12). EtOH added to the UV/PMS-treated ILs inhibited oxidation a few times compared to *t*-BuOH additions, showing thus also the substantial contribution of sulfate radicals into ILs degradation, which corresponds well with the PMS excitation reaction (R12).

4. Conclusions

Oxidation of aqueous imidazolium-based ionic liquids was successfully performed in PCD, PCD/oxidant and UV/oxidant combinations, showing the ILs oxidized with rates in the descending order [Emim][Cl] > [Omim][Cl] > [Emim][Br] in all methods. Compared to [Emim][Cl], the long alkyl chain of [Omim][Cl] had a low to moderate negative impact on the oxidation efficiency, making the imidazolium cation more recalcitrant towards degradation. Bromide anions greatly reduced the oxidation efficiency of [Emim]$^+$ cation due to the noticeable reactivity of bromide anions towards oxidation.

Oxidation of ILs PCD-treated in alkaline media proceeds with increased degradation efficiency due to cations' neutralization with hydroxyl anions to neutral molecules preferable as targets for electrophilic attacks of ROS, hydroxyl radicals and ozone.

Participation of ozone and, potentially, other long-living oxidants in the oxidation of ILs is seen from the difference in oxidation efficiencies at variations on pulse repetition frequency: lower frequency provides higher efficiency on account of long-living oxidants realizing their oxidation potential within longer pauses between pulses.

UV/persulfate combinations showed high efficiency in the degradation of ILs, although it is worth noting that their complete degradation was achieved only at increased dosages of the oxidant. The predominant role of sulfate radicals in ILs oxidation in UV/PDS treatment was observed in the experiments with the application of hydroxyl and sulfate radicals scavengers. A noticeable role of hydroxyl radicals in parity with sulfate ones in UV/PMS combination was observed.

For the PCD process, the effect of added persulfates ranged from a slight improvement to some inhibition of the ILs degradation rate. The fact that studies in the radicals' scavenging showed the substantial role of sulfate radicals in PCD/persulfate treatment at negligible or negative impact on the efficiency, the substitution of primary ROS with sulfate radicals may be considered proven.

The unassisted PCD and the UV/PDS combination showed the highest energy efficiency reaching, for example, 53.5 and 54.2 mmol kWh^{-1}, respectively, for the [Emim][Cl] degradation. Other ILs were also effectively oxidized by these reliable and promising methods.

CRediT authorship contribution statement

Dmitri Nikitin: Writing – review & editing, Writing – original draft, Visualization, Methodology, Investigation, Formal analysis,

Table 4
Results of hydroxyl and sulfate radical scavenging study in UV/oxidant combinations ([ILs]$_0$ = 100 μM, [PDS]$_0$ = [PMS]$_0$ = 500 μM, [EtOH]$_0$ = [*t*-BuOH]$_0$ = 25 mM, pH unadjusted).

Ionic liquid	Extrinsic oxidant		Ionic liquid degradation, %		
		Time, min	Reference	EtOH	*t*-BuOH
[Emim][Cl]	PDS	10	99	24	85
	PMS	20	99	11	52
[Omim][Cl]	PDS	10	99	38	90
	PMS	20	98	17	60
[Emim][Br]	PDS	40	97	44	83
	PMS	60	81	19	48

Conceptualization. **Sergei Preis:** Writing – review & editing, Resources, Methodology, Funding acquisition. **Niina Dulova:** Writing – review & editing, Writing – original draft, Validation, Supervision, Methodology, Formal analysis, Conceptualization.

Declaration of competing interest

The authors declare that they have no known competing financial interests or personal relationships that could have appeared to influence the work reported in this paper.

Data availability

Data will be made available on request.

Acknowledgement

Appendix A. Supplementary data

Supplementary data to this article can be found online at https://doi.org/10.1016/j.seppur.2024.127235.

References

[1] G. Kaur, H. Kumar, M. Singla, Diverse applications of ionic liquids: A comprehensive review, J. Mol. Liq. 351 (2022), https://doi.org/10.1016/j.molliq.2022.118556.

[2] R.F.M. Frade, C.A.M. Afonso, Impact of ionic liquids in environment and humans: An overview, Hum. Exp. Toxicol. 29 (2010) 1038–1054, https://doi.org/10.1177/0960327110371259.

[3] C.W. Cho, T.P.T. Pham, Y. Zhao, S. Stolte, Y.S. Yun, Review of the toxic effects of ionic liquids, Sci. Total Environ. 786 (2021), https://doi.org/10.1016/j.scitotenv.2021.147309.

[4] A. Romero, A. Santos, J. Tojo, A. Rodríguez, Toxicity and biodegradability of imidazolium ionic liquids, J. Hazard. Mater. 151 (2008) 268–273, https://doi.org/10.1016/j.jhazmat.2007.10.079.

[5] M.T. Garcia, N. Gathergood, P.J. Scammells, Biodegradable ionic liquids Part II. Effect of the anion and toxicology, Green Chem. 7 (2005) 9–14, https://doi.org/10.1039/B411922C.

[6] A. Jordan, N. Gathergood, Biodegradation of ionic liquids-a critical review, Chem. Soc. Rev. 44 (22) (2015) 8200–8237, https://doi.org/10.1039/C5CS00444F.

[7] N.V. Plechkova, K.R. Seddon, Applications of ionic liquids in the chemical industry, Chem. Soc. Rev. 37 (2008) 123–150, https://doi.org/10.1039/B006677J.

[8] K. Liu, Z. Wang, L. Shi, S. Jungsuttiwong, S. Yuan, Ionic liquids for high performance lithium metal batteries, J Energy Chem 59 (2021) 320–333, https://doi.org/10.1016/j.jechem.2020.11.017.

[9] P. Isosaari, V. Srivastava, M. Sillanpää, Ionic liquid-based water treatment technologies for organic pollutants: Current status and future prospects of ionic liquid mediated technologies, Sci. Total Environ. 690 (2019) 604–619, https://doi.org/10.1016/j.scitotenv.2019.06.421.

[10] E. Gomez-Herrero, M. Tobajas, A. Polo, J.J. Rodriguez, A.F. Mohedano, Toxicity and inhibition assessment of ionic liquids by activated sludge, Ecotoxicol. Environ. Saf. 187 (2020), https://doi.org/10.1016/j.ecoenv.2019.109836.

[11] M. Yu, S.M. Li, X.Y. Li, B.J. Zhang, J.J. Wang, Acute effects of 1-octyl-3-methyli-midazolium bromide ionic liquid on the antioxidant enzyme system of mouse liver, Ecotoxicol. Environ. Saf. 71 (2008) 903–908, https://doi.org/10.1016/j.ecoenv.2008.02.022.

[12] National Toxicology Program, Toxicity studies of select ionic liquids (1-ethyl-3-methylimidazolium chloride, 1-butyl-3-methylimidazolium chloride, 1-butyl-1-methylpyrrolidinium chloride, and n-butylpyridinium chloride) administered in drinking water to Sprague Dawley (Hsd:Sprague Dawley SD) rats and B6C3F1/N mice, NTP Developmental and Reproductive Toxicity Technical Report Series, no. TOX-103, pp. 1–209, 2022, doi: 10.22427/NTP-TOX-103.

[13] K.M. Docherty, J.K. Dixon, C.F. Kulpa, Biodegradability of imidazolium and pyridinium ionic liquids by an activated sludge microbial community, Biodegradation 18 (2007) 481–493, https://doi.org/10.1007/s10532-006-9081-7.

[14] I.F. Mena, E. Diaz, J.J. Rodriguez, A.F. Mohedano, An overview of ionic liquid degradation by advanced oxidation processes, Crit. Rev. Environ. Sci. Technol. (2021) 1–44, https://doi.org/10.1080/10643389.2021.1896273.

[15] S. Garcia-Segura, Á.S. Lima, E.B. Cavalcanti, E. Brillas, Anodic oxidation, electro-Fenton and photoelectro-Fenton degradations of pyridinium- and imidazolium-based ionic liquids in waters using a BDD/air-diffusion cell, Electrochim. Acta 198 (2016) 268–279, https://doi.org/10.1016/j.electacta.2016.03.057.

[16] T.L. Ren, X.W. Ma, X.Q. Wu, L. Yuan, Y.L. Lai, Z.H. Tong, Degradation of imidazolium ionic liquids in a thermally activated persulfate system, Chem. Eng. J. 412 (2021), https://doi.org/10.1016/j.cej.2021.128624.

[17] R. Guo, Y. Qi, B. Li, J. Tian, Z. Wang, R. Qu, Efficient degradation of alkyl imidazole ionic liquids in simulated sunlight irradiated periodate system: Kinetics, reaction mechanisms, and toxicity evolution, Water Res. 226 (2022), https://doi.org/10.1016/j.watres.2022.119316.

[18] W.-J. Liu, E. Kwon, B.X. Thanh, T.C. Khiem, D.D. Tuan, J.-Y. Lin, T. Wi-Afedzi, C. Hu, S. Sirivithayapakorn, K.-Y.-A. Lin, Hofmann-MOF derived nanoball assembled by FeNi alloy confined in carbon nanotubes as a magnetic catalyst for activating peroxydisulfate to degrade an ionic liquid, Sep. Purif. Technol. 295 (2022), https://doi.org/10.1016/j.seppur.2022.120945.

[19] C.A. Aggelopoulos, Recent advances of cold plasma technology for water and soil remediation: A critical review, Chem. Eng. J. 428 (2022), https://doi.org/10.1016/j.cej.2021.131657.

[20] M.A. Malik, Water purification by plasmas: Which reactors are most energy efficient? Plasma Chem. Plasma Process. 30 (2010) 21–31, https://doi.org/10.1007/s11090-009-9202-2.

[21] P. Ajo, I. Kornev, S. Preis, Pulsed Corona Discharge Induced Hydroxyl Radical Transfer Through the Gas-Liquid Interface, Sci. Rep. 7 (2017) 1–6, https://doi.org/10.1038/s41598-017-16333-1.

[22] H. Guo, S. Pan, Z. Hu, Y. Wang, W. Jiang, Y. Yang, Y. Wang, J. Han, Y. Wu, T. Wang, Persulfate activated by non-thermal plasma for organic pollutants degradation: A review, Chem. Eng. J. 470 (2023), https://doi.org/10.1016/j.cej.2023.144094.

[23] J. Wang, S. Wang, Activation of persulfate (PS) and peroxymonosulfate (PMS) and application for the degradation of emerging contaminants, Chem. Eng. J. 334 (2018) 1502–1517, https://doi.org/10.1016/j.cej.2017.11.059.

[24] G.M. Eisenberg, Colorimetric Determination of Hydrogen Peroxide, Ind Eng Chem - Anal Ed 15 (1943) 327–328, https://doi.org/10.1021/i560117a011.

[25] V. Derevshchikov, N. Dulova, S. Preis, Oxidation of ubiquitous aqueous pharmaceuticals with pulsed corona discharge, J. Electrostat. 110 (2021), https://doi.org/10.1016/j.elstat.2021.103567.

[26] J.E. Grebel, J.J. Pignatello, W.A. Mitch, Effect of halide ions and carbonates on organic contaminant degradation by hydroxyl radical-based advanced oxidation processes in saline waters, Environ. Sci. Tech. 44 (2010) 6822–6828, https://doi.org/10.1021/es1010225.

[27] P. Wardman, Reduction potentials of one electron couples involving free radicals in aqueous solution, J. Phys. Chem. Ref. Data 18 (1989) 1637–1755, https://doi.org/10.1063/1.555843.

[28] L. Onga, I. Kornev, S. Preis, Oxidation of reactive azo-dyes with pulsed corona discharge: Surface reaction enhancement, J. Electrostat. 103 (2020), https://doi.org/10.1016/j.elstat.2020.103420.

[29] U. Von Gunten, Ozonation of drinking water: Part II. Disinfection and by-product formation in presence of bromide, iodide or chlorine, Water Res. 37 (2003) 1469–1487, https://doi.org/10.1016/S0043-1354(02)00458-X.

[30] K. Tyrovola, E. Diamadopoulos, Bromate formation during ozonation of groundwater in coastal areas in Greece, Desalination 176 (2005) 201–209, https://doi.org/10.1016/j.desal.2004.10.018.

[31] K. Shang, R. Morent, N. Wang, Y. Wang, B. Peng, N. Jiang, N. Lu, J. Li, Degradation of sulfamethoxazole (SMX) by water falling film DBD Plasma/Persulfate: Reactive species identification and their role in SMX degradation, Chem. Eng. J. 431 (2022), https://doi.org/10.1016/j.cej.2021.133916.

[32] L. Wang, K. Jing, B. Hu, J. Lu, Hydrogen peroxide suppresses the formation of brominated oxidation by-products in heat-activated peroxydisulfate oxidation process, Chem. Eng. J. 417 (2021), https://doi.org/10.1016/j.cej.2021.129138.

[33] Y.X. Wang, I. Kornev, C.H. Wei, S. Preis, Surfactant and non-surfactant radical scavengers in aqueous reactions induced by pulsed corona discharge treatment, J. Electrostat. 98 (2019) 82–86, https://doi.org/10.1016/j.elstat.2019.03.001.

[34] D. Nikitin, B. Kaur, S. Preis, N. Dulova, Degradation of antibiotic vancomycin by UV photolysis and pulsed corona discharge combined with extrinsic oxidants, Catalysts 13 (2023), https://doi.org/10.3390/catal13030466.

[35] R.E. Brooks, S.B. Moore, Alkaline hydrogen peroxide bleaching of cellulose, Cellul. 7 (2000) 263–286, https://doi.org/10.1023/A:1009273701191.

[36] M.B. Heeb, J. Criquet, S.G. Zimmermann-Steffens, U. Von Gunten, Oxidative treatment of bromide-containing waters: Formation of bromine and its reactions with inorganic and organic compounds - A critical review, Water Res. 48 (2014) 15–42, https://doi.org/10.1016/j.watres.2013.08.030.

[37] L. Onga, E. Kattel-Salusoo, S. Preis, N. Dulova, Degradation of anti-inflammatory drug dexamethasone by pulsed corona discharge: The effect of peroxycompounds addition, J. Environ. Chem. Eng. 10 (2022), https://doi.org/10.1016/j.jece.2022.108042.

[38] P. Neta, V. Madhavan, H. Zemel, R.W. Fessenden, Rate constants and mechanism of reaction of sulfate radical anion with aromatic compounds, J. Am. Chem. Soc. 99 (1977) 163–164, https://doi.org/10.1021/ja00443a030.

[39] O.S. Furman, A.L. Teel, R.J. Watts, Mechanism of base activation of persulfate, Environ. Sci. Tech. 44 (2010) 6423–6428, https://doi.org/10.1021/es1013714.

[40] C. Qi, X. Liu, J. Ma, C. Lin, X. Li, H. Zhang, Activation of peroxymonosulfate by base: Implications for the degradation of organic pollutants, Chemosphere 151 (2016) 280–288, https://doi.org/10.1016/j.chemosphere.2016.02.089.

[41] Y.H. Guan, J. Chen, L.J. Chen, X.X. Jiang, Q. Fu, Comparison of UV/H₂O₂, UV/PMS, and UV/PDS in destruction of different reactivity compounds and formation of bromate and chlorate, Front. Chem. 8 (2020) 1–12, https://doi.org/10.3389/fchem.2020.581198.

[42] T. Mackuľak, L. Birošová, I. Bodík, R. Grabic, A. Takáčová, M. Smolinská, A. Hanusová, J. Híveš, M. Gál, Zerovalent iron and iron(VI): Effective means for the removal of psychoactive pharmaceuticals and illicit drugs from wastewaters, Sci. Total Environ. 539 (2016) 420–426, https://doi.org/10.1016/j.scitotenv.2015.08.138.

[43] Eurostat, Electricity prices for non-household consumers, 2023. https://ec.europa.eu/eurostat/statistics-explained/index.php?title=Electricity_price_statistics.

[44] P. Kumari, A. Kumar, Advanced oxidation processes: A remediation technique for organic and non-biodegradable pollutant, Results Surf Interfaces 11 (2023), https://doi.org/10.1016/j.rsurfi.2023.100122.

[45] G.P. Anipsitakis, D.D. Dionysiou, Radical generation by the interaction of transition metals with common oxidants, Environ. Sci. Tech. 38 (2004) 3705–3712, https://doi.org/10.1021/es035121o.

Curriculum vitae

Personal data:

Name:	Dmitri Nikitin
Date of birth:	22.07.1995
Place of birth:	Kohtla-Järve
Citizenship:	Estonia

Contact data:

E-mail:	dmitri.nikitin@taltech.ee

Education:

2020–2024	Tallinn University of Technology, Chemical and Materials Technology, PhD
2018–2020	Tallinn University of Technology, Chemical and Environmental Technology, Master of Science in Engineering (*Cum laude*)
2014–2017	Tallinn University of Technology, Chemical and Environmental Technology, Bachelor of Science in Engineering
2011–2014	Ahtme Gymnasium (Gold medal)

Language competence:

English	Fluent
Estonian	Fluent
Russian	Native speaker
Spanish	Basics

Professional employment:

2020–2024	Tallinn University of Technology, School of Engineering, Department of Materials and Environmental Technology, Junior Researcher
2019–2020	Eastman Specialties OÜ, Environmental Specialist

Defended thesis:

Master's Degree, 2020, (sup) Sergei Preis; Priit Tikker, Oxidation of bisphenol A by pulsed corona discharge: impacts of plasma-liquid contact surface and a surfactant radical scavenger, Tallinn University of Technology, School of Engineering, Department of Materials and Environmental Technology

Field of research:

1. Biosciences and Environment; 1.8. Research relating to the State of the Environment and to Environmental Protection; CERCS CLASSIFICATION: T270 Environmental technology, pollution control

4. Natural Sciences and Engineering; 4.11. Chemistry and Chemical Technology; CERCS CLASSIFICATION: T350 Chemical technology and engineering

Participation in research projects:

ETAG22018 Utilization of aluminium-bearing raw materials for the production of aluminium metal, other metals and compounds

VIR23025 Stormwater purification with construction and demolition waste

Awards:

2024	Kristjan Jaak Scholarship for the participation in the 19th IWA Leading Edge Conference on Water and Wastewater Technologies, 24-28 June 2024
2023	Tallinn City Council Scholarship
2022	Kristjan Jaak Scholarship for the participation in the International Conference on Green Energy and Environmental Technology (GEET-22), Rome, 27-29 July 2022.
2019	TalTech Development Fund, Eastman Specialties OÜ Scholarship

Supervised dissertations:

Joonas Nurges, Master's Degree, 2023, (sup) Niina Dulova; Dmitri Nikitin, Degradation of imidazolium-based ionic liquid by advanced oxidation processes, Tallinn University of Technology School of Engineering, Department of Materials and Environmental Technology

Roman Fadejev, Master's Degree, 2022, (sup) Niina Dulova; Dmitri Nikitin, Degradation of metformin by advanced oxidation processes, Tallinn University of Technology School of Engineering, Department of Materials and Environmental Technology

Helina Prükk, Master's Degree, 2022, (sup) Niina Dulova; Dmitri Nikitin, Degradation of 1-ethyl-3-methylimidazolium chloride in aqueous solution by advanced oxidation processes, Tallinn University of Technology School of Engineering, Department of Materials and Environmental Technology

Elulookirjeldus

Isikuandmed:

Nimi:	Dmitri Nikitin
Sünniaeg:	22.07.1995
Sünnikoht:	Kohtla-Järve
Kodakondsus:	Estonia

Kontaktandmed:

E-post:	dmiti.nikitin@taltech.ee

Hariduskäik:

2020–2024	Tallinna Tehnikaülikool, Keemia- ja materjalitehnoloogia, PhD
2018–2020	Tallinna Tehnikaülikool, Keemia- ja keskkonnakaitse tehnoloogia, tehnikateaduste magistrikraad (*Cum laude*)
2014–2017	Tallinna Tehnikaülikool, Keemia- ja keskkonnakaitse tehnoloogia, tehnikateaduste bakalaureusekraad
2011–2014	Ahtme Gümnaasium (Kuld medal)

Keelteoskus:

Inglise keel	Kõrgtase
Eesti keel	Kõrgtase
Vene keel	Emakeel
Hispaania keel	Algtase

Teenistuskäik:

2020–2024	Tallinna Tehnikaülikool, Inseneriteaduskond, Materjali- ja keskkonnatehnoloogia instituut, doktorant-nooremteadur
2019–2020	Eastman Specialties OÜ, Keskkonnaspetsialist

Kaitstud lõputööd:

Dmitri Nikitin, magistrikraad, 2020, (juh) Sergei Preis; Priit Tikker, Bisfenool A oksüdeerumine impulss-koroona elektrilahenduse toimel: plasma-vedelik kontaktpinna ja pindaktiivse radikaalpüüdja mõju, Tallinna Tehnikaülikool, Inseneriteaduskond, Materjali- ja keskkonnatehnoloogia instituut

Uurimustöö põhisuunad:

1. Bio- ja keskkonnateadused; 1.8. Keskkonnaseisundit ja keskkonnakaitset hõlmavad uuringud; CERCS KLASSIFIKAATOR: T270 Keskkonnatehnoloogia, reostuskontroll

4. Loodusteadused ja tehnika; 4.11. Keemia ja keemiatehnika; CERCS KLASSIFIKAATOR: T350 Keemiatehnoloogia ja -masinaehitus

Osalemine uurimisprojektides:

ETAG22018 Alumiiniumi sisaldavate toormaterjalide kasutamine alumiiniummetalli, muude metallide ja ühendite tootmiseks

VIR23025 Sademevee puhastamine ehitus- ja lammutusjäätmetega

Tunnustused:

2024	Kristjan Jaagu välislähetuse stipendium osalemiseks konverentsil "19th IWA Leading Edge Conference on Water and Wastewater Technologies", 24.-28. juuni 2024
2023	Tallinna linna Raestipendium
2022	Kristjan Jaagu välislähetuse stipendium osalemiseks konverentsil "International Conference on Green Energy and Environmental Technology (GEET-22)", Rooma, 27.-29. juuli 2022.
2019	TalTech Arengufond, Eastman Specialties OÜ Stipendium

Juhendatud magistritööd:

Joonas Nurges, magistrikraad, 2023, (juh) Niina Dulova; Dmitri Nikitin, Imidasooliumil põhineva ioonse vedeliku lagundamine süvaoksüdatsiooniprotsessidega, Tallinna Tehnikaülikool, Inseneriteaduskond, Materjali- ja keskkonnatehnoloogia instituut

Roman Fadejev, magistrikraad, 2022, (juh) Niina Dulova; Dmitri Nikitin, Metformiini lagundamine süvaoksüdatsiooniprotsessidega, Tallinna Tehnikaülikool, Inseneriteaduskond, Materjali- ja keskkonnatehnoloogia instituut

Helina Prükk, magistrikraad, 2022, (juh) Niina Dulova; Dmitri Nikitin, 1-etüül-3-metüülimidasooliumkloriidi lagundamine vesilahuses süvaoksüdatsiooniprotsessidega, Tallinna Tehnikaülikool, Inseneriteaduskond, Materjali- ja keskkonnatehnoloogia instituut